Technische Universität München

Fakultät für Chemie

Non-oxidative dehydroalkylation of benzene with methane over Co-ZSM-5

Martina Aigner

Vollständiger Abdruck der von der Fakultät für Chemie der Technischen Universität München zur Erlangung des akademischen Grades einer

Doktorin der Naturwissenschaften (Dr. rer. nat.)

genehmigten Dissertation.

Vorsitzender:	Prof. Dr. Tom Nilges
Prüfende der Dissertation:	1. Prof. Dr. Johannes A. Lercher
	2. Hon.- Prof. Dr. Richard W. Fischer

Die Dissertation wurde am 03.02.2022 bei der Technischen Universität München eingereicht und durch die Fakultät für Chemie am 30.03.2022 angenommen.

Die vorliegende Arbeit entstand im Zeitraum vom März 2017 bis Oktober 2021 an der Fakultät für Chemie und am Zentralinstitut für Katalyseforschung (CRC) der Technischen Universität München.

„Falls du glaubst, dass du zu klein bist um etwas zu bewirken,

dann versuche mal zu schlafen, wenn eine Mücke im Raum ist.“

Dalai Lama

Für meine Familie

Danksagung

Nach über zehn Jahren an der TU München mit einem kurzen Abstecher nach Kalifornien an die UC Berkeley, reiche ich nun endlich meine Dissertation ein. Es war eine sehr schöne, aber auch fordernde Zeit.

Ich möchte mich bei allen Menschen, die mich auf die eine oder andere Art und Weise unterstützt haben bedanken.

Insbesondere bei meinem Doktorvater Prof. **Johannes** A. Lercher für die Betreuung meiner Arbeit. Du hast mir die Chance gegeben mich an manchmal leichten, manchmal auch schweren Aufgaben zu beweisen und daran zu wachsen. Wir haben zwar hin und wieder aneinander vorbeigeredet, uns aber dann doch immer wieder zusammengefunden. Vielen Dank für deine Unterstützung!

Ich danke natürlich auch meinen beiden Mentoren **Ricardo** Bermejo de Val und **Maricruz** Sanchez Sanchez. Zu Beginn des Projektes hast du, Ricardo, mich tatkräftig dabei unterstützt mich in die Arbeitsweise der TC2 Gruppe einzufinden und mein Setup zum Laufen zu bringen. Somit haben die Basics meiner Forschung gepasst. Maricruz, du hast mich und das Projekt dann von Ricardo übernommen und mich tatkräftig insbesondere durch deine Schreibfähigkeiten unterstützt. Auch dir, **Andreas** Jentys möchte ich für deine Unterstützung und unterhaltsamen Gesprächen danken (auch wenn du mir oft meinen Stuhl geklaut hast). Vielen Dank euch dreien!

Ein großer Dank geht natürlich auch an das Dreiergespann aus **Bettina** Federmann, **Kateryna** Kryvko und **Stefanie** Seibold. Eure administrative Unterstützung hat vieles erst möglich gemacht!

Vieles im Labor wäre auch ohne euch, **Xaver** Hecht, **Muhammad** Iqbal, **Martin** Neukamm, **Andreas** Marx und dem ganzen Team der Feinmechanikwerkstatt nicht möglich gewesen. Daher ein großes Dankeschön an euch!

I am also very grateful to **Stijn** van Daele, **Nikolai** Nesterenko, and **Delphine** Minoux for supporting my project and fruitful scientific discussions.

Natürlich darf ich meine Studenten nicht vergessen, die mich alle tatkräftig unterstützt haben! **Andreas** Auernhammer, **Matthias** Bauer, **Michael** Bauer, **Angelina** Cuomo, **Lukas** Deffner, **Dominik** Grünwald und **Simon** Roßkopf. Das

Zusammenarbeiten mit euch hat mir immer große Freude bereitet. Und insbesondere euch, **Patrick** Gotthardt und **Felix** Simon, möchte ich danken. Durch eure unermüdliche Arbeit habt ihr das Projekt am Laufen gehalten, auch als ich nur von der Ersatzbank aus zusehen konnte.

Ein besonderer Dank gilt auch der gesamten Arbeitsgruppe. Es hat stets Spaß gemacht mit euch zu arbeiten! Especially to **Guanhua** Cheng, **Xi** Chen, **Lingli** Ni, **Iris** Yu, **Yong** Wang, and **Ruixue** Zhao for the funny evenings eating super tasty dumplings together. **Niklas** Pfriem**, Fischer** Philipp und **Jakub** Pazdera für die Gute Sitznachbarschaft. **Fuli** Deng**, Insu** Lee, **Lei** Tao**, Roland** Weindl und **Alex** Wellmann, für unvergessliche Stunden während des Ulm-Kurses. Den erfahrenden Hasen **Martin** Baumgärtl**, Christoph** Denk**, Verena** Höpfl**, Rachit** Khare und **Ferdinand** Vogelgsang. Und euch Jungspunden **Christoph** Gross, **Lennart** Wahl und **Florian** Zahn. Ich wünsche euch alles Gute und weiterhin viel Spaß und Erfolg in der TC2!

Und natürlich **Laura** Löbbert, **Madita** Einemann, **Simon** Krebs, **Teresa** Schachtl und **Mirjam** Wenig. Ihr habt mich durch so manche Kommentare in unserer WhatsApp Gruppe zum Lachen gebracht! Unsere gemeinsamen Ausflüge an den See oder Pausen zum Süßigkeiten essen waren immer eine willkommene Abwechslung zu den wissenschaftlichen Diskussionen bei der Arbeit.

Ein herzlicher Dank geht natürlich auch an alle meine Freunde außerhalb des Uniwahsinns. Ihr habt mich ertragen, als ich unverständliches chemisches Zeug erzählt habe und versucht habe euch mein Thema näher zu bringen.

Mein herzlichster Dank geht aber an meinen Freund **Paul**. Deine Ohren müssen schon kurz vor dem Abfallen sein, so oft wie ich dir schon von meinen Erlebnissen bei der Arbeit erzählt habe. Du hörst mir immer zu und bist immer für mich da! Vielen Dank!

Und das wichtigste zum Schluss: Vielen Dank **Mama** und **Papa**! Ihr habt mir meinen gesamten Werdegang erst ermöglicht! Für eure bedingungslose Unterstützung und Ausdauer meiner Geschichten zu Lauschen. Und mein **Bruder**, du warst erst richtig froh als ich das Elternhaus verlassen habe, aber du musst zugeben, dass du dich doch immer wieder freust wenn ich nach Hause komme ☺.

Abstract

In this study, ion-exchanged Co in ZSM-5 with mostly single Co^{2+} cations in Al pairs was found to be active at moderate temperatures for the direct methylation of benzene. Through kinetic experiments and temperature-programmed surface reactions, a tentative reaction scheme and a mechanism for that reaction were elucidated. Combining results of infrared and UV-Vis spectroscopy, the position of the active sites in Co-ZSM-5 was investigated. This allowed showing that the Co position influences the selectivity of various products.

Kurzzusammenfassung

In dieser Studie wurde festgestellt, dass ionenausgetauschtes Co in ZSM 5 mit überwiegend einzelnen Co^{2+}-Kationen in Al-Paaren bei moderaten Temperaturen aktiv für die direkte Methylierung von Benzol ist. Durch kinetische Experimente und temperaturprogrammierte Oberflächenreaktionen konnten, sowohl ein vorläufiges Reaktionsschema, als auch der Mechanismus dieser Reaktion aufgeklärt werden. Durch die Kombination von Ergebnissen aus Infrarot- und UV-Vis Spektroskopie, wurde die Position der aktiven Stellen in Co-ZSM-5 untersucht. Dadurch konnte gezeigt werden, dass die Co-Position die Selektivität der verschiedenen Produkte beeinflusst

Abbreviations and symbols

°C	degree Celsius
Å	Ångström
AAS	Atom absorption spectroscopy
AEI	Framework Type AEI
Al	Aluminum
BAS	Brønsted acid sites
bcm	billion cubic meters
BET	Brunauer-Emmett-Teller
CFI	Framework type CFI
CH_4	Methane
cm	Centimeter
CO	Carbon monoxide
CO_2	Carbon dioxide
Co	Cobalt
$Co(NO_3)_2$	Cobalt nitrate
Co_2O_3	Cobalt(III)-oxide
CoO	Cobalt oxide
$CoOAc_2$	Cobalt acetate

Cu	Copper
DFT	density functional theory
E_a	activation energy
EFAl	extra-framework aluminum
e.g.	exempli gratia
eq	equilibrium
eV	electron volt
EXAFS	extended X-ray absorption fine structure
Fe	Iron
FT	Fourier-transformed
FWHM	full width at half maximum
g	gram
GC	gas chromatography
GHG	greenhouse gas
h	hour
H_2	Hydrogen
H_2O	Water
IR	infrared
IZA-ZC	structure commission of the international zeolite association
K	Kelvin

k	kilo
kJ	kilojoule
LAS	Lewis acid site
M	metal
mbar	millibar
MDA	Methane dehydroaromatization
MFI	pentasil zeolites type MFI
mg	milligram
MHz	megahertz
min	minute
mL	milliliter
mmol	millimol
Mo	Molybdenum
MOR	Mordenite
MR	membered ring
N_2	Nitrogen
Na	Sodium
NMR	nuclear magnetic resonance
p	pressure
PBU	primary building unit

PFR	plug flow reactor
PXRD	powder X-ray diffraction
rds	Rate determining step
RT	room temperature
S	selectivity
s	second
SBU	secondary building unit
SEM	scanning electron microscopy
Si	silicon
SiC	silicon carbide
SiO_2	silica
SynAir	synthetic air
T	temperature
TGA	thermogravimetric analysis
Ti	Titanium
TOF	turnover frequency
TOS	time on stream
TPR	Temperature-programmed reaction
UV-Vis	ultraviolet-visible

WHSV	weight hourly space velocity
X	conversion
XANES	X-ray absorption near-edge structure
XAS	X-ray absorption spectroscopy
XRD	X-ray diffraction
Y	yield
Zn	Zinc
Zr	Zirconium
ZSM-5	Zeolite Socony Mobil–5
α	alpha
β	beta
γ	gamma

Table of Contents

1 Introduction

Climate change is on everyone's lips. In 2015, several countries decided in the Paris agreement that a limit of 2 °C for global warming is necessary to combat the climate crisis.[1] The main goal is the reduction of greenhouse gas emissions (GHG), mainly consisting of carbon dioxide (CO_2) and even more harmful methane (CH_4), to target the global warming to 1.5 °C above pre-industrial levels.[1-3] Large artificial sources for these greenhouse gases are, for instance, wells and petrochemical plants. This is mainly for safety reasons to release overpressure or a missing gas infrastructure, where the gas would reduce the flow velocity in liquid crude oil transportation.[4-5] Due to technical, regulatory, or economic constraints, CH_4 is primarily burned in large amounts to convert it into the slightly less damaging CO_2.[6] **Figure 1.1** shows such a gas flaring. This is not only a waste of energy but also money.

Figure 1.1: Example of a gas flare in the petrochemical industry.[7]

This so-called flaring accounted for 430 Mt (~1.2%) annual CO_2 emission worldwide in 2019.[8] Iran, and the USA, for example, contribute with more than 70 Mt CO_2 emission, each, and belong therefore to the countries with the highest emissions.[9] More beneficial approaches to manage excess CH_4 need to be established to avoid this malignant transformation.

Another big challenge to counter climate change is the investigation of renewable energy. Therefore, CH_4 from biogas plants plays an important role and is one of the most promising green energy sources. However, due to the high symmetry of CH_4, and its high C-H bond dissociation energy of ~440 kJ mol^{-1}, processes for CH_4 conversion on an industrial scale, are still very limited due to its limited activation in a controlled way.[10-12] They imply harsh conditions or the use of heterogeneous catalysts.

1.1 Turning CH_4 into a value-added product

The main component of natural gas is CH_4 with up to 96 mol%, followed by two mol% of ethane.[13] In 2019, about 4000 billion cubic meters (bcm) of natural gas was consumed worldwide.[14] Alone in the US, 871 bcm were used in several end-use sectors with the following distribution: 3% of the natural gas was used for transportation of the natural gas itself through pipelines; primarily for heating buildings and water, 15% of the natural gas was used by the residential sector, and 10% by commercial consumers; the electric power sector use 38% of natural gas to generate electricity; the industrial sector consumed 33% of natural gas typically as fuel for heating and power, but also the production of chemicals, fertilizer, and hydrogen.[15] As a fuel, CH_4 provides a very high heating value of ~ 56 kJ g^{-1}.[4] Therefore, CH_4 is indispensable as a fuel.

1.1.1 Most common processes converting CH_4

Around 25% of the U.S. natural gas consumption in industry is used to utilize CH_4 for chemical production.[15] Most of these processes consist of partial oxidation (1.1), dry reforming (1.2), steam reforming (1.3), and autothermal reforming (partial oxidation with oxygen and steam). The obtained products are CO and H_2, so-called syngas, which can then further be processed, for example for the methanol synthesis, the Haber-Bosch process (ammonia synthesis), or the Fisher-Tropsch process to synthesize liquid hydrocarbons.[6, 16]

$$CH_4 + \frac{1}{2} O_2 \rightleftharpoons CO + 2\,H_2 \qquad 1.1$$

$$CH_4 + CO_2 \rightleftharpoons 2\,CO + 2\,H_2 \qquad 1.2$$

$$CH_4 + H_2O \rightleftharpoons CO + 3\,H_2 \qquad 1.3$$

Dry reforming is the most efficient method to convert two GHG simultaneously. Nevertheless, the downside of this reaction is that high temperatures of 450-900 °C are needed, as well as the requirement of catalysts to reach sufficient conversions, since this reaction is endothermic by 247 kJ mol^{-1}.[17-18] Nobel metals such as Ru, Rh, Ni and Co supported on amorphous supports (*e.g.*, TiO_2, SiO_2) or mesoporous material (*e.g.*, SBA-15) are highly active to support this reaction. However, a significant disadvantage of these materials consists of sintering (agglomeration and fusion of smaller particles to larger ones) and coking (carbon depositing).

Methanol is the most crucial downstream product of CH_4 chemistry in terms of volume.[19] Approximately 157 million metric tons of methanol were produced worldwide in 2020.[20]

Besides syngas production, several more processes in the industry use CH_4 as reactant: chlorination, Degussa and the Andrussow process for hydrogen cyanide production, carbon disulfide production, and high-temperature pyrolysis for acetylene production.[21]

In addition to the above-listed industrial-relevant processes, CH_4 valorization is also often explored in academic studies. These include the direct selective oxidation towards methanol or formaldehyde, the oxidative coupling towards ethane or ethylene, and the dehydro-aromatization towards benzene.[22-25] Nevertheless, limited yield of the product of interest , and high coke formation hinder such processes from being implemented in large-scale industrial processes.[23] A deeper understanding and development is desirable.

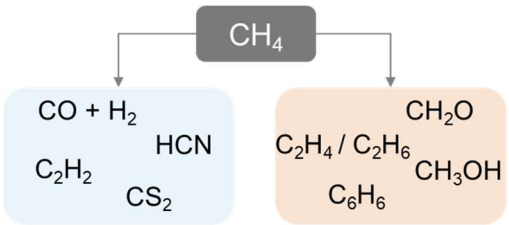

Figure 1.2: Products directly converted from CH_4. Left: commercial; right: non-commercial processes.

1.1.2 The challenge of CH_4 activation

As already mentioned, the C-H bond dissociation energy in CH_4 is ~440 kJ mol^{-1}.[26] It is a highly symmetric tetrahedral molecule with a carbon atom in the center, surrounded by four hydrogen atoms with a C-H bond length of 1.09 Å.[10] To overcome such a low reactivity of CH_4, it is necessary to find a highly active catalyst for the CH_4 activation.

It is widely accepted that the CH_4 activation follows either a homolytic or heterolytic C-H bond breaking mechanism on metal oxide supported catalysts.[27-31] Such a dissociative cleavage of CH_x-H on an active site is generally considered the rate-determining step (rds) in CH_4 reactions.[32-33] A selection of non-oxidative routes of CH_4 activation is presented within the following section. Due to its thematic relevance in this thesis, oxidative mechanisms are not further discussed in this section.

One example for the direct conversion of CH_4 to valued products such as benzene, toluene, naphthalene, and hydrogen by methane dehydroaromatization (MDA). Besides a small fraction of toluene and naphthalene, the primary reaction of CH_4 in MDA is the aromatization towards benzene (*1.4*):

$$6\,CH_4 \longrightarrow C_6H_6 + 9\,H_2 \qquad 1.4$$

Several studies report that Cu, Co, Mo, or Zn modified zeolites (ZSM-5 or MCM-22) and Fe on amorphous SiO_2 or GaN nanowire are capable catalysts reaching notable conversion of CH_4 with high selectivity towards benzene.[11, 23, 30, 34-37] The first step is always the C-H bond cleavage. Different studies report controversial mechanisms, discussing whether this step is homolytic or heterolytic. Sun *et al.* report the formation of free methyl radicals on Fe supported H-ZSM-5 observed by vacuum ultraviolet-soft photoionization-molecular beam mass spectrometry.[37] They propose a homolytic mechanism where C_2H_6 is formed by $CH_3^{\cdot}$ followed by dehydrogenation and cyclization forming benzene. On the other hand, Wang *et al.* using Zn on H-ZSM-5, have reported a heterolytic dissociation. They report the formation of CH_3^+ species, interacting with the support, and a $[Zn\text{-}H]^+$ species.[34] A similar mechanism was proposed on Cu zeolites by Gabrienko *et al.* in 2020.[38] A heterolytic cleavage includes the formation of a surface methoxy species and the H adsorbs on a Cu^{2+} ion.

Nevertheless, the literature proposing heterolytic dissociation is divided. Recent studies by Xu *et al.* report a heterolytic dissociative cleavage using Co on ZSM-5 material.[30] They suggest the C atom of the resulting CH_3 bonds to the Lewis acid metal sites, and the remaining H atom interacts with an O atom nearby.[30]

In MDA processes using M^{2+} supported zeolites, alkylated aromatics were also observed besides benzene production.[35, 37, 39] This opens another field about the direct methylation of benzene.

In the 90s and 2000, there was an ongoing discussion about the involvement of CH_4 in the toluene formation from benzene and CH_4.[5, 28, 40-43] Two different pathways in various catalyst systems were proposed: one hypothesis was that the additional C atom in of the methyl group of toluene was formed by fragmentation, coke deposition and rearrangement of benzene without the direct involvement of methane, while the other hypothesis indicated the participation of CH_4 by witnessing the appearance of labeled ^{13}C from $^{13}CH_4$ in the methyl group of toluene.

Furthermore, similar to MDA, there is a constant debate, whether the methyl group adsorbs on the metal of a catalyst or the neighboring O atom of the support (see **Figure 1.3**).[28, 31, 38, 44]

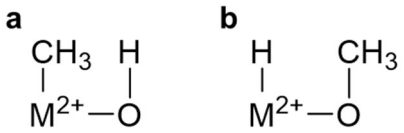

Figure 1.3: CH_4 activation in two different pathways. M^{2+} can be, *e.g.*, Cu, Co, Zn.

Xu *et al.* reported that if a heterolytic cleavage occurs, species **a** is formed, while methoxy species **b** is formed after a homolytic separation.[31] And Wang *et al.* proposed that both formations are possible, but the reaction between benzene and methane is only possible if the formed M-CH_3 has been further oxidized to a methoxy species.[28] In constellation **a**, CH_3 is negatively charged and cannot react via an electrophilic substitution with benzene. Recent publications by Matsubara *et al.* suggested a possible mechanism for the direct methylation over Co-ZSM-5.[29] They propose that benzene is the only molecule that adsorbs on the metal site. The Co^{2+} is suggested to retain its electron-withdrawing properties. This allows CH_4 from the gas phase to be

polarized by the Co-cation so that a CH_3^+ species is formed under the separation of a hydride ion. The CH_3^+ species then readily react with benzene to form toluene and hydrogen.

This discussion about the CH activation and the mechanism in total will be investigated further in this thesis.

1.2 Benzene and its derivates

Benzene is considered one of the essential basic petrochemical molecules. It is the simplest aromatic molecule with a unique delocalized π-system of C_6H_6 with a CH bond length of 140 pm.[21] Despite its carcinogenicity benzene is used in many applications. The total benzene consumption of ~ 57 million metric tons per year (stated 2021) can be categorized into five main products: ethylbenzene, cumene, cyclohexane, nitrobenzene, and linear alkylbenzenes.[20, 45-46] The main consumable products are polystyrene, pharmaceuticals, nylon, or polyethylene terephthalate plastic (PET). Together with toluene and xylene, it builds the mixture of BTX (benzene, toluene, and xylene isomers) hydrocarbons. More than 100 million tons of BTX per year were produced in 2018.[47] A significant fraction of BTX is made from crude oil by catalytic naphtha reforming in a refinery. **Figure 1.4** shows a diagram of the fractional distillation of crude oil. The C_5-C_{10} products are within the boiling range of naphtha. This can further be processed to BTX among others, using metal-modified zeolites (*e.g.,* Pt-Zn-ZSM-5). [48]

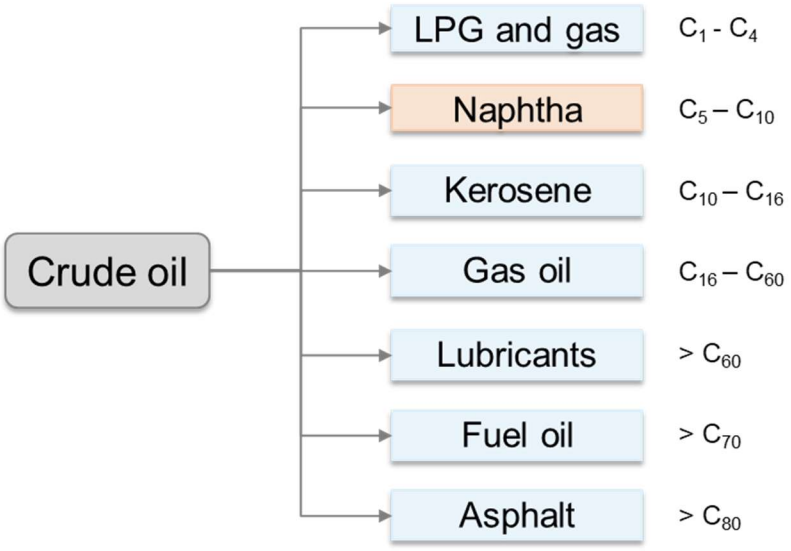

Figure 1.4: Overview of crude oil fractional distillation (adapted from ref. [49]).

The market of BTX is in steady growth. However, if the relevance of petroleum-based resources may decline due to hydrogen-powered and electrified mass transport, BTX generated in refineries might also be limited. Consequentially, alternative routes for

BTX production need to be developed. A valuable carbon source for that can be natural gas, as already described in section 1.1.2.

Furthermore, electricity will be the ultimate energy provider through the energy transition. As an energy storage vector, hydrogen plays a very important role. However, there are several disadvantages in terms of storage of hydrogen, which have not been the case with traditional sources. Hydrogen can form flammable mixtures, it diffuses relatively well through various materials, and it has a low energy density by volume. Solutions for effectively storing hydrogen have been discussed for years. One promising method is using a liquid organic hydrogen carrier (LOHC).[50-53] LOHCs are unsaturated liquid organic hydrocarbons - mostly aromatic compounds. H_2 can be absorbed via hydrogenation reactions, then LOHCs can serve as a carrier material. By dehydrogenation, the chemically stored H_2 can be released on demand. As a result, LOHCs provide transport safety and efficient storage for H_2.[51-54] One example of a LOHC is perhydro-dibenzyl-toluene. **Figure 1.5** shows a catalytic cycle with the hydrogenation of dibenzyltoluene towards perhydro-dibenzyltoluene. This hydrogenation is exothermic and requires nine H_2. During the dehydrogenation, nine H_2 are released in an endothermic process with + 65 kJ mol^{-1}.[55]

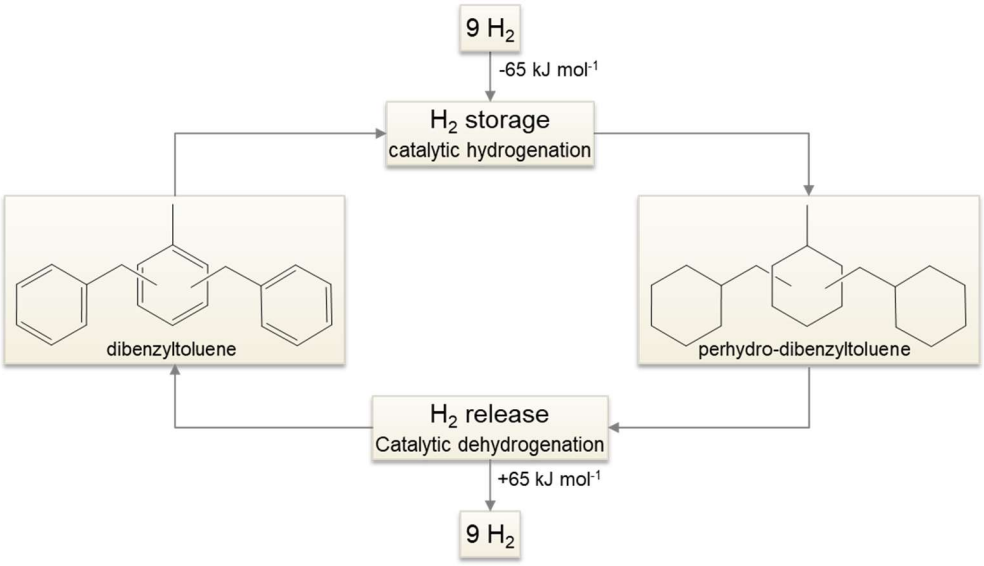

Figure 1.5: Scheme of the catalytic circle of dibenzyltoluene function as LOHC (adapted from ref. [51]).

The source material for dibenzyltoluene is benzyl chloride, which in turn is obtained from toluene.[56-57] These various applications of BTX result in its higher demands, and

alternative paths for the production of BTX are required. In section 1.4, an alternative way for toluene and H_2 production is introduced.

1.3 Zeolites – high-quality catalysts

Industry-relevant cracking, alkylation, and Mobil-oil processes utilize heterogeneous catalysts to activate CH bonds from crude oil and natural gas.[21] In such extensive scale procedures, primarily zeolites are efficient materials.

Zeolites are porous materials with a three-dimensional structure consisting of channels and cavities. The pores differ in their diameters and their dimensionality. These structures can be assigned to a Framework Type Code (FTC) by the Structure Commission of the International Zeolite Association (IZA-SC). Currently, already 255 different frameworks are accepted.[58]

Zeolites were initially defined by Axel Frederick Cronstedt in 1756 and named after the Greek words –"ζέω" (zeō) - to boil/cook - and "λίθος" (lithos) – stone.[59-60] Zeolites are aluminosilicate minerals consisting of $[SiO_4]^-$ and $[AlO_4]^-$ tetrahedra – so-called basic building units (BBU).[61] A connection of these BBU via the oxygen atoms forms secondary building blocks, generating a highly porous three-dimensional and uniform pore structure. The resulting negative charges of the tetrahedra containing Al^{3+} can be balanced by non-metallic cations such as NH_4^+ or H^+, or metallic ions such as, *e.g.*, Co^{2+} or Ni^{2+}. One specific property of zeolites is exchanging these cations with other ions. The protonated form is highly acidic, acts as a solid Brønsted acid site (BAS) and are commonly referred to as solid acids. This acidity depends on the Si/Al ratio, specifically the aluminum content in the network. However, the more Al content, the less stable the zeolite is since a structure with high Si contents is thermodynamically favored.[60-61] Zeolites can also contain electrophilic Lewis acid sites (LAS), *e.g.*, if the zeolite is exchanged with divalent metal ions. With these properties, the options to modify and adapt such a catalyst material to various applications seem to be almost infinite.

Generally, the structures are classified by their pore size in small-pore, medium-pore, large-pore, and extra-large pore zeolites, according to the number of tetrahedral sites

(T-atoms) per pore opening. The grouping and examples for each dimension are shown in **Table 1.1**. Most industry-relevant zeolites consist of 8 membered-ring (MR), 10 MR, and 12 MR. Due to its importance for this study, section 1.3.3 focuses on a medium-sized zeolite - the MFI type.

Table 1.1: Grouping of zeolites in four different pore sizes (adapted from ref. [62]).

Pore size	Number of T-sites (MR)	Pore diameter (Å)	Example
Small	8	4	AEI
Medium	10	5.5	MFI
Large	12	7.5	MOR
Extra-large	> 12	> 7.5	CFI

1.3.1 Shape selectivity of zeolites

The confined and well-defined pore structure is the main advantage of crystalline materials compared to amorphous supports as catalysts. It provides a shape selectivity with three main effects:

i) the reactant selectivity,

ii) the product selectivity, and

iii) the transition state-type selectivity.[63]

Figure 1.6 shows the different types of shape selectivitie. In the first case, the pore diameter excludes constraint substrates sterically to enter the catalytic sites inside the pores. In the second case, bulky products formed inside the pores are hindered from leaving the pores due to steric reasons. A standard example is the formation of xylenes, where only the kinetically smaller *para*- isomers can leave the pores while *meta*- and *ortho*- isomers are captured inside the pores.[60, 64-65] And in the third case,

the formation of a transition state is sterically hindered, while another less constrained one is favored. Therefore, one speaks from a restricted transition state-type selectivity. Typical applications can be found in transalkylation reactions.[66]

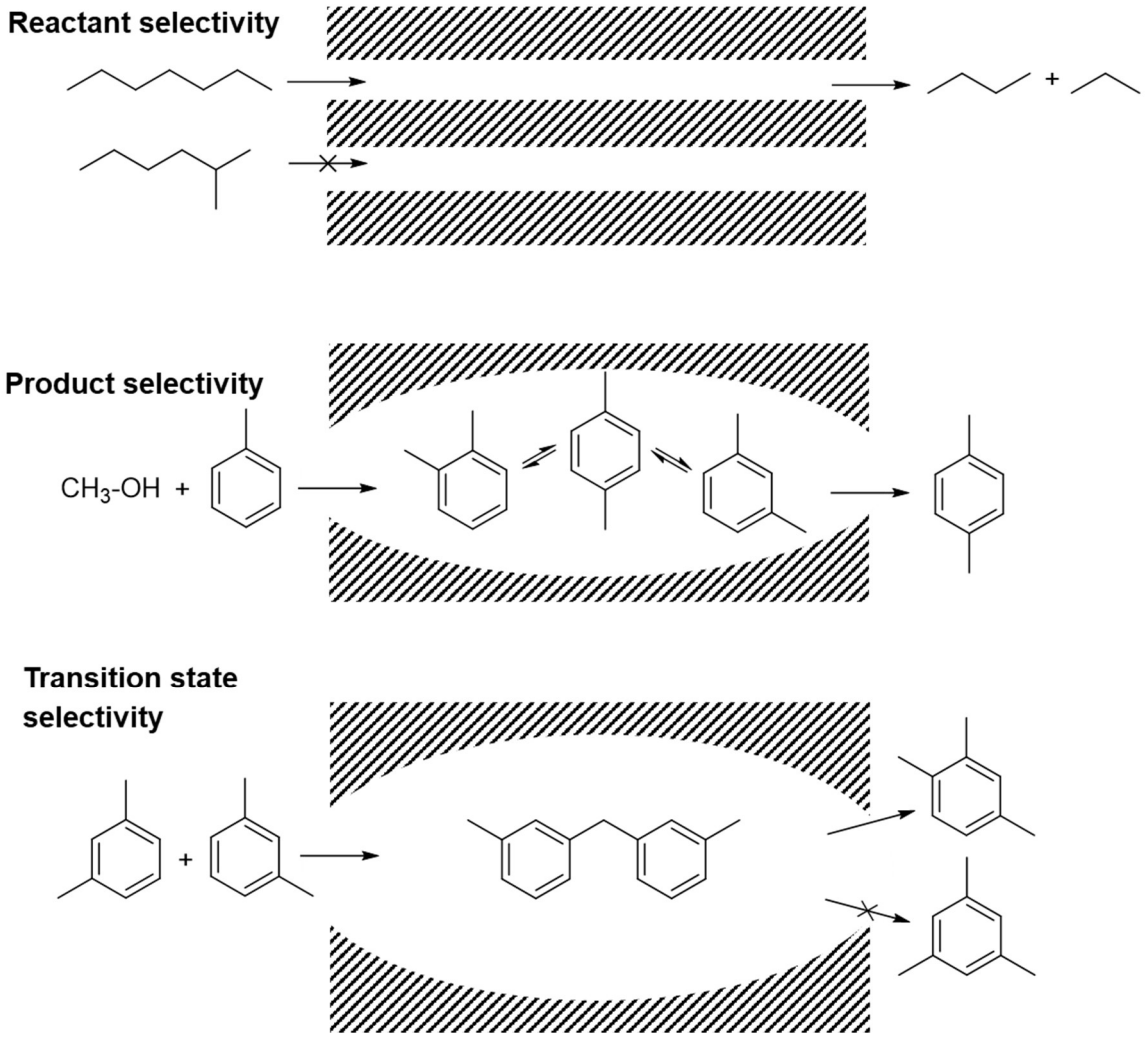

Figure 1.6: Illustration of three different shape selectivities in zeolite pores (adapted from ref. [63]).

1.3.2 Acidity in zeolites

As mentioned above, zeolites with SiO_4 and AlO_4 BBU contain BAS and LAS, depending on the ion which compensates for the lattice charge.[67] This makes these materials very attractive as bifunctional catalysts. In case that a proton is attached to

the bridging oxygen atom, a BAS is generated as [Si-OH-Al].[68] Scheme 1.1 shows such bridging hydroxyl groups (BAS). LAS are present when Al is in an extra framework position – so-called extra framework Al (EFAL). Another possibility of LAS is that a Si from the zeolite framework gets exchanged by another metal such as, *e.g.* Ti^{4+} or Zr^{4+}.[69-70] And the third description of LAS can be if the counter-balancing ions of Al and Si tetrahedra are metals such as, *e.g.* Cu^{2+}, $Co^{2+,}$ or Zn^{2+}. These different options of LAS in a zeolite are also shown in Scheme 1.1.

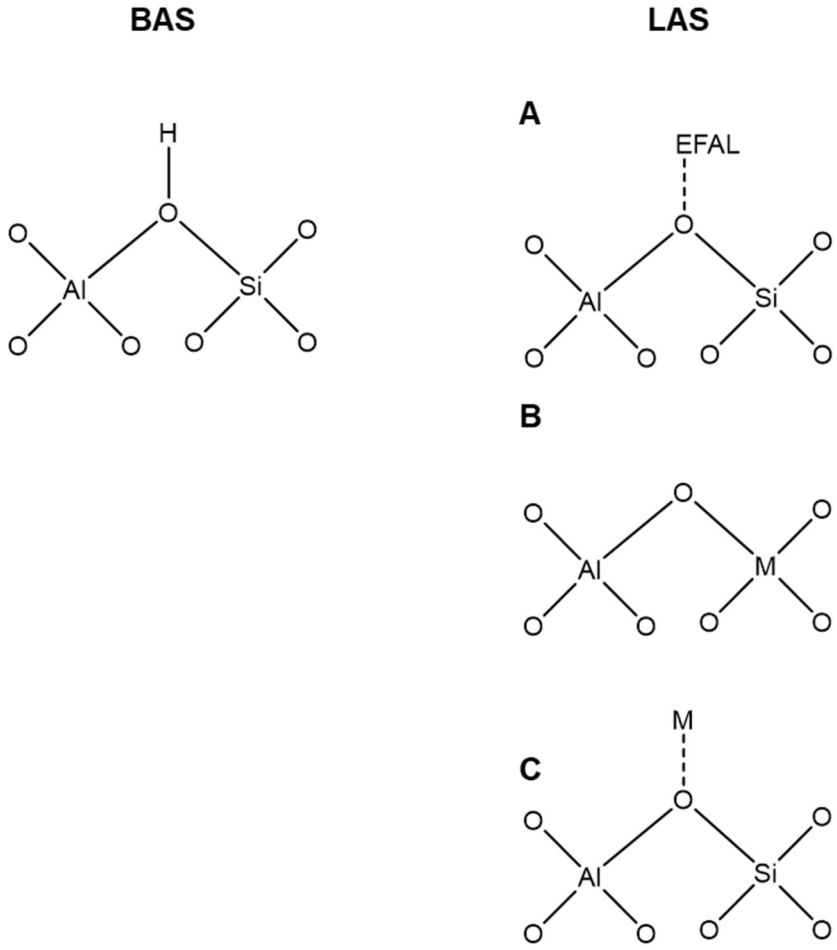

Scheme 1.1: BAS and LAS within a zeolite generated from **A** EFAL, **B** isomorphic substitution of Si by a metal, and **C** metal cation (adapted from ref. [71]). M = metal, in **B** *e.g.* Zr, Sn, Ti; in **C** *e.g.* Co, Cu, Zn.

Mostly, EFAL is formed during post-synthesis either by contact with mild acids during ion exchange or calcination or steaming. Besides this, EFAL can already be formed during the synthesis of the zeolite framework. In the post-synthesis, the cations such

as Na^+ or NH_4^+ interacting with the tetrahedrally coordinated Si and Al framework can be replaced by H_3O^+ ions.[60, 70, 72] The water molecule then competes with the framework oxygen atom for the proton, and the structure can then break down.[73] Thus, the Al can be removed from the framework and form several different species such as $Al(OH)^{2+}$, $Al(OH)_2^+$, and $Al(OH)_3$. [60, 70, 72] This dealumination generating EFAL is more likely at a low Si/Al ratio due to the thermodynamic instability of the framework. EFAL can act as LAS and influence the catalyst's performance in some reactions.[74]

The second type of LAS (Scheme 1.1 B) are generated by introducing heteroatoms, such as Zr, Sn, or Ti into the framework.[70] This incorporation can either be done isomorph during hydrothermal synthesis or post-synthesis by exchanging a T-atom via acid treatment or impregnation. Such LAS are active, *e.g.*, for isomerization, oxidation, and epoxidation.[75-77]

The most designed type of LAS for heterogeneous catalysis is the exchange of the lattice charge compensating cation NH_4^+ or H^+ (BAS) primarily by univalent and bivalent metals (Scheme 1.1 C). In the case of divalent ions such as Cu^{2+}, Co^{2+}, or Zn^{2+} two Al in proximity are required for stabilization. The capability of ion exchange depends on the Al content. There are different methods for this post-synthetic introduction of most transition metals: i) solid-state ion exchange, ii) sublimation of metal chlorides in the gas phase, iii) impregnation and iv) liquid phase ion exchange.[60, 78-80] This study will be focused on liquid phase ion exchange with divalent Co^{2+} ions. More details can be found in the experimental part.

Divalent metals, to which Co^{2+} belongs, need two $[AlO_4]$ tetrahedra to compensate for the charge in the ion exchange. One schematic example is shown in Scheme 1.2.

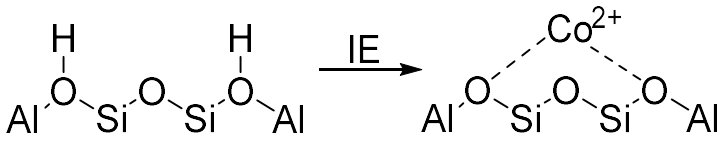

Scheme 1.2 Structure of two BAS exchanged by one Co^{2+} ion.

Other Co species in ZSM-5 can be Co-OH exchanged on one BAS, Co-oxide clusters with Co^{2+} and Co^{3+} inside the zeolite channel, or at the external surface area primarily as bulk CoO or Co_3O_4. Single Co^{2+} species can be built by liquid ion exchange, while Co oxides are mainly generated by impregnation caused by an over-exchange.

As per the definition of Löwenstein's rule, the presence of Al–O–Al connections is prohibited, but two BAS needs to be nearby to stabilize Co^{2+} ions.[81] Therefore, the Al distribution guides the Cobalt location in the zeolite. Al-O-$(Si\text{-}O)_n$-Al sequence with $n \leq 2$ – so-called Al pairs - favor coordination of Co^{2+}, while unpaired Al sites - Al-O-$(Si\text{-}O)_n$-Al with $n > 2$ - can only stabilize a divalent ion if the Al-OH still faces into the same channel, so that the sites are "visible" for each other. [82-84] If the Al sites are too far, they are called isolated sites.[82-84] The possibilities of Al distribution and Co sites within a ZSM-5 are discussed in 1.3.3.

Besides the structure and the Al distribution, the Co precursor can also affect the distribution and nature of Co sites. In an aqueous solution of organic precursors such as cobalt acetate, Co particles are known to disperse very uniformly, while using nitrate salts as a precursor, Co particles are less dispersed.[85-87] However, it has been reported that Co nitrate predominantly exchanges in well-defined Al pairs, while Co acetate tends easier to lead to over exchanged materials - meaning to build also oxide-like clusters with non-octahedral symmetry- at relatively high Co contents.[82, 84] The origin from the different behavior building hexa-aqua-complexes depends on the pH during synthesis (octahedral or non-octahedral).[84]

1.3.3 ZSM-5 – benefits of its structure

The framework of the zeolite influences the properties and, therefore, its activity as a catalyst, controlled mainly by the pore size and acidity. The MFI type zeolites consist of pentasil secondary building units (SBU) forming chains, which are ordered to create three-dimensional 10 MR straight channels (5.3 × 5.6 Å) and sinusoidal channels (5.1 × 5.5 Å).[88] **Figure 1.7** and **Figure 1.8** show images of the framework units and the three-dimensional structure. The intersection of these two 10 MR

channels can accommodate a sphere diameter of 6.36 Å, compared to 4.7 Å in the main channel and 4.5 Å inside the sinusoidal channel.[89]

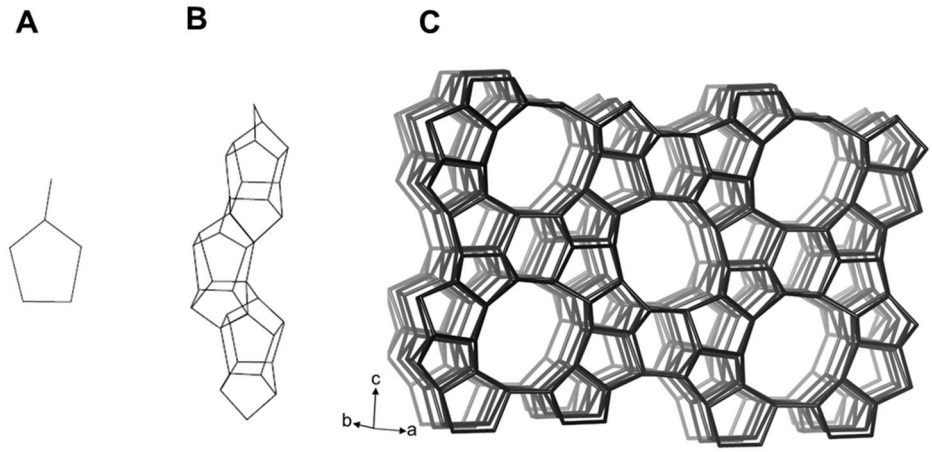

Figure 1.7: The framework structure of MFI: A) Type 5-1 SBUs, B) pentasil chains C) 3D MFI structure. [58]

As mentioned in 1.3.1, the cation distribution depends on the Al location within the zeolite structure. The location of Al is affected by several factors during the hydrothermal synthesis such as the sequence of mixing and the ratio of the precursors, the Si and Al source, structure-directing agents, the temperature, and time - to name only a few. [83, 90-93]

To get more information about the Al sites within the zeolite framework, it needs to be distinguished from EFAL. One possibility is via ^{27}Al MAS NMR. Here, tetra-coordinated Al resonates between 70 and 40 ppm, while hexa-coordinated EFAL can be found from +10 to −20 ppm.[94-95] Furthermore, infrared spectroscopy can differentiate different hydroxyl groups. A band around 3660-3665 cm^{-1} gives evidence about EFAL. In contrast, the band for Al-OH-Si groups appears at 3610 cm^{-1}.[94, 96] When combined this ratio of tetra-coordinated Al and hexa-coordinated EFAL with elemental analysis, one can determine the Al content present according to its coordination within ZSM-5.

Next, the location of Al sites can be determined. One method is to test the ability to exchange Co^{2+} or Cu^{2+}.[83, 97] Knowing that two BAS in proximity are needed to exchange one divalent ion, the number of paired sites can be calculated. Moreover, several studies reported to determine the Al location by the Co^{2+} position within the

ZSM-5 structure.[90, 97-98] Co^{2+} ions in ZSM-5 have been assigned to different positions according to its parallels to MOR structures: α-, β-, and γ – sites. [82, 97-98] **Figure 1.8A** shows the location of these sites within the ZSM-5 channels. Co^{2+} ions in the straight channel represent the α-site, Co^{2+} in the intersection of the main channel and sinusoidal channel are in β- sites, and Co exchanged in the sinusoidal channel are located in γ sites.[98] The detailed structures of the α-, β-, and γ – sites are also shown in **Figure 1.8B**. Co^{2+} in α position is coordinated to the rectangle of four framework oxygen atoms of the channel wall. Moreover, an extended six-membered ring is formed by two folded 5-MR.[98] Co^{2+} located in β –sites are coordinated to a twisted 6-MR connected to another 6-MR forming a wall in the intersection of the straight and sinusoidal channels.[98] And in γ – sites, the Co^{2+} ions are in a boat-shaped 6-MR ring accessible only through the sinusoidal channel.

Different bands in diffuse reflectance UV-Vis spectroscopy can differentiate these sites. A single band at 15100 cm^{-1} represents Co^{2+} at α position, four bands at 16000, 17150, 18600 and 21200 cm^{-1} represent Co^{2+} in β position, and two bands at 20100 and 22000 cm^{-1} represent Co^{2+} at γ position. [82, 97-98]

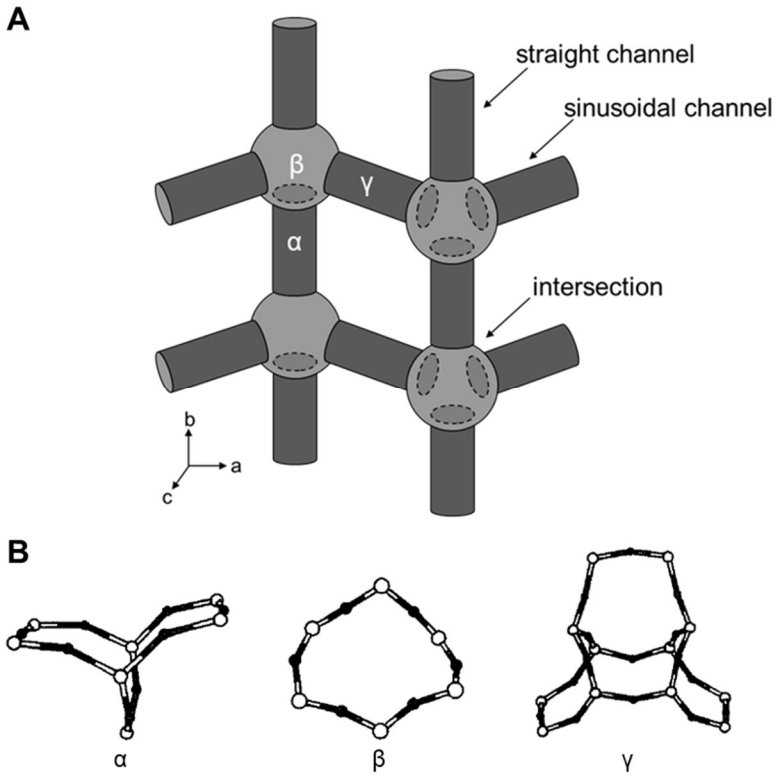

Figure 1.8: A) Schematic illustration of the MFI framework with straight and sinusoidal channel including α-, β-, and γ − site positions, and B) framework structures of the α-, β-, and γ - sites (adapted from ref. [58] and [82]).

The zeolite used in this thesis is a commercially available ZSM-5 with a Si/Al of 15 (manufactured by Zeolyst). It has 96 T atoms and 6 Al per unit cell.[99] According to literature, ~55% of all framework Al atoms are located in the intersection of the straight channel and sinusoidal channel.[89]

1.3.4 Sorption properties of zeolites

One established way to characterize the surface sites of zeolites and get more insight into molecule surface interactions is to adsorb probe molecules followed by IR spectroscopically or gravimetric measurements.

Adsorption is a binding interaction between an adsorbate - a molecule from the gas or liquid phase, and an adsorbent – a solid surface.[100] One differentiates between physisorption and chemisorption: physisorbed molecules are weakly non-specific bonded to a surface via, *e.g.*, van-der-Waals forces, while chemisorbed molecules are firmly held on the surface by site-specific chemical bonds.[101]

Irving Langmuir established the most commonly applied theory for adsorption in 1916 about the adsorption behavior of gases on metal surfaces.[100] In this Langmuir isotherm model, the central postulations are:

i) only one adsorbate can adsorb on one sorption site,

ii) adsorption as well as desorption is independent of the surface coverage and is homiletically presumable through all adsorption sites,

iii) a monolayer of adsorbates covers the surface of the adsorbent,

iv) there are no molecule-molecule interactions.

v) the heat of adsorption is independent of the surface coverage.[102-103]

In Langmuir isotherms, the adsorption is always in equilibrium with the desorption of molecules. Hence, their rate constants k_{ads} and k_{des} are equal:[103]

$$A_g + * \underset{k_{des}}{\overset{k_{ads}}{\rightleftharpoons}} A^* \qquad 1.5$$

A typical Langmuir isotherm is shown in **Figure 1.9**. The coverage is defined as follows:

$$\theta_A = \frac{K_A\, p_A}{1 + K_A\, p_A} \qquad 1.6$$

With the coverage of adsorbate A $\boldsymbol{\theta_A}$, the equilibrium constant of adsorbate A $\boldsymbol{K_A}$, and the partial pressure of adsorbate A $\boldsymbol{p_A}$.

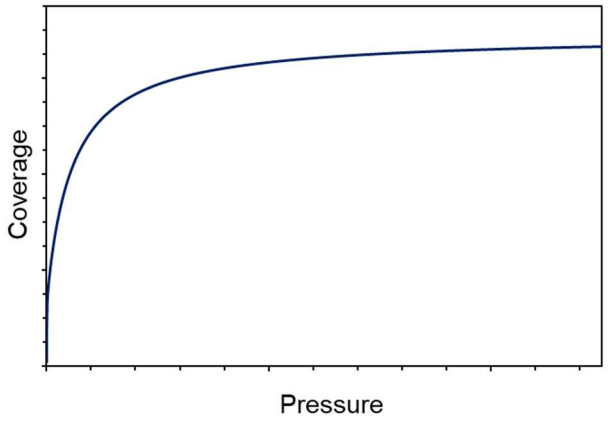

Figure 1.9: Coverage as a function of partial pressure at a constant temperature.

1.3.5 Characteristics of zeolites as catalysts in heterogeneous catalysis

To utilize metal supported zeolites as heterogeneous catalysts, they must first be prepared and activated. This happens within four steps:[61]

i) Interaction between zeolite and precursor (*e.g.* impregnation)

ii) Drying of the material

iii) Calcination

iv) Reduction

The interaction between zeolite and precursor can be used to introduce metal ions by aqueous ion exchange. During the material drying step, the water will be removed without the decomposition of the precursor. The structure of the precursor is transferred into an oxide site by calcination. And the last step, in many applications, is the activation of the metal by reduction.[103]

After these steps, a metal-supported catalyst is formed. **Figure 1.10** shows the interaction of several factors. Only if these are balanced, a successful system is built. A catalyst is considered a suitable one if it leads to high conversion, high yields, and high selectivity towards desired products. This can only happen if active sites with suitable acidity have been synthesized. There, also the part of stability and structure plays a role. In order to reach high conversion, parameters such as pressure and

temperatures must be optimized which is, only possible if the material is stable enough to stand such demanding conditions. Moreover, the zeolite structure influences product formation significantly (see 1.3.1). In most cases, a balance is maintained between high conversion rates and selectivity depending on the product.

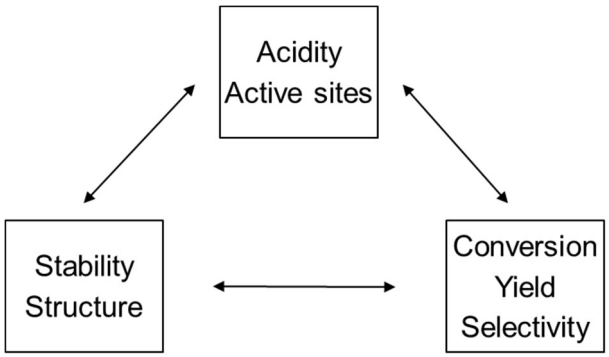

Figure 1.10: Interaction of different characteristics of a catalyst.

Once a fruitful process was finally reached, deactivation might also play an important role. Active sites of catalysts can either be blocked or changed. This can happen by the formation of coke or organics by undesirable products, which might block active sites or pores, or active sites are modified by reduction/oxidation or migration.[60] The topic of deactivation will not be further discussed in this thesis.

1.4 Scope of the thesis

This project aims to activate CH_4 and integrate it directly into crude oil as an alternative strategy to valorize the energy stored in the molecule. This study focuses on benzene as a model molecule to test direct methylation of aromatics. **Scheme 1.3** shows the reaction scheme of that direct methylation of benzene.

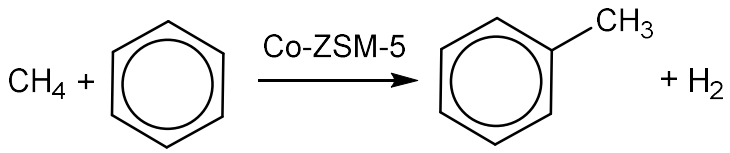

Scheme 1.3: Reaction scheme of direct benzene methylation towards toluene and hydrogen using Co-ZSM-5 as the catalyst.

The first chapter of this thesis introduces the problem with flaring CH_4 and a way how to turn CH_4 into values. In most cases, CH_4 is used for the production of synthesis gas or the oxidization to methanol. Moreover, zeolites, which are often used for C-H activation, are introduced. In particular, Co supported on ZSM-5 is a highly active catalyst for such reactions and therefore considered more in detail.

The second chapter presents the most common procedures and methods used for this study.

Then, in the first stage, a reaction scheme of the reaction of methane and benzene is elucidated. Furthermore, the product distribution, including secondary products and products from side reactions, is described. With the help of various kinetic measurements, the mechanism for the direct methylation of benzene is enlightened.

The last stage considered within this thesis, in particular, is the nature of active sites catalyzing the direct methylation of benzene. The specific role of their distribution is considered more closely.

Therefore, the scope of this thesis is to understand the elementary reaction steps in benzene methylation.

1.5 References

1. Schleussner, C.-F.; Rogelj, J.; Schaeffer, M.; Lissner, T.; Licker, R.; Fischer, E. M.; Knutti, R.; Levermann, A.; Frieler, K.; Hare, W., Science and policy characteristics of the Paris Agreement temperature goal. *Nature Climate Change* **2016,** *6* (9), 827-835.

2. Minx, J. C.; Lamb, W. F.; Andrew, R. M.; Canadell, J. G.; Crippa, M.; Döbbeling, N.; Forster, P. M.; Guizzardi, D.; Olivier, J.; Peters, G. P.; Pongratz, J.; Reisinger, A.; Rigby, M.; Saunois, M.; Smith, S. J.; Solazzo, E.; Tian, H., A comprehensive dataset for global, regional and national greenhouse gas emissions by sector 1970–2019. *Earth Syst. Sci. Data Discuss.* **2021,** *2021*, 1-63.

3. Emam, E. A., Gas flaring in industry: an overview. *Petroleum & coal* **2015,** *57* (5).

4. Caballero, A.; Pérez, P. J., Methane as raw material in synthetic chemistry: the final frontier. *Chemical Society Reviews* **2013,** *42* (23), 8809-8820.

5. Lunsford, J. H., Catalytic conversion of methane to more useful chemicals and fuels: a challenge for the 21st century. *Catalysis Today* **2000,** *63* (2), 165-174.

6. Mansoor, R.; Tahir, M., Recent Developments in Natural Gas Flaring Reduction and Reformation to Energy-Efficient Fuels: A Review. *Energy & Fuels* **2021,** *35* (5), 3675-3714.

7. currahee_shutter, *stock.adobe.com*.

8. Ritchie, H.; Rose, M., CO_2 and Greenhouse Gas Emission. *Our World in Data* **2020**.

9. Elvidge, C. D.; Bazilian, M. D.; Zhizhin, M.; Ghosh, T.; Baugh, K.; Hsu, F.-C., The potential role of natural gas flaring in meeting greenhouse gas mitigation targets. *Energy Strategy Reviews* **2018,** *20*, 156-162.

10. Horn, R.; Schlögl, R., Methane Activation by Heterogeneous Catalysis. *Catalysis Letters* **2015,** *145* (1), 23-39.

11. Spivey, J. J.; Hutchings, G., Catalytic aromatization of methane. *Chemical Society Reviews* **2014,** *43* (3), 792-803.

12. Taifan, W.; Baltrusaitis, J., CH 4 conversion to value added products: Potential, limitations and extensions of a single step heterogeneous catalysis. *Applied Catalysis B: Environmental* **2016,** *198*, 525-547.

13. Abd, A. A.; Naji, S. Z.; Hashim, A. S., Effects of non-hydrocarbons impurities on the typical natural gas mixture flows through a pipeline. *Journal of Natural Gas Science and Engineering* **2020,** *76*, 103218.

14. Gaedicke, C.; Franke, D.; Ladage, S.; Lutz, R.; Pein, M.; Rebscher, D.; Schauer, M.; Schmidt, S.; Goerne, G., Daten und Entwicklungen der deutschen und globalen Energieversorgung. In ***Bundesanstalt für Geowissenschaften und Rohstoffe (BGR)***, Hannover, 2018.

15. U., S. Energy Information Administration, Monthly Energy Review, DOE/EIA-0035(2021/11) Nov 2021.

16. Pinaeva, L.; Noskov, A.; Parmon, V., Prospects for the direct catalytic conversion of methane into useful chemical products. *Catalysis in Industry* **2017,** *9* (4), 283-298.

17. Abdulrasheed, A.; Jalil, A. A.; Gambo, Y.; Ibrahim, M.; Hambali, H. U.; Hamid, M. Y. S., A review on catalyst development for dry reforming of methane to syngas: Recent advances. *Renewable and Sustainable Energy Reviews* **2019,** *108*, 175-193.

18. Challiwala, M. S.; Ghouri, M. M.; Linke, P.; El-Halwagi, M. M.; Elbashir, N. O., A combined thermo-kinetic analysis of various methane reforming technologies: Comparison with dry reforming. *Journal of CO2 Utilization* **2017,** *17*, 99-111.

19. Fiedler, E.; Grossmann, G.; Kersebohm, D. B.; Weiss, G.; Witte, C., Methanol. *Ullmann's encyclopedia of industrial chemistry* **2000**.

20. Fernández, L., GlobalData: Statista - The Statistics Portal; URL: https://www.statista.com/statistics/1065891/global-methanol-production-capacity/, 2021.

21. Baerns, M.; Behr, A.; Brehm, A.; Gmehling, J.; Hofmann, H.; Onken, U., *Technische chemie*. John Wiley & Sons: 2013.

22. Olivos-Suarez, A. I.; Szecsenyi, A.; Hensen, E. J.; Ruiz-Martinez, J.; Pidko, E. A.; Gascon, J., Strategies for the direct catalytic valorization of methane using heterogeneous catalysis: challenges and opportunities. *Acs Catalysis* **2016,** *6* (5), 2965-2981.

23. Huang, K.; Maravelias, C. T., Synthesis and analysis of nonoxidative methane aromatization strategies. *Energy Technology* **2020,** *8* (8), 1900650.

24. Kondratenko, E. V.; Peppel, T.; Seeburg, D.; Kondratenko, V. A.; Kalevaru, N.; Martin, A.; Wohlrab, S., Methane conversion into different hydrocarbons or oxygenates: current status and future perspectives in catalyst development and reactor operation. *Catalysis Science & Technology* **2017,** *7* (2), 366-381.

25. Kondratenko, E. V.; Rodemerck, U., Recent Progress in Oxidative Conversion of Methane to Value-Added Products. *Perovskites and Related Mixed Oxides* **2016**, 517-538.

26. Anggoro, D.; Chamdani, F.; Buchori, L. In *One step catalytic oxidation process of methane to methanol at low reaction temperature: A Brief Review*, IOP Conference Series: Materials Science and Engineering, IOP Publishing: 2021; p 012056.

27. Lukyanov, D. B.; Vazhnova, T., Selective and stable benzene alkylation with methane into toluene over PtH-MFI bifunctional catalyst. *Journal of Molecular Catalysis A: Chemical* **2009,** *305* (1-2), 95-99.

28. Wang, X.; Xu, J.; Qi, G.; Li, B.; Wang, C.; Deng, F., Alkylation of Benzene with Methane over ZnZSM-5 Zeolites Studied with Solid-State NMR Spectroscopy. *The Journal of Physical Chemistry C* **2013,** *117* (8), 4018-4023.

29. Matsubara, H.; Yamamoto, K.; Tsuji, E.; Okumura, K.; Nakamura, K.; Suganuma, S.; Katada, N., Position and Lewis acidic property of active cobalt species on MFI zeolite for catalytic methylation of benzene with methane. *Microporous and Mesoporous Materials* **2021,** *310*.

30. Xu, Y.; Chen, M.; Wang, T.; Liu, B.; Jiang, F.; Liu, X., Probing cobalt localization on HZSM-5 for efficient methane dehydroaromatization catalysts. *Journal of Catalysis* **2020,** *387*, 102-118.

31. Xu, J.; Zheng, A.; Wang, X.; Qi, G.; Su, J.; Du, J.; Gan, Z.; Wu, J.; Wang, W.; Deng, F., Room temperature activation of methane over Zn modified H-ZSM-5 zeolites: Insight from solid-state NMR and theoretical calculations. *Chemical Science* **2012,** *3* (10).

32. Cowan, A. D.; Dumpelmann, R.; Cant, N. W., The rate-determining step in the selective reduction of nitric-oxide by methane over a Co-ZSM5 catalyst in the presence of oxygen. *Journal of Catalysis* **1995,** *151* (2), 356-363.

33. Kiani, D.; Sourav, S.; Tang, Y.; Baltrusaitis, J.; Wachs, I. E., Methane activation by ZSM-5-supported transition metal centers. *Chemical Society Reviews* **2021,** *50* (2), 1251-1268.

34. Wang, L.; Tao, L.; Xie, M.; Xu, G.; Huang, J.; Xu, Y., Dehydrogenation and aromatization of methane under non-oxidizing conditions. *Catalysis Letters* **1993,** *21* (1), 35-41.

35. Luzgin, M. V.; Rogov, V. A.; Arzumanov, S. S.; Toktarev, A. V.; Stepanov, A. G.; Parmon, V. N., Understanding methane aromatization on a Zn-modified high-silica zeolite. *Angew Chem Int Ed Engl* **2008,** *47* (24), 4559-62.

36. Liu, B. S.; Zhang, Y.; Liu, J. F.; Tian, M.; Zhang, F. M.; Au, C. T.; Cheung, A. S. C., Characteristic and Mechanism of Methane Dehydroaromatization over Zn-Based/HZSM-5 Catalysts under Conditions of Atmospheric Pressure and Supersonic Jet Expansion. *The Journal of Physical Chemistry C* **2011,** *115* (34), 16954-16962.

37. Sun, K.; Ginosar, D. M.; He, T.; Zhang, Y.; Fan, M.; Chen, R., Progress in Nonoxidative Dehydroaromatization of Methane in the Last 6 Years. *Industrial & Engineering Chemistry Research* **2018,** *57* (6), 1768-1789.

38. Gabrienko, A. A.; Yashnik, S. A.; Kolganov, A. A.; Sheveleva, A. M.; Arzumanov, S. S.; Fedin, M. V.; Tuna, F.; Stepanov, A. G., Methane Activation on H-ZSM-5 Zeolite with Low Copper Loading. The Nature of Active Sites and Intermediates Identified with the Combination of Spectroscopic Methods. *Inorg Chem* **2020,** *59* (3), 2037-2050.

39. He, P.; Wang, A.; Meng, S.; Bernard, G. M.; Liu, L.; Michaelis, V. K.; Song, H., Impact of Al sites on the methane co-aromatization with alkanes over Zn/HZSM-5. *Catalysis Today* **2019,** *323*, 94-104.

40. Kennedy, E. M.; Lonyi, F.; Ballinger, T. H.; Rosynek, M. P.; Lunsford, J. H., Conversion of benzene to substituted aromatic products over zeolite catalysts at elevated pressures. *Energy & fuels* **1994,** *8* (4), 846-850.

41. Adebajo, M.; Long, M. A.; Howe, R. F., Methane activation over zeolite catalysts: The methylation of benzene. *Research on Chemical Intermediates* **2000,** *26* (2), 185-191.

42. Adebajo, M. O., Green chemistry perspectives of methane conversion via oxidative methylation of aromatics over zeolite catalysts. *Green Chemistry* **2007,** *9* (6).

43. He, S. J.; Long, M. A.; Wilson, M. A.; Gorbaty, M. L.; Maa, P. S., Methylation of Benzene by Methane-13C over Zeolitic Catalysts at 400. degree. C. *Energy & fuels* **1995,** *9* (4), 616-619.

44. Gabrienko, A. A.; Arzumanov, S. S.; Moroz, I. B.; Toktarev, A. V.; Wang, W.; Stepanov, A. G., Methane Activation and Transformation on Ag/H-ZSM-5 Zeolite Studied with Solid-State NMR. *The Journal of Physical Chemistry C* **2013,** *117* (15), 7690-7702.

45. Perego, C.; Pollesel, P., Advances in aromatics processing using zeolite catalysts. *Advances in Nanoporous Materials* **2010,** *1*, 97-149.

46. Speight, J.; Özüm, B., Hydrotreating. *Petroleum refining processes. New York: Marcel Dekker Inc* **2002**, 472-519.

47. Yushkin, A. A.; Anokhina, T. S.; Bazhenov, S. D.; Borisov, I. L.; Budd, P. M.; Volkov, A. V., Sorption and Nanofiltration Characteristics of PIM-1 Material in Polar and Non-Polar Solvents. *Petroleum Chemistry* **2018,** *58* (13), 1154-1158.

48. Ellouh, M.; Qureshi, Z. S.; Aitani, A.; Akhtar, M. N.; Jin, Y.; Koseoglu, O.; Alasiri, H., Light Paraffinic Naphtha to BTX Aromatics over Metal-Modified Pt/ZSM-5. *ChemistrySelect* **2020,** *5* (44), 13807-13813.

49. Fahim, M. A.; Al-Sahhaf, T. A.; Elkilani, A., *Fundamentals of petroleum refining*. Elsevier: 2009.

50. Sekine, Y.; Higo, T., Recent Trends on the Dehydrogenation Catalysis of Liquid Organic Hydrogen Carrier (LOHC): A Review. *Topics in Catalysis* **2021**, 1-11.

51. Wunsch, A.; Berg, T.; Pfeifer, P., Hydrogen Production from the LOHC Perhydro-Dibenzyl-Toluene and Purification Using a 5 μm PdAg-Membrane in a Coupled Microstructured System. *Materials* **2020,** *13* (2), 277.

52. Rao, P. C.; Yoon, M., Potential Liquid-Organic Hydrogen Carrier (LOHC) Systems: A Review on Recent Progress. *Energies* **2020,** *13* (22).

53. Niermann, M.; Beckendorff, A.; Kaltschmitt, M.; Bonhoff, K., Liquid Organic Hydrogen Carrier (LOHC)–Assessment based on chemical and economic properties. *International Journal of Hydrogen Energy* **2019,** *44* (13), 6631-6654.

54. Teichmann, D.; Arlt, W.; Wasserscheid, P.; Freymann, R., A future energy supply based on Liquid Organic Hydrogen Carriers (LOHC). *Energy & Environmental Science* **2011,** *4* (8), 2767-2773.

55. Brückner, N.; Obesser, K.; Bösmann, A.; Teichmann, D.; Arlt, W.; Dungs, J.; Wasserscheid, P., Evaluation of Industrially applied heat-transfer fluids as liquid organic hydrogen carrier systems. *ChemSusChem* **2014,** *7* (1), 229-235.

56. Coq, B.; Gourves, V.; Figuéras, F., Benzylation of toluene by benzyl chloride over protonic zeolites. *Applied Catalysis A: General* **1993,** *100* (1), 69-75.

57. Lipper, K. A.; Löser, E.; Brücher, O., Benzyl Chloride and other Side-Chain Chlorinated Aromatic Hydrocarbons. *Ullmann's Encyclopedia of Industrial Chemistry* **2000**, 367-384.

58. Baerlocher, C.; McCusker, L. B. Database of Zeolite Structures. http://www.iza-structure.org/databases/.

59. Cronstedt, A., Observation and description of an unknown kind of rock to be named zeolites. *Kongl Vetenskaps Acad Handl Stockh* **1756,** *17*, 120-123.

60. Weitkamp, J.; Puppe, L., *Catalysis and zeolites: fundamentals and applications*. Springer Science & Business Media: 2013.

61. Cejka, J.; Corma, A.; Zones, S., *Zeolites and catalysis: synthesis, reactions and applications*. John Wiley & Sons: 2010.

62. Pergher, S. B. C.; Vinaches, P.; Gusmão, K. B., An introduction to zeolite synthesis using imidazolium-based cations as organic structure-directing agents. **2017**.

63. Csicsery, S. M., Shape-selective catalysis in zeolites. *Zeolites* **1984,** *4* (3), 202-213.

64. Mirth, G.; Lercher, J. A., On the role of product isomerization for shape selective toluene methylation over HZSM5. *Journal of catalysis* **1994,** *147* (1), 199-206.

65. Klemm, E.; Emig, G., A method for the determination of diffusion coefficients in product-shape-selective catalysis on zeolites under reaction conditions. *Chemical engineering science* **1997,** *52* (23), 4329-4344.

66. Derouane, E. G., New Aspects of Molecular Shape-Selectivity: Catalysis by Zeolite ZSM - 5. In *Studies in Surface Science and Catalysis*, Imelik, B.; Naccache, C.; Taarit, Y. B.; Vedrine, J. C.; Coudurier, G.; Praliaud, H., Eds. Elsevier: 1980; Vol. 5, pp 5-18.

67. Niwa, M.; Katada, N.; Okumura, K., *Characterization and design of zeolite catalysts: solid acidity, shape selectivity and loading properties*. Springer Science & Business Media: 2010; Vol. 141.

68. Hadjiivanov, K., Chapter Two - Identification and Characterization of Surface Hydroxyl Groups by Infrared Spectroscopy. In *Advances in Catalysis*, Jentoft, F. C., Ed. Academic Press: 2014; Vol. 57, pp 99-318.

69. Rahimi, N.; Karimzadeh, R., Catalytic cracking of hydrocarbons over modified ZSM-5 zeolites to produce light olefins: A review. *Applied Catalysis A: General* **2011,** *398* (1-2), 1-17.

70. Ravi, M.; Sushkevich, V. L.; van Bokhoven, J. A., Towards a better understanding of Lewis acidic aluminium in zeolites. *Nature Materials* **2020,** *19* (10), 1047-1056.

71. Zhao, X.; Xu, J.; Deng, F., Solid-state NMR for metal-containing zeolites: From active sites to reaction mechanism. *Frontiers of Chemical Science and Engineering* **2020,** *14*.

72. Primo, A.; Garcia, H., Zeolites as catalysts in oil refining. *Chemical Society Reviews* **2014,** *43* (22), 7548-7561.

73. Fyfe, C.; Gobbi, G.; Kennedy, G., Investigation of the dealumination of zeolite ZSM-5 by solid-state magic-angle spinning NMR. *Chemistry Letters* **1983,** *12* (10), 1551-1554.

74. Zhang, Y.; Zhao, R.; Sanchez-Sanchez, M.; Haller, G. L.; Hu, J.; Bermejo-Deval, R.; Liu, Y.; Lercher, J. A., Promotion of protolytic pentane conversion on H-MFI zeolite by proximity of extra-framework aluminum oxide and Brønsted acid sites. *Journal of Catalysis* **2019,** *370*, 424-433.

75. Cavani, F.; Teles, J. H., Sustainability in Catalytic Oxidation: An Alternative Approach or a Structural Evolution? *ChemSusChem* **2009,** *2* (6), 508-534.

76. Aigner, M.; Grosso-Giordano, N. A.; Okrut, A.; Zones, S.; Katz, A., Epoxidation of 1-octene under harsh tail-end conditions in a flow reactor I: a comparative study of crystalline vs. amorphous catalysts. *Reaction Chemistry & Engineering* **2017,** *2* (6), 842-851.

77. Hammond, C.; Conrad, S.; Hermans, I., Simple and scalable preparation of highly active lewis acidic Sn-β. *Angewandte Chemie International Edition* **2012,** *51* (47), 11736-11739.

78. Inui, T., Zeolite today. Part 6.; Progress of zeolite catalysts for hydrocarbon synthesis. Zeolite no konnichi. 6.; Tanka suiso gosei shokubai to shite no zeolite no shinpo. *Petrotech (Tokyo);(Japan)* **1993,** *16* (5).

79. Karge, H. G., Solid-state reactions of zeolites. In *Studies in Surface Science and Catalysis*, Elsevier: 1994; Vol. 83, pp 135-146.

80. Pierella, L. B.; Saux, C.; Caglieri, S. C.; Bertorello, H. R.; Bercoff, P. G., Catalytic activity and magnetic properties of Co–ZSM-5 zeolites prepared by different methods. *Applied Catalysis A: General* **2008,** *347* (1), 55-61.

81. Rice, M. J.; Chakraborty, A. K.; Bell, A. T., Site Availability and Competitive Siting of Divalent Metal Cations in ZSM-5. *Journal of Catalysis* **2000,** *194* (2), 278-285.

82. Dědeček, J.; Sobalík, Z.; Wichterlová, B., Siting and distribution of framework aluminium atoms in silicon-rich zeolites and impact on catalysis. *Catalysis Reviews* **2012,** *54* (2), 135-223.

83. Dědeček, J.; Kaucký, D.; Wichterlová, B., Al distribution in ZSM-5 zeolites: An experimental study. *Chemical Communications* **2001,** (11), 970-971.

84. Dědeček, J.; Kaucký, D.; Wichterlová, B.; Gonsiorová, O., Co2+ions as probes of Al distribution in the framework of zeolites. ZSM-5 study. *Phys. Chem. Chem. Phys.* **2002,** *4* (21), 5406-5413.

85. Panpranot, J.; Kaewkun, S.; Praserthdam, P.; Goodwin, J. G., Effect of Cobalt Precursors on the Dispersion of Cobalt on MCM-41. *Catalysis Letters* **2003,** *91* (1), 95-102.

86. van de Loosdrecht, J.; van der Haar, M.; van der Kraan, A. M.; van Dillen, A. J.; Geus, J. W., Preparation and properties of supported cobalt catalysts for Fischer-Tropsch synthesis. *Applied Catalysis A: General* **1997,** *150* (2), 365-376.

87. Martins, L.; Peguin, R. P. S.; Urquiet-González, E. A., Cu and Co exchanged ZSM-5 zeolites: activity towards no reduction and hydrocarbon oxidation. *Quimica Nova* **2006,** *29*, 223-229.

88. Newsam, J. M., The Zeolite Cage Structure. *Science* **1986,** *231* (4742), 1093-1099.

89. Pashkova, V.; Sklenak, S.; Klein, P.; Urbanova, M.; Dědeček, J., Location of Framework Al Atoms in the Channels of ZSM-5: Effect of the (Hydrothermal) Synthesis. *Chemistry–A European Journal* **2016,** *22* (12), 3937-3941.

90. Dedecek, J.; Balgová, V.; Pashkova, V.; Klein, P.; Wichterlová, B., Synthesis of ZSM-5 Zeolites with Defined Distribution of Al Atoms in the Framework and Multinuclear MAS NMR Analysis of the Control of Al Distribution. *Chemistry of Materials* **2012,** *24* (16), 3231-3239.

91. Kim, S.; Park, G.; Woo, M. H.; Kwak, G.; Kim, S. K., Control of Hierarchical Structure and Framework-Al Distribution of ZSM-5 via Adjusting Crystallization Temperature and Their Effects on Methanol Conversion. *ACS Catalysis* **2019,** *9* (4), 2880-2892.

92. Biligetu, T.; Wang, Y.; Nishitoba, T.; Otomo, R.; Park, S.; Mochizuki, H.; Kondo, J. N.; Tatsumi, T.; Yokoi, T., Al distribution and catalytic performance of ZSM-5 zeolites synthesized with various alcohols. *Journal of Catalysis* **2017,** *353*, 1-10.

93. Liu, M.; Yokoi, T.; Yoshioka, M.; Imai, H.; Kondo, J. N.; Tatsumi, T., Differences in Al distribution and acidic properties between RTH-type zeolites synthesized with OSDAs and without OSDAs. *Physical Chemistry Chemical Physics* **2014,** *16* (9), 4155-4164.

94. Treps, L.; Demaret, C.; Wisser, D.; Harbuzaru, B.; Méthivier, A.; Guillon, E.; Benedis, D. V.; Gomez, A.; Bruin, T. d.; Rivallan, M.; Catita, L.; Lesage, A.; Chizallet, C., Spectroscopic Expression of the External Surface Sites of H-ZSM-5. *The Journal of Physical Chemistry C* **2021,** *125* (3), 2163-2181.

95. Fyfe, C. A.; Thomas, J. M.; Klinowski, J.; Gobbi, G. C., Magic-Angle-Spinning NMR (MAS-NMR) Spectroscopy and the Structure of Zeolites. *Angewandte Chemie International Edition in English* **1983,** *22* (4), 259-275.

96. Rahman, A. F. A.; Jalil, A. A.; Siang, T. J.; Aziz, M. A. H.; Abdullah, T. A. T.; Mohamed, M.; Prasetyoko, D., Mechanistic insight into low temperature toluene production via benzene methylation over mesopore-rich fibrous silica HZSM-5 zeolite. *Journal of Porous Materials* **2021,** *28* (6), 1765-1777.

97. Pashkova, V.; Sklenak, S.; Klein, P.; Urbanova, M.; Dědeček, J., Location of Framework Al Atoms in the Channels of ZSM-5: Effect of the (Hydrothermal) Synthesis. *Chemistry – A European Journal* **2016,** *22* (12), 3937-3941.

98. Dědeček, J.; Kaucký, D.; Wichterlová, B., Co2+ ion siting in pentasil-containing zeolites, part 3.: Co2+ ion sites and their occupation in ZSM-5: a VIS diffuse reflectance spectroscopy study. *Microporous and Mesoporous Materials* **2000,** *35*, 483-494.

99. Argauer, R. J.; Landolt, G. R. Crystalline zeolite zsm-5 and method of preparing the same. 1969.

100. Öhlmann, G.; Pfeifer, H.; Fricke, R., *Catalysis and Adsorption by Zeolites*. Elsevier Science: 1991.

101. Gaspard, J. P. In *Physisorption and Chemisorption*, Dordrecht, Springer Netherlands: Dordrecht, 1982; pp 103-118.

102. Kecili, R.; Hussain, C. M., Chapter 4 - Mechanism of Adsorption on Nanomaterials. In *Nanomaterials in Chromatography*, Hussain, C. M., Ed. Elsevier: 2018; pp 89-115.

103. Davis, M. E.; Davis, R. J., *Fundamentals of chemical reaction engineering*. Courier Corporation: 2012.

2 Procedures and Methods

In this study, several techniques for the synthesis, characterization, and kinetic behavior of catalysts were used. The basic principles of these methods are briefly explained in this chapter below.

2.1 Synthesis

In heterogeneous catalysis, it is mandatory to prepare a catalyst that is highly active and selective towards desired products on the one hand side. From an industry-relevant point of view, this preparation needs to be simple and scalable, and the resulting material must be stable even at harsh conditions (*e.g.*, high temperature, high pressure).

The material screening of this project and optimization were performed to find the best material to support benzene's direct alkylation with CH_4. The most promising candidate was Co-ZSM-5 with a Si/Al of 15. A commercially available zeolite NH_4-ZSM-5 from the supplier Zeolyst was used as the support material. In order to get an active catalyst, an effective active component is applied to the carrier material via ion exchange.

An ion exchange needs to be performed for the transformation of NH_4-ZSM-5 into Co-ZSM-5. Therefore, the NH_4 form is first converted into the zeolite's H form by calcination, where NH_4 decomposes.[1] The standard method for calcination uses 100 mL min^{-1} flow of synthetic air (*Westfalen* AG) with a temperature program shown in **Figure 2.1**.

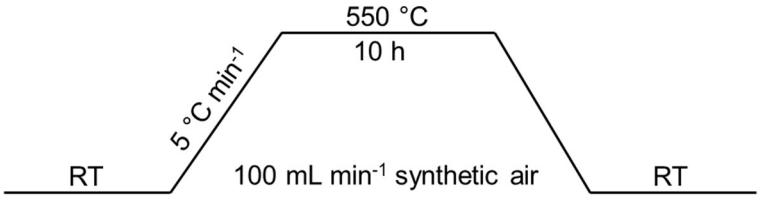

Figure 2.1: Standard temperature program for calcination.

With the H-form zeolite, aqueous ion exchange was performed. Hence, 50 mL $Co(OAc)_2$ (99.99% Merck) solution or $Co(NO_3)_2$ (99.99% Merck) solution per gram of H-ZSM-5 were adjusted to a pH of 5.8 with acetic acid or nitric acid, respectively. Then the Co solution and the zeolite were stirred for 15 h at 80 °C. The resulting product was then isolated via centrifugation and washed three times with ultra-pure water (18.2 MΩ cm resistance) and dried at 80 °C.

In order to remove the precursor acetate or nitrate and activate the catalyst, the material was further calcined again, following the standard procedure (**Figure 2.1**). Before utilization as a catalyst, it was also shaped into particles of 150-250 μm size via pressing and sieving to prevent pressure drops in the reactor tube.

2.2 Most commonly used characterization techniques

2.2.1 Fourier-transform infrared spectroscopy

Type and concentration of acid sites

Probe molecules are chosen by their interaction with a specific type of site. Moreover, the concentration and location of acid sites can be determined by adequately selecting probe molecules. An overview of probe molecules used within this study is given in **Table 2.1**.

Table 2.1: Probe molecules applied in this study and their type of sites.[2-3]

Probe molecule	Type of site
benzene	strength and location of acidic sites
CO	concentration and type of acidic sites and metal cations
NO	concentration and type of acidic sites and metal cations
pyridine	concentration and type of acidic sites

Pyridine adsorption

The evidence and classification of acid centers were provided via pyridine adsorption. For this technique, a material was pressed into a very thin wafer (~10 mg·cm^{-2}) and installed in an FT - IR spectrometer *Nicolet 5700*. The MCT (Mercury-Cadmium-Telluride) detector was cooled with liquid nitrogen. At a pressure below ~10^{-6} mbar, the sample was heated up to 450 °C for one hour with 10 °C min^{-1}. Then, at 150 °C, the material was exposed to $5 \cdot 10^{-1}$ mbar and equilibrated for 1 h. After removing physisorbed pyridine by outgassing for 1 h, a spectrum was taken. Typical spectra of

an activated Co-ZSM-5 and one with pyridine adsorbed on Co-ZSM-5 is shown in **Figure 2.2**. In the spectrum after activation one can see the assignment of bands as shown in **Table 2.2**.[4-6] At 3720 $cm^{-1,}$ the stretching vibration resulting from Si-OH vibrations can be seen. The band at 3608 cm^{-1} indicates BAS-OH stretching modes, and three bands between 2050 –1500 cm^{-1} represent the skeletal vibrations of ZSM-5.

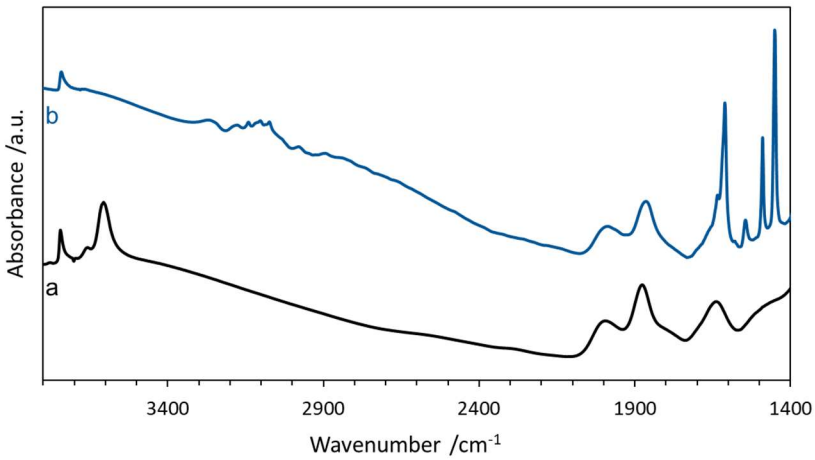

Figure 2.2: FTIR spectra of an **a**) activated Co-ZSM-5 and **b**) chemisorbed pyridine on Co-ZSM-5. The spectra are background corrected.

The acid sites can then be categorized into LAS and BAS. A band shows pyridinium ions (PyH+) over BAS at 1544 cm^{-1} and, coordinated pyridine (LPy) on strong LAS – mostly Co sites - are displayed at 1455 cm^{-1}.[5-6] The concentration of acid sites $c_{\text{acid sites}}$ was determined as shown in equation 2.1 with the area of the integral of the corresponding bands A_{integral}, the area of the wafer A_{wafer}, the mass of the wafer m_{wafer} and the corresponding extinction coefficient 0.73 cm mol^{-1} for BAS and 0.96 cm mol^{-1} for LAS.[7]

$$\boldsymbol{c}_{\text{acid sites}}\left[\frac{mol}{g}\right] = \frac{A_{integral}\,[cm^{-1}]\cdot A_{wafer}[cm^2]}{m_{wafer}[g]\cdot \epsilon\left[\frac{cm}{mol}\right]} \qquad 2.1$$

Table 2.2: Assignment of IR adsorption bands.[8-10]

Wavenumber /cm^{-1}	Functional group
3720	Si-OH stretching modes
3608	BAS-OH stretching modes
3500 - 3100	Perturbed SiOHAl stretching modes
3350 – 2200	N-H & C-H stretching modes
2207	C–O stretching modes of Co^{2+} - CO
2173	C–O stretching modes of CO - BAS
2089	C–O stretching modes of $Co^{+}(CO)_3$
2050 –1500	skeletal vibrations
1620	N-H bending
1545	PyH^+
1477	CC stretching modes
1450	PyH^+ + LPy
1455	LPy

CO adsorption

The oxidation state of Co cations in Co-ZSM-5 was determined amongst others via CO adsorption. At ambient temperature, it has been reported that Co cations can coordinate up to three CO molecules, while up to four carbonyls can be coordinated at low temperatures (liq. N_2).[9, 11-12]

Figure 2.3 shows an FTIR spectrum with chemisorbed CO on a Co-ZSM-5 sample at liq. N_2 temperature. Besides the Si-OH, BAS-OH, and lattice vibrations described in the previous paragraph, CO stretching modes can be seen at 2207 cm^{-1} presenting Co^{2+} - CO, 2173 cm^{-1} from CO – interacting with BAS and bands at 2089 cm^{-1} representing C–O stretching modes of $Co^{+}(CO)_3$. Moreover, a broad band from 3500 – 3100 cm^{-1} presents perturbed SiOHAl. The assignment can be seen in **Table 2.2**. With this experiment, one can distinguish between Co^{2+} and Co^{+} sites.

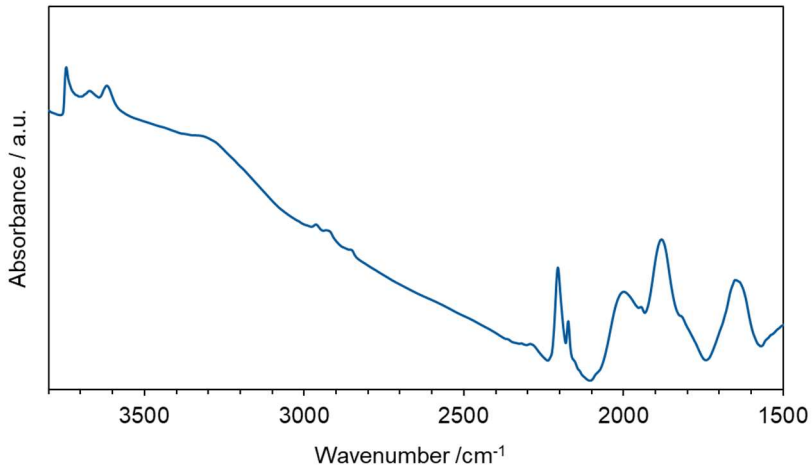

Figure 2.3: FTIR spectrum of chemisorbed CO on Co-ZSM-5. The spectra are background corrected.

Benzene adsorption

Benzene was adsorbed on Co-ZSM-5 at 100 °C. **Figure 2.4** shows one related example. Besides the bands coming from the zeolite itself, three regions are related to adsorbed benzene: CH out-of-plane deformation vibrations of benzene vibration at 3100 – 2800 cm^{-1}, and CC stretching vibrational bands at 1477 cm^{-1} from benzene adsorbed on LAS.[13] With increasing partial pressure of benzene, the intensity of the CC band increases, which indicates benzene being adsorbed. One can then differentiate between benzene adsorbed on BAS or Co sites. In the case of benzene adsorbed on BAS, the intensity of the band of SiOHAl decreases while the CC band increases. However, if the CC band intensity increases while the BAS are not affected, benzene is adsorbed elsewhere - in our case, on Co sites. With the help of the area of

the CC band of benzene and the area of SiOHAl band of ZSM-5, the amount of benzene and the amount of BAS can be determined, respectively. The molar extinction coefficients used for calculation are ε(C=C) = 0.356 cm^2 μmol^{-1} and ε(SiOHAl) = 0.325 cm^2 μmol^{-1}. These molar extinction coefficients were determined with the help of thermogravimetric analysis.

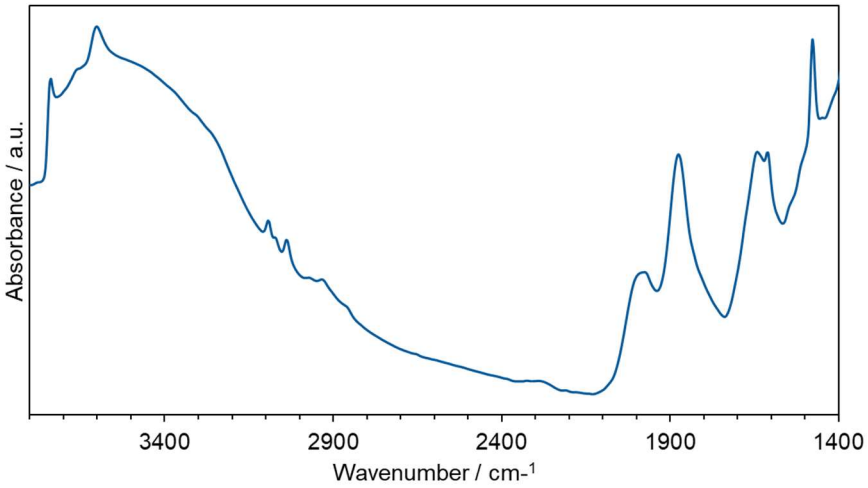

Figure 2.4: FTIR spectrum of benzene adsorbed on Co-ZSM-5.

2.2.2 Thermogravimetric analysis

The interaction between adsorbent and adsorbate can be studied more in detail by measuring adsorption isotherms. The direct method to measure the heat of adsorption is possible by thermogravimetric analysis.[14] The adsorption isotherms of benzene on H-ZSM-5 and Co-ZSM-5 were measured using thermogravimetric analysis (TGA) in combination with differential scanning calorimetry (TG-DSC) analysis performed on a TG-DCS 111 calorimeter in a high vacuum system ($< 5 \cdot 10^{-6}$ mbar). The heat flux signal was used to determine the released heat by adsorption, and the uptake of benzene was determined via the increase of sample weight. The adsorption isotherms were further analyzed in terms of a Langmuir adsorption model as discussed in section 1.3.4.

2.2.3 Gas analysis

Gas chromatography

The gas-phase composition was analyzed with a gas chromatography (GC) system 7890B GC from *AgilentTechnologies*. One column (HayeSep T 80-100, 0.5 m × 1/8") was used to separate low-boiling components (mainly H_2 and CH_4) from high-boiling compounds (aromatics). The low-boiling components were further separated in a ShinCarbon ST 50/80 UM column (2 m × 1/16" × 1 mm, *AgilentTechnologies*) and analyzed via a thermal conductivity detector (TCD). The high-boiling compounds were separated by a DB-WAX Ultra Inert column (30 m × 0.32 mm, *AgilentTechnologies*) and analyzed with a flame ionization detector (FID). It was possible to determine the exact feed concentration by calibration. A suitable method was chosen to measure the feed composition every 30 min.

Mass spectrometry

Mass spectrometry was used for the analysis of the gas-phase composition within seconds. A compact system ThermoStar GSD 320 from *PfeifferVacuum* working at 10^{-6} mbar was used.

2.3 Reaction kinetics

All data regarding the reaction kinetics were performed in a continuous plug flow reactor (PFR). The process diagram is shown in **Figure 2.5**. The setup was made in-house.

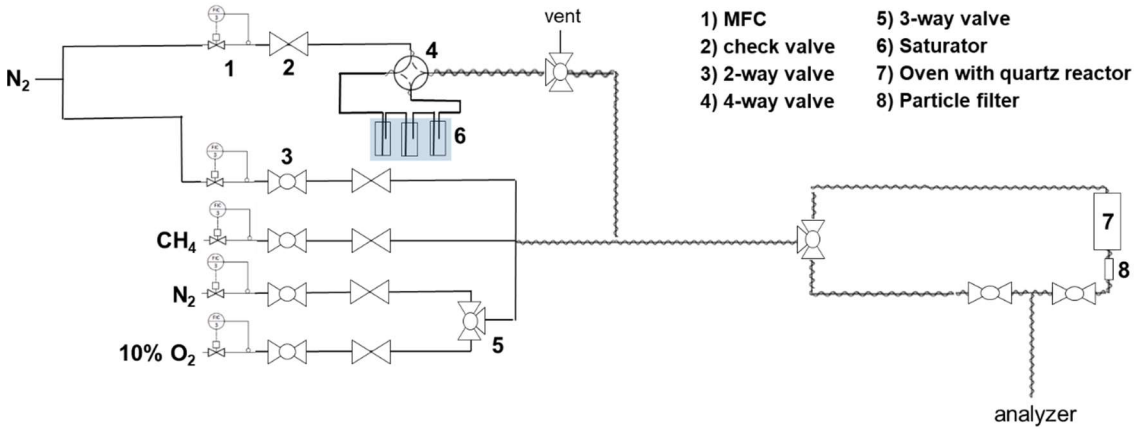

Figure 2.5 Process flow diagram for plug flow reactor setup with GC or MS used for analysis.

The fixed bed reactor consists of a 280 mm length and inner diameter of 4 mm. The catalyst in various masses was pretreated in 10% O_2 in He at 550°C for 2h. Before the reaction, the reactor system was purged with inert for 1h. The gas composition was determined at the end of the reactor using either an online GC- (*Agilent*) or MS-system (*PfeifferVacuum*).

2.3.1 Calculation of basic kinetic numbers: reaction rates, conversion, yield, and selectivity

One of the essential characteristics of a reaction is how fast that conversion takes place and how much product is generated. This can be determined by measuring the reaction rate and the conversion of a reactant. Moreover, it is essential to determine to quantity and the identify into which product the reactants were converted. This is

represented by yield Y and selectivity S. [15] It is important to mention, that for this work that the selectivities reported are all carbon based.

For the reaction rate r, the change of the amount of a reactant with time is normalized to its stoichiometric coefficient v, and either per mass of catalyst m_{cat} or per active species $mol_{active\ site}$. The mathematics are represented in equation 2.2. [15]

The conversion of a reactant is given by the proportion of the converted quantity of component *i* in relation to the used quantity $n_{i,0}$ (compare equation 2.3). In this study, the amount of converted reactant is given by the total amount of products formed (product-based calculation). [15]

The yield is defined as the amount of product produced $\dot{n}_k$, normalized to the amount of reactant $\dot{n}_{i,0}$, see equation 2.4. [15]

$$r_i = \frac{dn_i}{dt} \cdot \frac{1}{v_i} \cdot \frac{1}{m_{cat}} \qquad 2.2$$

$$X_i = \frac{n_{i,0} - n_p}{n_{i,0}} \qquad 2.3$$

$$Y_k = \frac{n_k}{n_{i,0}} \qquad 2.4$$

$$S = \frac{Y_k}{X_i} \qquad 2.5$$

$$TOF = \frac{r_i}{n_{active\ sites}} \qquad 2.6$$

Consequently, selectivities correspond to the ratio of yield and associated conversion – see equation 2.5. [15]

A particularly meaningful form of the reaction speed r is the so-called Turnover Frequency (TOF). For heterogeneously catalyzed reactions, Boudart defined turnover frequencies as "the number of runs of the catalytic cycle per unit time".[16] It gives a insight into the performance of the evaluated catalytic material. [15]

2.3.2 Determination of reaction order

The reaction rate r can also be described by the product of the reaction rate constant k and the concentration of reactant with the exponent reaction order n:

$$\boldsymbol{r = k \cdot c_{i,0}^{\,n}} \qquad 2.7$$

In an ideal system, the concentration **c** equals the partial pressure **p**. Experimentally the reaction order can be calculated using the initial rates method. The mathematic term for that method is:

$$\boldsymbol{\ln(r) = \ln(k) \cdot \ln(c_{i,0})} \qquad 2.8$$

By a series of experiments for various initial concentrations $c_{i,0}$ and the corresponding reaction rates according to equation 2.2, a straight line is obtained by plotting ln(r) versus ln($c_{i,0}$) (see **Figure 2.6**). The resulting slope corresponds to the reaction order n, and the y-axis interception can determine the rate constant k.

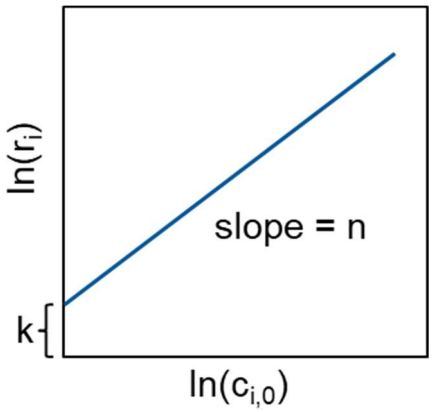

Figure 2.6: Linearization and graphical illustration of the reaction rate equation.

2.3.3 Determination of activation energy

The critical challenge of a catalyst is to offer an alternative reaction pathway that subsequently reduces the activation energy required for a specific reaction. The relation between reaction constant k and the activation energy E_A is described by the Arrhenius equation (2.9). A temperature dependency of the reaction rate constant can be seen. With the help of the linearized equation 2.10 and its illustration by the Arrhenius plot - ln (k) vs. 1/T - one can determine the activation energy. Experimentally, this can be determined by measuring reaction rates at different temperatures.

$$k = k_0 \cdot e^{-E_A/RT} \qquad 2.9$$

$$\ln k = \ln k_0 - \frac{1}{T} \cdot \frac{E_A}{R} \qquad 2.10$$

2.3.4 Temperature programmed surface reaction

By performing temperature-programmed surface reaction (TPSR) experiments, the sorption properties of reactants can be investigated.

The standard procedure followed the temperature program, as shown in **Figure 2.7**. First, the catalyst was activated at 550 °C under a flow of 10% O_2 in He. The second step was to cool down to 200 °C under He atmosphere. The exposure to either CH_4 or benzene diluted in He took place at 200 °C. After that, the system was purged with He again until no reactant in the gas phase was detected via MS. Before starting the TPSR, the catalyst was cooled down to 150°C.

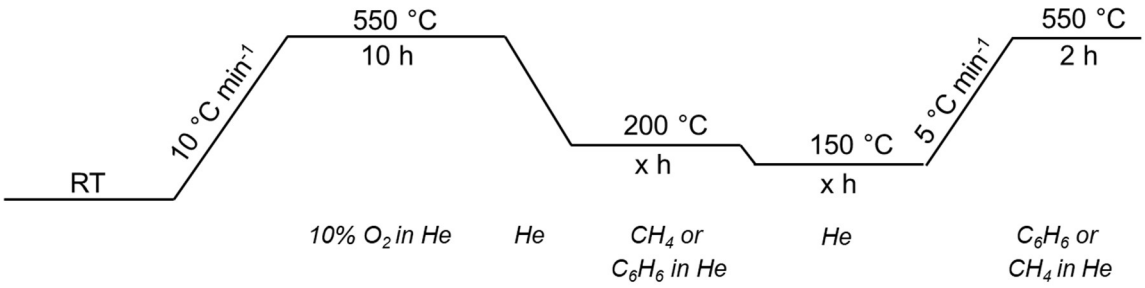

Figure 2.7: Temperature program and gas composition of a typical TPSR.

During TPSR, the gas atmosphere contained either benzene or CH_4, according to the pre-exposure medium. With this method, it can be possible to determine the required temperature for a specific reaction and the concentration of products formed. Moreover, one can distinguish between an Eley-Rideal and Langmuir-Hinshelwood mechanism since only one reactant was feed at a time, whole another reactant was already pre-adsorbed on the catalyst's surface.

2.4 References

1. Xue, T.; Wang, Y. M.; He, M.-Y., Facile synthesis of nano-sized NH4-ZSM-5 zeolites. *Microporous and Mesoporous Materials* **2012,** *156*, 29-35.

2. Cejka, J.; van Bekkum, H.; Corma, A.; Schueth, F., *Introduction to zeolite molecular sieves*. Elsevier: 2007.

3. Kulprathipanja, S., *Zeolites in industrial separation and catalysis*. John Wiley & Sons: 2010.

4. Zecchina, A.; Spoto, G.; Bordiga, S., Vibrational Spectroscopy of Zeolites. In *Handbook of Vibrational Spectroscopy*, John Wiley & Sons, Ltd.: 2006.

5. Khalil, I.; Celis-Cornejo, C. M.; Thomas, K.; Bazin, P.; Travert, A.; Pérez-Martínez, D. J.; Baldovino-Medrano, V. G.; Paul, J. F.; Maugé, F., In Situ IR-ATR Study of the Interaction of Nitrogen Heteroaromatic Compounds with HY Zeolites: Experimental and Theoretical Approaches. *ChemCatChem* **2020,** *12* (4), 1095-1108.

6. Auerbach, S. M.; Carrado, K. A.; Dutta, P. K., *Handbook of zeolite science and technology*. CRC press: 2003.

7. Schüßler, F.; Schallmoser, S.; Shi, H.; Haller, G. L.; Ember, E.; Lercher, J. A., Enhancement of dehydrogenation and hydride transfer by La3+ cations in zeolites during acid catalyzed alkane reactions. *ACS Catalysis* **2014,** *4* (6), 1743-1752.

8. Borade, R.; Sayari, A.; Adnot, A.; Kaliaguine, S., Characterization of acidity in ZSM-5 zeolites: an X-ray photoelectron and IR spectroscopy study. *Journal of Physical Chemistry* **1990,** *94* (15), 5989-5994.

9. Hadjiivanov, K.; Tsyntsarski, B.; Venkov, T.; Klissurski, D.; Daturi, M.; Saussey, J.; Lavalley, J. C., FTIR spectroscopic study of CO adsorption on Co–ZSM-5: Evidence of formation of Co+(CO)4 species. *Physical Chemistry Chemical Physics* **2003,** *5* (8), 1695-1702.

10. Tzoulaki, D.; Jentys, A.; Pérez-Ramírez, J.; Egeblad, K.; Lercher, J. A., On the location, strength and accessibility of Brønsted acid sites in hierarchical ZSM-5 particles. *Catalysis today* **2012,** *198* (1), 3-11.

11. Bellmann, A.; Rautenberg, C.; Bentrup, U.; Brückner, A., Determining the Location of Co2+ in Zeolites by UV-Vis Diffuse Reflection Spectroscopy: A Critical View. *Catalysts* **2020,** *10* (1), 123.

12. Campa, M. C.; De Rossi, S.; Ferraris, G.; Indovina, V., Catalytic activity of Co-ZSM-5 for the abatement of NOx with methane in the presence of oxygen. *Applied Catalysis B: Environmental* **1996,** *8* (3), 315-331.

13. Datka, J., Adsorption of benzene and toluene on Y zeolites studied by infrared spectroscopy. *Journal of the Chemical Society, Faraday Transactions 1: Physical Chemistry in Condensed Phases* **1981,** *77* (3), 511-517.

14. Bolis, V.; Vedrine, J. C.; Van de Berg, J. P.; Wolthuizen, J. P.; Derouane, E. G., Adsorption and activation of ethene by zeolite-H-ZSM-5. *Journal of the Chemical Society, Faraday Transactions 1: Physical Chemistry in Condensed Phases* **1980,** *76*, 1606-1616.

15. Draxler, J.; Siebenhofer, M., Reaktionstechnik. In *Verfahrenstechnik in Beispielen*, Springer Vieweg, Wiesbaden: 2014.

16. Boudart, M., Turnover rates in heterogeneous catalysis. *Chemical reviews* **1995,** *95* (3), 661-666.

3 Basic characterization results

3.1.1 Chemical composition

The metal content of materials was determined by graphite furnace atomic absorption spectroscopy (GT-AAS). The measurements were performed using a Solaar M5 Dual-Flame AAS spectrometer from ThermoFischer. For sample preparation, the dry material (0.03 g) was dissolved in a mixture of HF (10%, 1 mL) and HNO_3 (3 mL) followed by heating. With this procedure a revealing of the zeolite is possible

For the standard support ZSM-5 used for this study, a Si/Al of 15 was determined. The Co content is stated in chapters 4 and 5.

3.1.2 Crystallinity

A powder X-ray diffractometer was used to determine the sample crystal structure. It is based on the ability of crystalline solids to diffract electromagnetic radiation of an appropriate wavelength. Measurements were performed on an Empyrean diffractometer from Malvern PANalytical. Cu-Kα radiation ($K\alpha_2/K\alpha_1$ = 0.5) at 45 kV and 40 mA was used. XRD patterns were recorded for 2θ between 3° and 60°.

The crystallinity parent ZSM-5 sample (H & NH_4) was examined. As shown in **Figure 3.1**, all reflections were consistent with the structure of a ZSM-5 reference taken from a database.[1] A high crystallinity is given. The calcination step did not affect the structure of the zeolite.

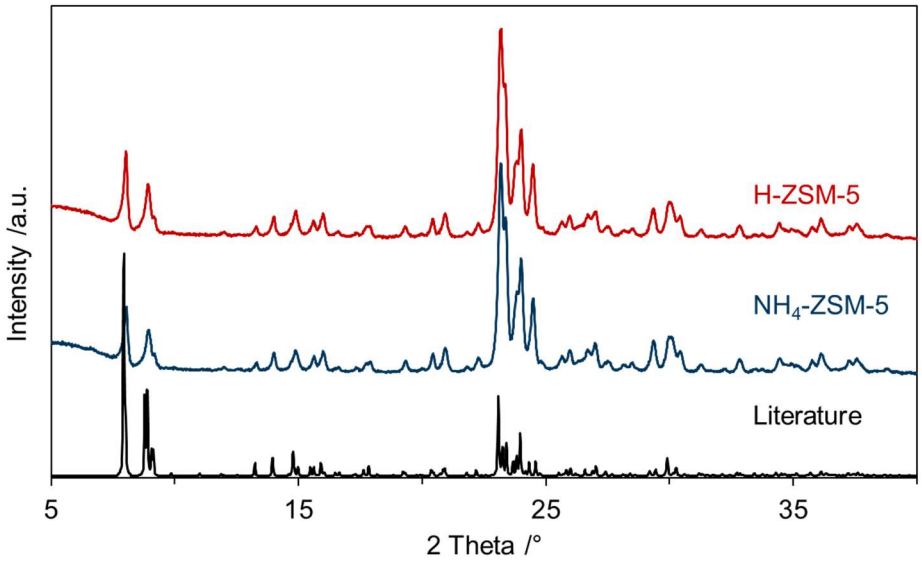

Figure 3.1: PXRD spectra of H-ZSM-5, NH_4-ZSM- 5, and a reference.[1]

3.1.3 Crystallite size

Scanning electron spectroscopy is a method to analyze and image bulk materials. SEM measurements were performed with a Jeol JSM 7500F ultrahigh-resolution field microscope using secondary electron imaging. The primary electron beam used an accelerating voltage of 1.0 kV.

The resulting images of two samples are shown in **Figure 3.2**. The crystal size of H-ZSM-5 was determined to be 110 ± 20 nm, while the crystal size of Co-ZSM-5 was determined slightly smaller with 100 ± 20 nm. Morphology and crystallinity of the zeolite were not changed during the ion exchange procedure. However, the purity was somewhat lower.

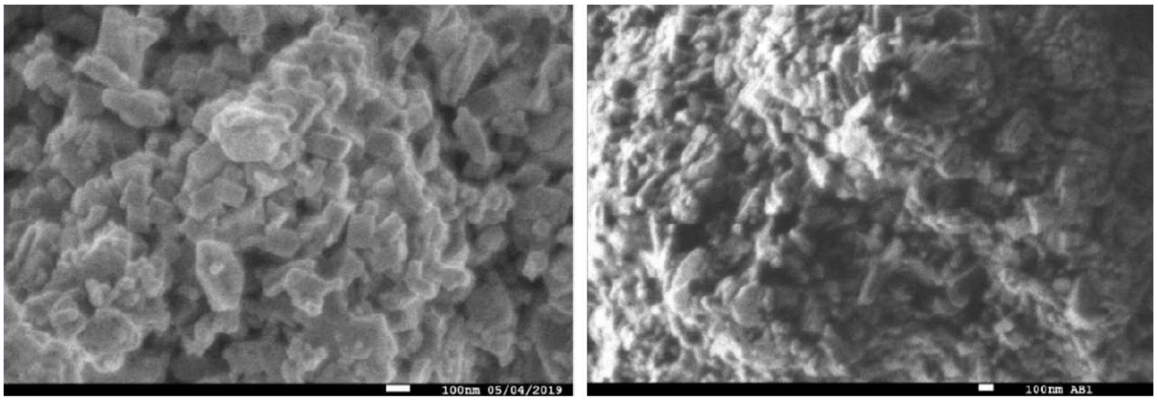

Figure 3.2: SEM image of H-ZSM-5, left; and Co-ZSM-5 (326 µmol g^{-1}), right (Si/Al = 15).

3.1.4 Aluminum structure

Solid-state ^{27}Al- nuclear magnetic resonance spectroscopy (NMR) was used to calculate the amount of extra-framework aluminum (EFAL) in the zeolite. Measurements were conducted on a Bruker AV500 WB, with a 500 MHz wide-bore magnet from Oxford Instruments and a Bruker AVI console. The dried material was packed inside a rotor (4mm) from Rototec Spintec GmbH. The measurement took place at a spinning rate of 12 kHz.

Figure 3.3 shows a ^{27}Al-NMR spectra of H-ZSM-5. From this it can be seen that 4% of all Al in the material is octahedral coordinated Al (δ = 0 ppm), while the rest is tetrahedral coordinated (δ = 54).

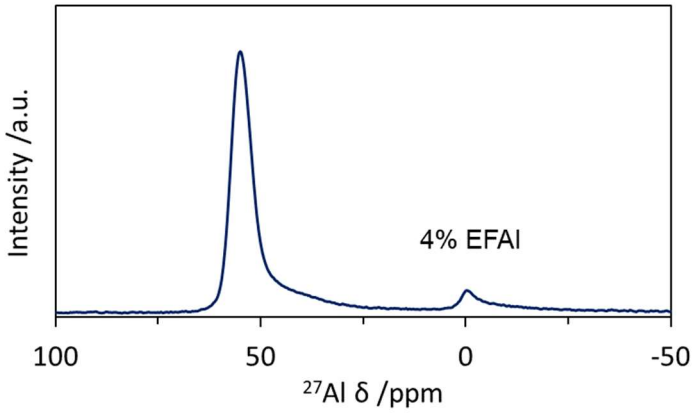

Figure 3.3: ^{27}Al-NMR spectra of the H-ZSM-5 (Si/Al = 15).

3.1.5 Pore volume

N_2-physisorption was performed according to Brunauer–Emmett–Teller method. These measurements provide information about pore volume. The analysis was performed on a Thermo Sorptomatic instrument. The activated sample (2h at 160 °C) was exposed to N_2 at -196 °C. To determine the surface area of a sample BET theory was applied to the obtained isotherm over a pressure range from 0.05 to 0.30 p/p_0. The mesopore volume was determined on the desorption branch in a range of 0.30 to 0.95 p/p_0. Using the t-plot method, the micropore volume was determined.[2]

Table 3.1 lists the micropore and mesopore volume of main materials as following: NH_4- and H-ZSM-5 contain the same micropore volume of 0.15 and 0.16 $cm^3\ g^{-1}$, respectively, while the micropore volume of Co-ZSM-5 with 326 $\mu mol_{Co}\ g^{-1}$ is slightly lower with 0.13 $cm^3\ g^{-1}$. This indicates to block some micropores with Co atoms. However, the mesopore volume of all three materials remains constant with 0.08 and 0.07 $cm^3\ g^{-1}$.

Table 3.1: Micropore and mesopore volume of the basic material of this study.

Material	Micropore volume /$cm^3\ g^{-1}$	Mesopore volume /$cm^3\ g^{-1}$
NH_4-ZSM-5	0.15	0.08
H-ZSM-5	0.16	0.07
Co-ZSM-5	0.13	0.07

3.2 References

1. Baerlocher, C.; McCusker, L. B. Database of Zeolite Structures. http://www.iza-structure.org/databases/.

2. Scherdel, C.; Reichenauer, G.; Wiener, M., Relationship between pore volumes and surface areas derived from the evaluation of N2-sorption data by DR-, BET-and t-plot. *Microporous and Mesoporous Materials* **2010,** *132* (3), 572-575

4 Reaction network and kinetics of the alkylation of benzene with CH_4 over Co-ZSM-5 catalysts

The following chapter is based on unpublished results. The manuscript will be submitted by Martina Aigner[1], Stijn Van Daele,[2] Maricruz Sanchez-Sanchez[1], and Johannes A. Lercher[1].

Martina Aigner performed all experiments and the manuscript preparation. Stijn Van Daele, Maricruz Sanchez-Sanchez, and Johannes A. Lercher supported the research. The manuscript was written with the involvement of all named authors.

Abstract

Ion exchanged Co^{2+} in ZSM-5 was found active for the direct methylation of benzene with CH_4. While toluene is the main product, a competitive reaction pathway leading to biphenyl and phenyltoluene decreases selectivities and contributes to catalyst deactivation. Spectroscopic characterization showed that the material only contained exchanged Co species, the majority as single Co^{2+} ions compensating the negative charges of two Al T-sites in the ZSM-5 framework. This species has a strong Lewis acid character and strongly adsorbs benzene. Temperature Programmed Surface Reaction (TPSR) studies showed the competitive adsorption of CH_4 and benzene on active Co sites at moderate temperatures, with toluene formation only detected when CH_4 is activated on the surface of Co-ZSM-5 before benzene exposure. Reaction under high CH_4 to benzene ratios promotes the alkylation route to toluene over the competitive biphenyl formation. The kinetic parameters obtained indicate that the reaction at temperatures > 500°C follows a Langmuir-Hinshelwood mechanism. It is proposed that the activation of CH_4 and alkylation mechanism occurs via heterolytic dissociation of CH_4 on Co^{2+} sites followed by a nucleophilic attack on electron-poor benzene coordinated an adjacent strong Lewis acid Co^{2+} site.

4.1 Introduction

CH_4 contributes ~ 16% of the global greenhouse gas and is underutilized in many processes. Large amounts of CH_4 are flared or burned as fuel in a gas turbine or steam generator. CH_4 is - due to its strong C-H bond- thermodynamically very stable and therefore relatively unreactive. Nevertheless, it can be converted into valuable chemicals (via steam reforming, partial oxidation, or oxyhalogenation), but so far, the commercially used processes need several steps.[1-2]

In the last decades, multiple research groups have applied Mo-based catalysts for the CH4 dehydroaromatization (MDA) reaction.[3-5] A critical disadvantage of this process is the strong catalyst deactivation due to rapid coke formation. Elements of the VIII group such as Fe, Co, and Ni are suitable metals to activate CH_4 for MDA. Recently, Y. Xu *et al.* reported Co on HZSM-5 as an active model MDA catalyst for converting CH_4 towards benzene and naphthalene.[6]

Another interesting approach is the direct alkylation of aromatic feeds from crude oil with CH_4. Here we will study the CH_4 alkylation of benzene to toluene, which can be used as a commodity chemical.

It has been recently reported that some transition metals hosted on zeolites catalyze the alkylation of benzene with CH_4 to toluene and hydrogen.[7-12] Among the metals and zeolites tested, Co exchanged in an MFI type zeolite (ZSM-5) is one of the most promising catalysts for this reaction.[8] Nakamura *et al.* recently proposed that the active sites for the CH_4 alkylation of benzene are Co^{2+} ions compensating the two negative charges of an Al pair in the α position in MFI.[9] In a later work, the same group, suggested a non-oxidative activation of CH_4 by heterolytic C-H cleavage on strong Lewis acid sites.[13] However, an overall molecular understanding of the reaction mechanism and the reaction parameters that can influence the different pathways is not yet available.

This work has optimized reaction conditions for a potential industrial application of CH_4 methylation of benzene over Co/ZSM-5 catalysts. The materials are prepared to avoid the formation of precipitated Co particles, and only ion-exchanged Co^{2+} species are present in the zeolite micropores. We perform a kinetic study and provide a

detailed description of the reaction network, pinpointing the main competitive reaction pathways that affect the selectivity to toluene.

4.2 Results and discussion

4.2.1 Synthesis and characterization of Co-ZSM-5 catalysts

For this study, we used the H-form of a commercial ZSM-5 (Zeolyst, CBV 3024E) with Si/Al ratio of 15 with ~40 % of Al pairs according to the quantification method by Dědeček *et al.* using cobalt(II) nitrate.[14] The samples for this study were synthesized via an ion exchange methodology using cobalt(II) acetate to achieve a higher concentration of Co ions exchanged in the zeolite.[15-16] By pyridine adsorption, we have quantified the amount of Brønsted acid sites (BAS) and Lewis acid sites (LAS) in the parent sample H-ZSM-5 as 950 μmol g^{-1} and 173 μmol g^{-1}, respectively. We have prepared a Co-ZSM-5 catalyst by our ion exchange protocol, and the highest Co loading achieved without precipitation was 314 μmol g^{-1}. The success of the ion exchange step in Co-ZSM-5 can be followed by measuring the remaining BAS available in ZSM-5 after Co exchange. For this highest Co-exchanged loading, we have detected 227 μmol g^{-1} BAS. Therefore, the number of BAS that Co ions have exchanged is 1.8 ± 0.1. This indicates that a significant fraction of Co cations has exchanged as single Co^{2+} ions on Al pairs (with a nominal BAS/Co =2), and a small fraction of Co is exchanged, compensating 1 BAS per Co. Tentatively, such exchanged Co species are exchanged in isolated Al T-sites with a $[CoOH]^{+}$ or a [Co-O-Co] structure.[14] The presence of Co oxide nanoparticles was not observed by TEM (see **Figure S 4.1** in Supporting Information) but cannot be excluded entirely.

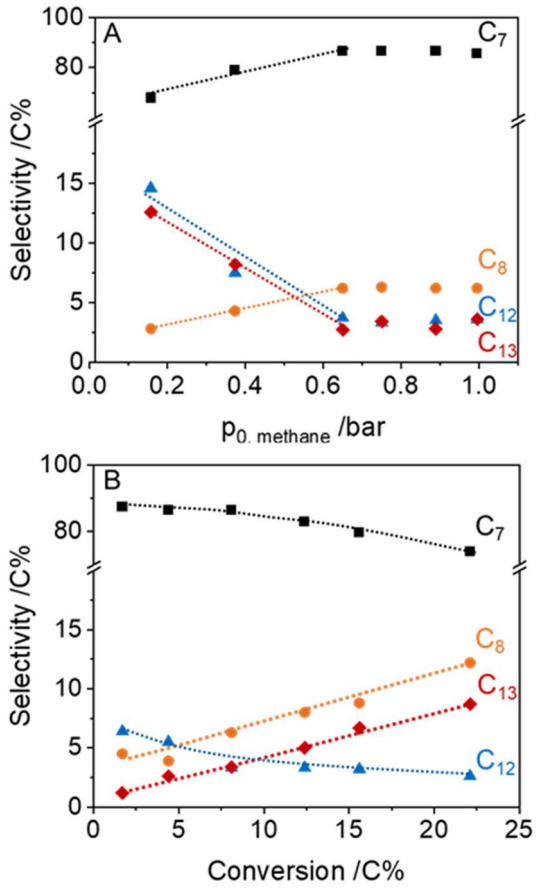

Figure 4.1: Selectivity towards products in the CH_4 alkylation of benzene over Co-ZSM-5 catalyst (314 $\mu mol_{Co}\ g^{-1}$). C_7 (toluene, square), C_8 (xylenes, circle), C_{12} (biphenyl, triangle) and C_{13} (phenyltoluene, diamond) as a function of A) the partial pressure of CH_4, and B) the conversion of benzene T = 550 °C, 1 atm, CH_4/benzene = 166, WHSV = 0.1-2.5 h^{-1}.

4.2.2 Product distribution and reaction pathway.

We determined the theoretically achievable conversion of benzene depending on temperature and the varying ratio of the reactants from the thermodynamic equilibrium (**Figure S 4.2** in Supporting Information). For a reaction temperature of 550 °C, the equilibrium conversion increases from 4% to 40% when the methane to benzene ratio (M/B) increases from 1 to 166. We tested a Co-ZSM-5 with 314 µmol g^{-1} Co loading at increasing M/B ratios by increasing partial pressures of CH_4 at a constant benzene partial pressure of 5 mbar. External diffusion limitations can be ruled out (see **Figure S 4.3** in Supporting Information). Moreover, the carbon balance is considered to be closed with 100 ± 2 %. The product selectivity is shown in **Figure**

4.1A. Firstly, it should be noted that apart from the main products, toluene and hydrogen, also xylenes, phenyltoluene, and biphenyl are formed over Co-ZSM-5. The selectivity towards toluene and xylenes increases with CH_4 partial pressure. Conversely, the selectivity towards phenyltoluene and biphenyl decreased at higher CH_4 partial pressures. Above a CH_4 to benzene ratio of 166 ($p_{0,CH4}$ = 750 mbar), the selectivities for all products reached a constant value and did not further change. This is due to constant consumption rates at p_{CH4} > 750 mbar, indicating a zero-order reaction and thus suggesting that full CH_4 coverage of surface sites has been achieved.

Setting the operating CH_4 to benzene ratio at 166, the reaction over the selected Co-ZSM-5 catalyst reached a conversion of benzene of up to ca. 22 % at a WHSV of 2.5 h^{-1}. **Figure 4.1B** shows how toluene and biphenyl selectivities decrease with conversion at the expense of an increase in selectivities to xylene and phenyltoluene. The evolution of selectivity with conversion shows that toluene and biphenyl are primary products, while xylenes and phenyltoluene are secondary products.

We performed catalytic tests over Co-ZSM-5 using different feeds: mixtures of benzene, toluene, and CH_4 in various combinations (**Table 4.1**). Together with the selectivities discussed above, these experiments provide insight into the reaction pathways involved in the alkylation of benzene with CH_4. When the only reactant available is benzene (test 1 in **Table 4.1**), only the formation of biphenyl was detected. A feed of toluene (test 2) produced xylenes together with small fractions of benzene, CH_4, and phenyltoluene. In this experiment, biphenyl was not detected. The formation of xylenes and benzene is attributed to the toluene disproportionation reaction. Moreover, the formation of phenyltoluene in the absence of biphenyl suggests that this product stems from the reaction of toluene with benzene and not from the methylation of biphenyl. In good agreement with this, when benzene and toluene are fed together – in the absence of CH_4, test 3 - the highest rates in the formation of phenyltoluene are achieved ($3.3 \cdot 10^{-8}$ mol s^{-1} g^{-1}). Finally, a feed with toluene and CH_4 (test 5) mainly produced xylenes, indicating that the catalyst is also active in the methylation of toluene with CH_4. When feeding only CH_4 on Co-ZSM-5, we have detected benzene formation by methane dehydroaromatization.

Table 4.1: Formation rates of CH_4, benzene, toluene, xylenes, biphenyl and phenyltoluene with different feed compositions. T = 550 °C, 1 atm, $p_{0, CH4}$ = 400 mbar, WHSV = 0.6 h^{-1}. * ~10% conversion.

Test number	Reactants	Partial pressure aromatics /mbar	X benzene /toluene / %	Formation rate CH_4 / mol s^{-1} g^{-1}	Formation rate C_7/ C_6 / mol s^{-1} g^{-1}	Formation rate C_8 / mol s^{-1} g^{-1}	Formation rate C_{12} / mol s^{-1} g^{-1}	Formation rate C_{13} / mol s^{-1} g^{-1}
1	benzene	5.1	0.7	-	-	-	$1.4 \cdot 10^{-8}$	-
2	toluene	4.9	12.4	$5.1 \cdot 10^{-9}$	$6.6 \cdot 10^{-8}$	$3.2 \cdot 10^{-8}$	-	$2.5 \cdot 10^{-9}$
3	benzene + toluene	2.5 / 2.5	-	$3.8 \cdot 10^{-9}$	-	$3.2 \cdot 10^{-8}$	$6.1 \cdot 10^{-10}$	$3.3 \cdot 10^{-8}$
4	benzene + CH_4	5.1	3.7	-	$4.9 \cdot 10^{-8}$	$0.2 \cdot 10^{-8}$	$1.1 \cdot 10^{-8}$	$0.9 \cdot 10^{-8}$
5	toluene + CH_4	5.1	14.1	-	$6.1 \cdot 10^{-8}$	$5.3 \cdot 10^{-8}$	-	$1.1 \cdot 10^{-9}$

We propose a reaction network for CH4 and benzene based on these experiments, as shown in **Scheme 4.1**. There are two main pathways: i) the CH_4 alkylation of benzene to toluene, and subsequently to xylenes and a small fraction of C_{9-11}, and ii) in parallel, benzene can undergo a bimolecular reaction to form biphenyl. The toluene formed via pathway i) reacts with benzene to produce phenyltoluene and undergoes disproportionation to xylene and benzene. According to the increase in toluene and xylenes selectivities shown in **Figure 4.1A**, alkylation reactions are favored at high CH_4 partial pressures, indicating a positive reaction order with respect to CH_4. Under these conditions, the formation of xylene via toluene disproportionation is negligible. Given these results, we attribute the effect of the CH_4/C_6H_6 ratio on products selectivities (**Figure 4.1A**) to the competition between pathways i) and ii).

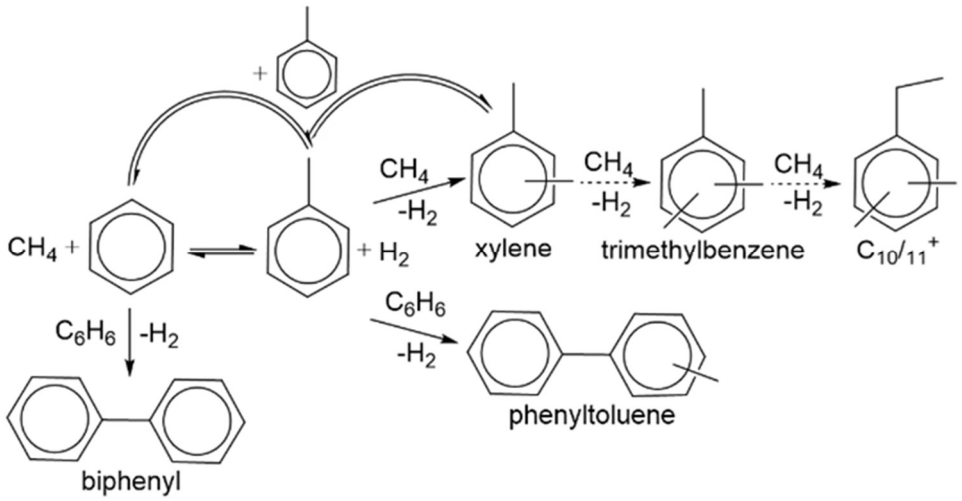

Scheme 4.1: Reaction network of benzene with CH_4 over Co-ZSM-5.

4.2.3 Adsorption properties of benzene on H-ZSM-5 and Co-ZSM-5.

We determined the heat of benzene adsorption on BAS and Co sites (see Figure 4 in Supporting Information). Over H-ZSM-5, we measured a ΔH_{ads} value of ~65 kJ mol^{-1}, characteristic of the adsorption of benzene over BAS.[17] For Co-ZSM-5 with 314 µmol g^{-1} of Co, we observe a ΔH_{ads} of 260 kJ mol^{-1} for benzene uptakes well below 200 µmol g^{-1}. This indicates a strong benzene interaction with a fraction of Co sites.

We also monitored the adsorption of benzene at 100 °C by in-situ FTIR. **Figure S 4.5** in SI shows the BAS coverage, measured by the decrease of AlOHSi vibrations (3610 cm^{-1}), in dependency of the benzene uptake for H-ZSM-5 and Co-ZSM-5. **Figure S 4.6** shows the corresponding FTIR spectra. We observe that adsorbing up to ~ 100 µmol g^{-1} benzene did not lead to any decrease in the O-H vibration of BAS. Above 100 µmol g^{-1} of benzene uptake, a linear increase of the coverage of BAS with increasing benzene adsorption can be seen up to a coverage of BAS of ~ 230 µmol g^{-1}, in good agreement with the total BAS concentration measured for this Co-ZSM-5 by pyridine IR Therefore; we conclude that there are at least 100 µmol g^{-1} of Co sites with strong Lewis acidity leading to the preferential adsorption of benzene.

4.2.4 Kinetics of benzene alkylation with CH_4

First, we tested the effect of Co loadings on the activity of Co exchanged ZSM-5 catalysts in benzene alkylation with CH_4. It should be noted that, in the absence of Co, H-ZSM-5 does not form any toluene. An increase in the formation rate of toluene with Co loading is observed for samples below the exchange limit of the parent H-ZSM-5. Based on our data, such a limit is ~340 $\mu mol_{Co}\ g^{-1}$. Introducing higher Co loadings (600 - 800 $\mu mol_{Co}\ g^{-1}$) via impregnation or repeated ion-exchange protocols did not achieve similar activities per catalyst mass nor per Co (**Figure S 4.7** in SI). We have performed our kinetic study on the sample with the highest rates per Co, a ZSM-5 with a Co loading of 314 $\mu mol_{Co}\ g^{-1}$. The apparent activation energy obtained for toluene formation at 550°C is 122 kJ mol^{-1} - see **Figure S 4.8A**.

On the other hand, the formation rate of biphenyl was not affected by temperature, leading to an E_{app} of only 2 kJ mol^{-1}. Given the high heat of adsorption measured for benzene over our Co-ZSM-5 catalyst (~ 260 kJ mol^{-1}, **Figure S 4.4**), we attribute this low E_{app} to an energetic compensation of the reaction barrier of biphenyl formation by the benzene adsorption step.

We measured the reaction orders with respect to CH_4 and respect to benzene for toluene formation and obtained values of 0.7 and 0.4, respectively. This indicates that the reaction occurs via co-adsorption of both reactants in an L-H mechanism. The reaction order in benzene for biphenyl formation is 1.0. In addition, we have measured a negative reaction order of biphenyl formation with CH_4 of -0.5 that indicates that the reaction of benzene methylation competes with benzene dimerization (**Figure S 4.8B**).

4.2.5 Surface reactivity of CH_4 and benzene over Co-ZSM-5

As mentioned above, blank experiments testing the reaction on H-ZSM-5 (950 $\mu mol\ g^{-1}$ BAS) show that BAS alone do not achieve significant conversions at the conditions tested here (except for a 0.1% yield of H_2 that, together with a change of color of the catalyst after reaction, points to certain coking of the catalyst). Therefore, both the

methylation of benzene and the biphenyl formation pathways are attributed to Co-based Lewis acid sites.

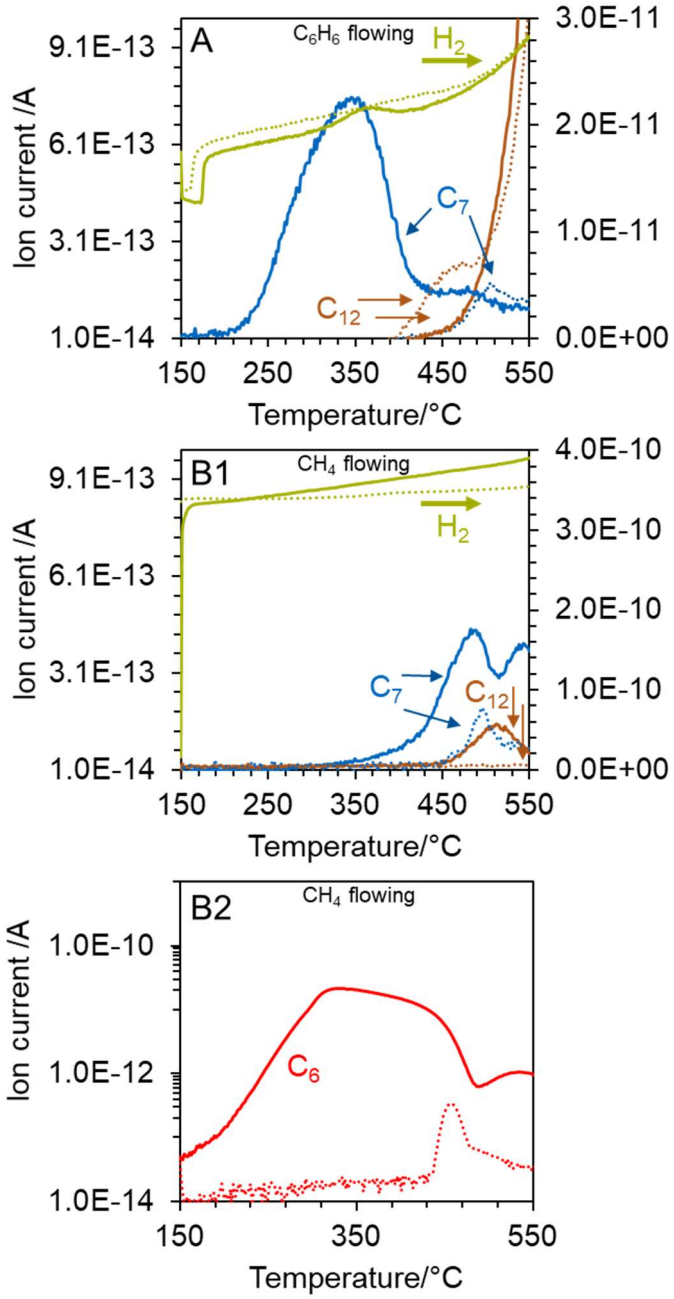

Figure 4.2: Temperature programmed reaction over Co-ZSM-5 of A) benzene (5 mbar) after the catalyst was exposed to CH_4 (200°C, 750 mbar, 2.5 h), and B1) CH_4 (750 mbar) after the catalyst was exposed to benzene (200°C, 5 mbar, 0.5 h) with 5 °C min^{-1}. In B2), it represents the signal of benzene corresponding to experiment B1. The y-axis represents the ion current measured by mass spectroscopy: toluene (C_7, blue), benzene (C_6, red), and biphenyl (C_{12}, brown) left, and hydrogen (green) on the right axis. Blank experiments in which the TPRs were performed on a clean Co-ZSM-5 without pre-exposure to any reactant are shown in dotted lines.

To determine the catalytic steps and sites at the surface of Co-ZSM-5 catalysts, we have performed temperature-programmed surface reaction (TPSR) experiments over the highly active Co-ZSM-5 with 314 $\mu mol_{Co}\ g^{-1}$. In these measurements, we first expose the activated catalyst to either CH_4 or benzene and subsequently monitor the gas products while heating under a flow of the other reactant. When the catalyst was first exposed to CH_4, the TPRS profile under benzene flow showed toluene, hydrogen, and biphenyl (**Figure 4.2A**, solid lines). The maximum toluene production under flowing benzene is centered at 350 °C. A concomitant local maximum is observed in the hydrogen formation. It should be noted that H_2 production increased continuously with temperature indicating that coking of the catalyst is likely taking place via benzene dehydrogenation. The increasing H_2 formation confirms this with T observed in a benzene TPRS experiment using Co-ZSM-5 without preabsorbed CH_4 (**Figure 4.2A**). After the low-temperature production of toluene in the region of 200 – 400 °C, the second peak of formation of toluene is detected at ~490 °C, which will be discussed later. Biphenyl formation is detected at 400 °C and increases exponentially above 450 °C. In the blank TPSR without CH_4 preexposure (**Figure 4.2A** dashed lines), a shoulder of biphenyl entered at ~450 °C precedes the predominant formation at 500 °C. We attribute the absence of the biphenyl formation peak in the region of 370-470 °C in the TPRS in the presence of preadsorbed CH_4 to surface CH_x species competing for the sites that are active in benzene dimerization to biphenyl.

When the catalyst was exposed to benzene, and subsequently, the temperature was increased under CH_4 flow, the formation of toluene was not observed until temperatures above 350 °C (**Figure 4.2B1**). Only a minor production of toluene was detected in the temperature region of 350-420 °C, followed by two resolved toluene formation peaks centered at 490 and 550 °C. Biphenyl was observed in the high-temperature region with a maximum at 500 °C. It should be noted that in the temperature region of 200 - 450 °C ~350 $\mu mol\ g^{-1}$ of unreacted benzene desorbed (**Figure 4.2B2**, solid line). We have quantified the desorption of a similar amount of benzene (349 ± 7 $\mu mol\ g^{-1}$) up to ~ 450 °C, with a broad maximum at 310-440 °C, in the absence of CH_4 flow (**Figure S 4.9**). Based on this, we suggest that in the TPRS shown in **Figure 4.2B1,** the lack of significant toluene formation below 450 °C is due to strongly adsorbed benzene hindering the activation of CH_4 by the active Co sites. In other words, the alkylation is only possible once the benzene has been desorbed

and the sites are available for activation of flowing CH_4, leading to toluene formation at T > 400 °C. All this indicates that the low-temperature formation of toluene in Figure 2A follows an Eley-Rideal mechanism, with CH_4 as the adsorbed reactant. Integration of the curve of toluene formation in the temperature range 200 – 440 °C of the TPSR profile in **Figure 4.2A** gives a production of 183 ± 5 μmol g^{-1} of toluene. Assuming a 1 to 1 adsorption stoichiometry of CH_4 on Co sites, this would correspond to ~ 58% of Co ions able to activate CH_4 for this Eley-Rideal mechanism of benzene alkylation. Conversely, the quantification of benzene desorption in **Figure 4.2B2** and **Figure S 4.9** points to benzene strongly adsorbing 1 to 1 in all Co sites in the absence of CH_4. The toluene formation at high temperatures (450-550 °C) in **Figure 4.2A**is attributed to the reaction of remaining adsorbed CH_4 via the L-H mechanism with flowing C_6H_6, predominant in this temperature region as inferred from reaction orders obtained at 550 °C (**Figure S 4.8**).

Finally, the TPSR profile under CH_4 flow without preadsorbed benzene (**Figure 4.2B2**) shows a benzene formation peak arising at 450 °C. This indicates that Co-ZSM-5 can catalyze the dehydroaromatization of CH_4 to form benzene in this temperature range.[6] In good agreement, toluene is detected under CH_4 flow only (**Figure 4.2B1** dashed line) due to the benzene formed with CH_4. Therefore, we conclude that the reaction of benzene formed from CH_4 contributes to the high-temperature toluene formation (peak at ~550 °C) and biphenyl formation at T > 460 °C in Figure 2 B1.

4.2.6 Mechanism of reaction of benzene CH_4 methylation on Co-ZSM-5.

Combining the results of TPSR experiments and the kinetic analysis, a picture emerges of the different steps involved in the surface activation and reaction of CH_4 and benzene. Based on the quantification of covered BAS per Co by FTIR of pyridine and the changes in activity with Co loading, we have concluded that the active sites are Co^{2+} ions exchanged on the zeolite, in good agreement with earlier studies.[9] Toluene formation reaction orders with respect to benzene (0.4) and CH_4 (0.7) point to a Langmuir-Hinshelwood type of mechanism. This implies that adsorption of benzene and CH_4 in adjacent Co sites is necessary for the reaction to take place at 550 °C.

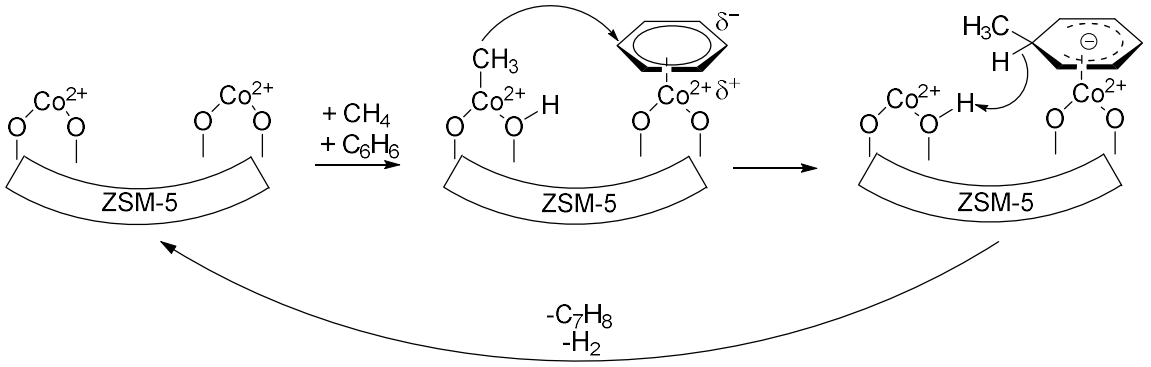

Scheme 4.2: Proposed mechanism of alkylation of benzene with CH_4 over Co-ZSM-5.

TPSR shows that when CH_4 is adsorbed first on Co sites, the formation of toluene in the presence of benzene can occur even at moderate temperatures (starting at 200 °C, **Figure 4.2A**). Conversely, if benzene is adsorbed first on active sites, it either undergoes a bimolecular reaction to form biphenyl or dehydrogenates to coke. However, due to the higher heat of adsorption of benzene on Co sites in comparison to CH_4, it will block sites for the activation of CH_4, hindering the formation of toluene. However, it should be noted that the strongly adsorbed benzene on Co sites is observed to desorb almost entirely at T > 450 °C. At the temperature used in our catalytic tests (550 °C) and the relatively low pressures of benzene used in our tests, we expect that the coverage of Co sites is low.

There is an ongoing discussion if the alkylation of aromatics follows an Eley-Rideal (ER) or a Langmuir-Hinshelwood (LH) mechanism.[18-21] The TPSR results show that activated CH_3 on Co sites can react with benzene following an ER mechanism in the temperature region of 200-400 °C. From the integral of the total toluene formation curve, it can be estimated that the percentage of Co sites that have activated one CH_4 (assuming a 1:1 stoichiometry) is 70%, and 58 % are capable of alkylating benzene via ER mechanism. From the onset of the TPRS profile, we measured 69 kJ mol^{-1} as E_{app} value for the ER alkylation, which is significantly lower than the E_{app} obtained in continuous feed of CH_4 and benzene at T = 500 - 550 °C of 122 kJ mol^{-1}. In this temperature region, reaction orders of 0.7 in CH_4 and 0.4 in benzene point to an L-H mechanism, which dominates the rates because of its higher activation energy. Therefore, we propose that, at the industrially applicable conditions, CH_4 alkylation of benzene proceeds via a concerted mechanism, with the C-C formation as the rate-

determining step on two adjacent Co sites of Co-ZSM-5 as illustrated in Scheme 2. On the one hand, heterolytic activation of CH_4 leads to the formation of CH_3 on Co-based LAS sites and H interacting with framework oxygen. The presence of methoxy species or oxidative activation of CH_4 has been ruled out as described in the SI. This heterolytic dissociation of CH_4 is analogous to reports of CH_4 activation on Co-ZSM-5 or Zn-ZSM-5 for CH_4 dehydroaromatization (MDA).[6, 22-23] Consistently, Co-ZSM-5 catalysts are observed to be active in MDA at temperatures above 500 °C (**Figure 4.2B2,** dashed lines). On the other hand, based on the high ΔH_{ads} of benzene measured on Co-ZSM-5 (~ 260 kJ mol^{-1}), we propose that Co^{2+} species with a strong Lewis acid character are the preferred adsorption sites of benzene. The Lewis acid center decreases the electron density of the aromatic ring, enabling a nucleophilic attack by a CH_3 from a vicinal Co site (**Scheme 4.2**). In a final step, an H- leaving the transition state combines with the H from CH_4 cleavage and forms H_2 and toluene.

The proposed mechanism requires two Co^{2+} sites nearby in the zeolite. Given the nature of the Co sites – exchanged ions in Al pairs that are stochastically distributed on the T sites of the MFI framework – the likelihood of two sites being close to each other increases nonlinearly with Co loading. In good agreement, we have observed an increase in TOF when the concentration of exchanged Co increases in the zeolite (**Figure S 4.10**) following a function that points to a reaction order of 2.6 with respect to Co sites. However, due to this dependency above two, involvement of a third Co site cannot be ruled out at the current status of this study. Moreover, the participation of radicals can also not be completely ruled out at this point. Further studies to clarify this coherence need to be done.

4.3 Chapter conclusion

We have synthesized Co-ZSM-5 materials with most Co exchanged as single Co^{2+} ions on Al pairs. Activity tests in benzene methylation with CH_4 showed that these single Co^{2+} sites are active and form toluene at 550 °C with high selectivity. The benzene adsorption studies on H-ZSM-5 and Co-ZSM-5 showed a strong interaction between benzene and Co sites (ΔH_{ads} = 260 kJ mol^{-1}). Co-ZSM-5 catalyzes two main reaction pathways: the dimerization of benzene to form biphenyl and the alkylation with methane to form toluene. CH_4 partial pressure has a positive impact on the selectivity to toluene because it decreases the rate of the competitive biphenyl formation reaction.

Temperature programmed surface reactions showed that toluene formation by CH_4 alkylation of benzene is possible at mild temperatures (200-400 °C). In this temperature region, an ER mechanism operates with CH_4 as the adsorbed reactant with an energy barrier of 69 kJ/mol. However, the high heat of benzene adsorption on the same Co sites means that, under a feed with both benzene and CH_4, the sites will be poisoned by benzene, hindering this reaction pathway. Lower benzene coverage allows the reaction at higher temperatures, but the dominant pathway is then a concerted mechanism with a higher E_{app} of 112 kJ/mol. Based on the kinetic parameters obtained, we conclude that the activation of CH_4 and benzene is performed by similar Co^{2+} sites. At the industrially compatible temperatures for this application (550 °C), two Co sites must be close to complete the reaction by a concerted mechanism. Therefore, the increase of TOF with the concentration of Co exchanged in ZSM-5 is attributed to a second reaction order of toluene formation with respect to Co sites. Nevertheless, the involvement of a third Co site in this mechanism cannot be ruled out.

4.4 Experimental section

4.4.1 Chemicals

High-purity nitrogen (99.999%), synthetic air (99.995%), 10% oxygen in helium (99.995%), and CH_4 (99.995%) gases were purchased from Westfalen and used without further purification. Cobalt(II)-acetate (99.99%) and benzene (anhydrous, 99.8%) were purchased from Merck.

4.4.2 Material synthesis

NH_4-ZSM-5 zeolite (Si/Al = 15, Zeolyst) was calcined in synthetic air (100 mL min^{-1}) for 10h at 550 °C (10 °C min^{-1}) to obtain the H-form. To prepare the metal exchanged catalysts, 1 g of H-form zeolite was stirred in 50 mL g^{-1} metal salt solution (2.5 mM – 10 mM) at 80 °C for 15 h. The pH value was adjusted to 6.5 with acetic acid. The resulting suspensions were filtered and washed with water, and dried in air.

4.4.3 Infra-Red spectroscopy measurement

The catalysts were characterized by FTIR measurements with a Nicolet iS50 spectrometer from Thermo Scientific to obtain their acid site concentrations. The spectra were recorded in the range of 4000 - 650 cm^{-1} on thin catalyst pellets. After heating to 450 °C for 1h under vacuum (10 °C min^{-1}, 10^{-7} mbar), pyridine (0.5 mbar) was adsorbed at 150 °C for 1h. To obtain only chemisorbed pyridine, the sample was under vacuum (10^{-7} mbar) for one hour.

Benzene adsorption measurements were carried out in a Bruker ifs 66v/S FTIR spectrometer. The spectra were recorded in the range of 8000 - 650 cm^{-1} on thin catalyst pellets. After heating to 450 °C for 1h under vacuum (10 °C min^{-1}, 10^{-7} mbar), benzene was adsorbed stepwise from $7.0 \cdot 10^{-3}$ – 11 mbar. For analysis, the SiOHAl band at 3610 cm^{-1} and C-C band at 1478 cm^{-1} were used for BAS coverage and benzene uptake, respectively.

4.4.4 Atomic absorption spectroscopy

To investigate the element contents in the prepared catalysts, graphite-tube atomic absorption spectroscopy (GT-AAS) was performed on a Solaar M5 AA-Spectrometer from ThermoFischer.

4.4.5 Catalytic testing

The activity of the catalysts was tested in a 1/4" quartz glass plug flow reactor between 500 and 560 °C, under atmospheric pressure. The catalysts were activated in a mixture of 10% oxygen in helium at 550 °C (10 °C min^{-1}) for 2 h. Before starting the reaction, the reactor was purged with nitrogen. The reaction was conducted in nitrogen atmosphere with varied ratios of CH_4/benzene = 33- 170, and WHSV= 0.2 - 2.2 h^{-1}. Reactants and products were analyzed by a GC System Agilent 7890B or a mass spectrometer Omnistar® by Pfeiffer Vacuum.

4.4.6 Temperature programmed surface reaction

For TPSR, the catalyst was activated in a 1/4" quartz glass plug flow reactor at 550 °C in a mixture of 10% oxygen in helium (atm). After purging with inert for 1 h, the catalyst was exposed to CH_4 or benzene at 200 °C for 2.5 h and 0.5 h, respectively. After purging with inert, the catalyst was heated up to 550 °C (5 °C min^{-1}) in benzene (5 mbar) or CH_4 (750 mbar). Reactants and products were analyzed by a mass spectrometer Omnistar® by Pfeiffer Vacuum.

4.5 Supporting Information

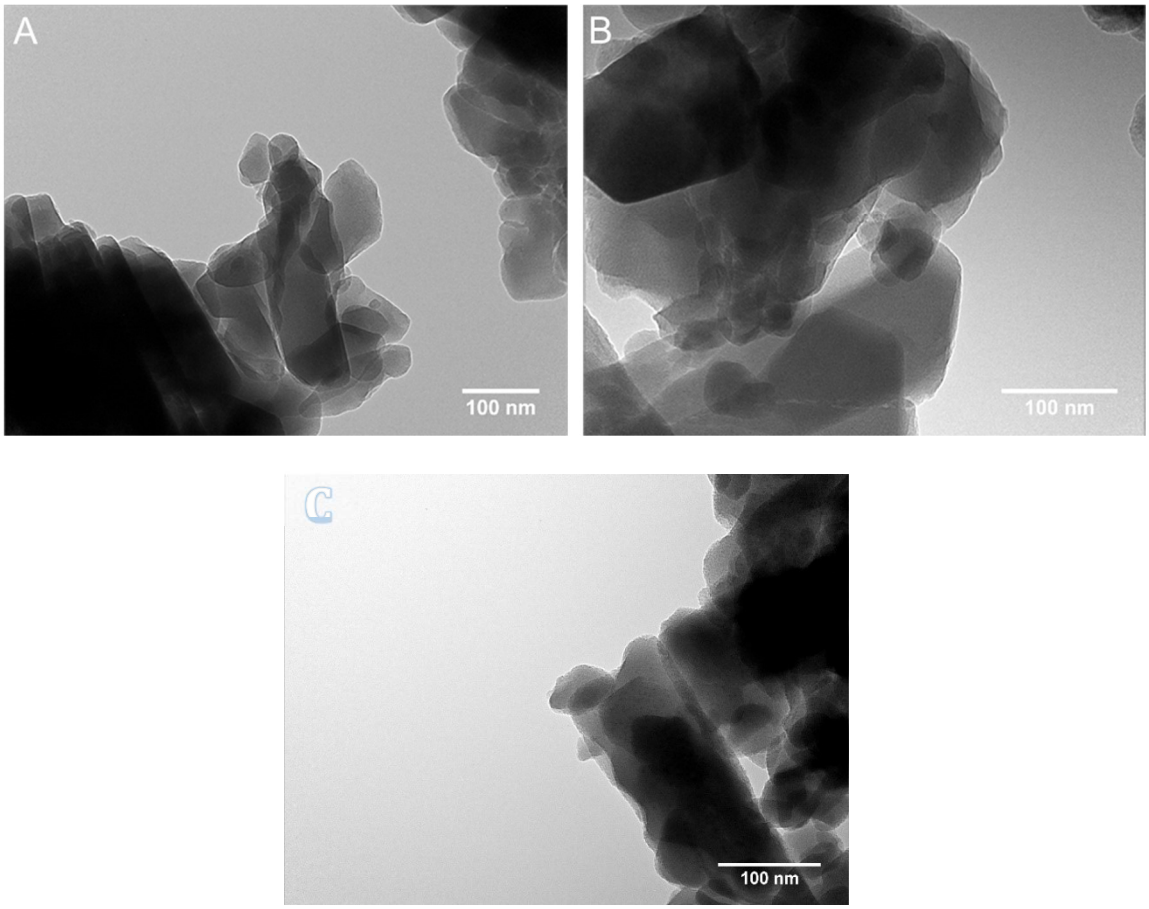

Figure S 4.1 : TEM images of A) H-ZSM-5, B) 314 $\mu mol_{Co}\ g^{-1}$, and C) 453 $\mu mol_{Co}\ g^{-1}$.

TEM was performed using a JEOL JEM 2011 microscope with an accelerating voltage of 120 kV. Prior to measurement, the powdered samples were ultrasonically dispersed and deposited onto a carbon-coated copper tape

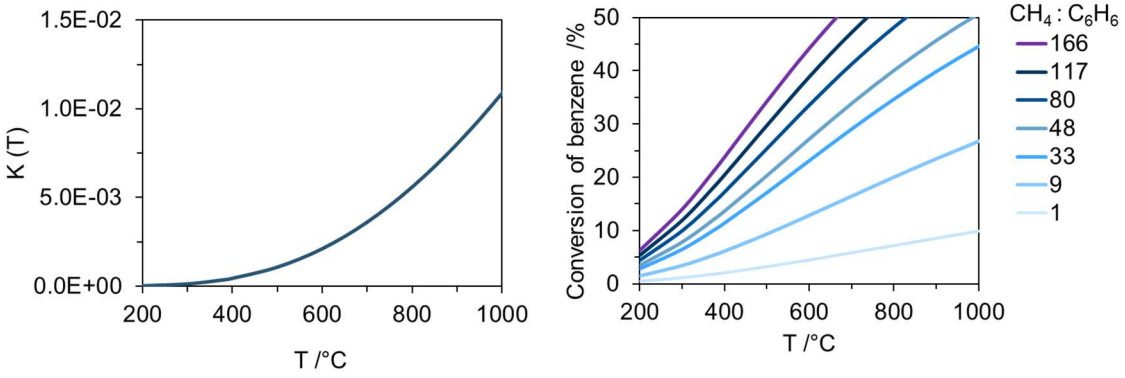

Figure S 4.2: The thermodynamic equilibrium constant K (left) and benzene conversion at different methane to benzene ratios (right) as a function of the temperature.

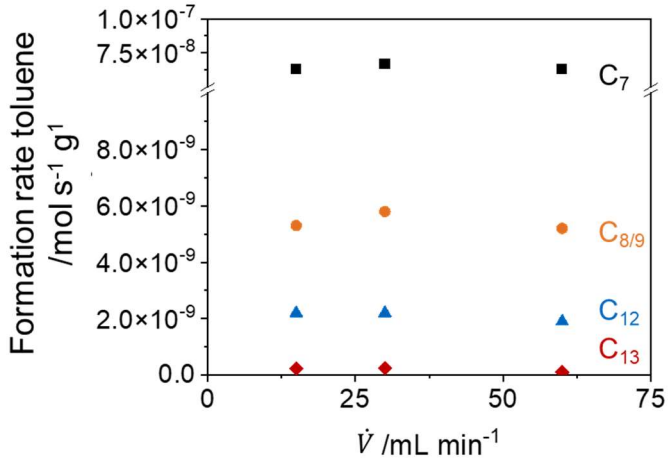

Figure S 4.3: Formation rate of toluene per gram catalyst as a function of volumetric flow rate. toluene (black square), xylenes (orange circle), biphenyl (blue triangle) and phenyltoluene (red diamond). Co content = 321 µmol g^{-1}, T = 550 °C, 1 atm, CH_4: benzene = 160, WHSV = 0.2 h^{-1}.

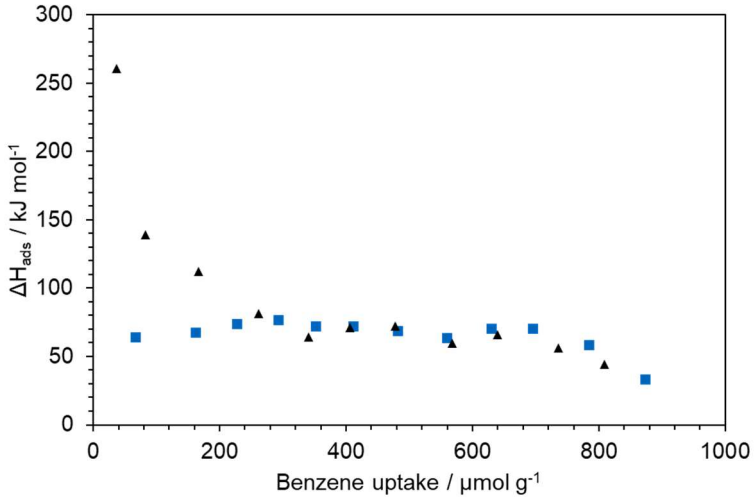

Figure S 4.4*:* Differential heat of sorption on H-ZSM-5 (square, blue) and Co-ZSM-5 (314) (triangle, black) as a function of the benzene uptake at 100°C.

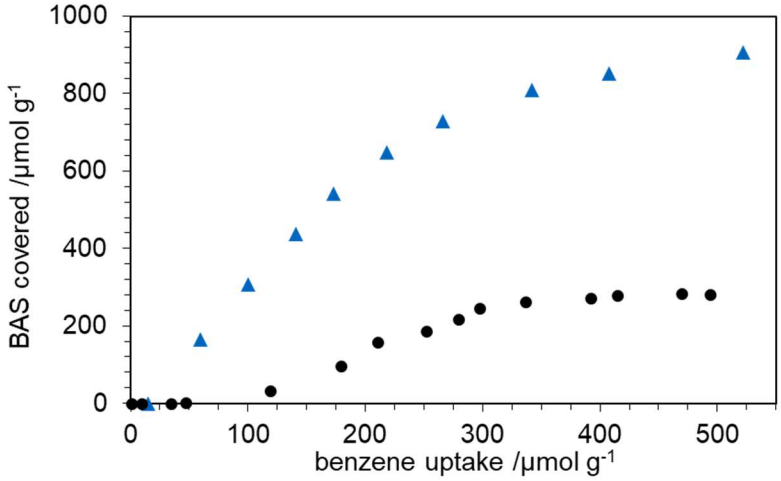

Figure S 4.5: Benzene adsorption on H-ZSM-5 (blue triangle), and Co-ZSM-5 (black circle). Activation for 1 h, 400 °C at $p < 10^{-7}$ mbar. $p_{0,benzene} = 7.0 \cdot 10^{-3} - 1.1 \cdot 10^{1}$ mbar, T = 100 °C.

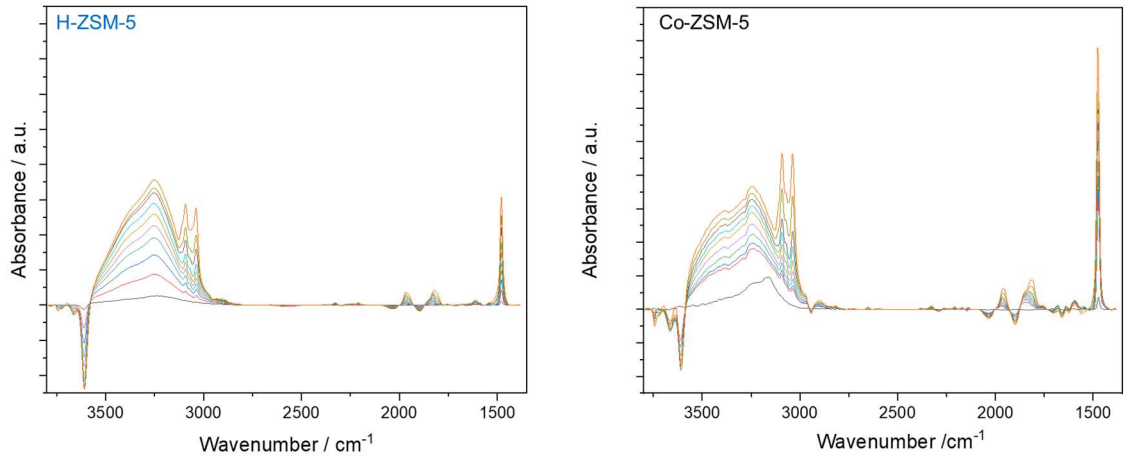

Figure S 4.6: FTIR spectra of benzene adsorption on H-ZSM-5 (left) and Co-ZSM-5 (right). Activation for 1 h, 400 °C at p < 10^{-7} mbar. $p_{0,benzene}$ = $7.0 \cdot 10^{-3}$ – $1.1 \cdot 10^{1}$ mbar, T = 100 °C.

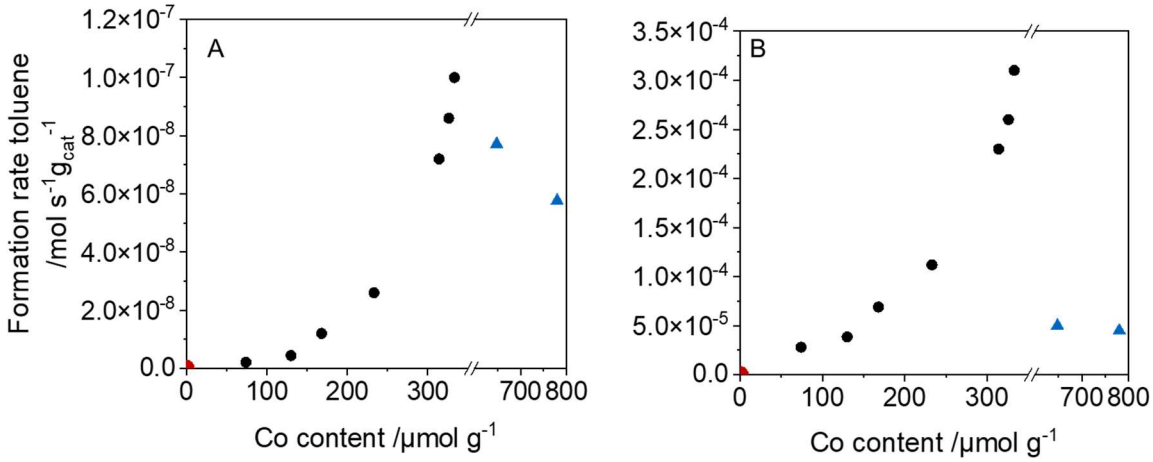

Figure S 4.7: Formation rate of toluene per gram catalyst (A) and per mol Co (B) as a function of Co content. H-ZSM-5 (red square), ion exchanged Co-ZSM-5 (black circle), impregnated Co-ZSM-5 (blue triangle). T = 550 °C, 1 atm, CH_4/ benzene = 80, WHSV = 0.6 h^{-1}.

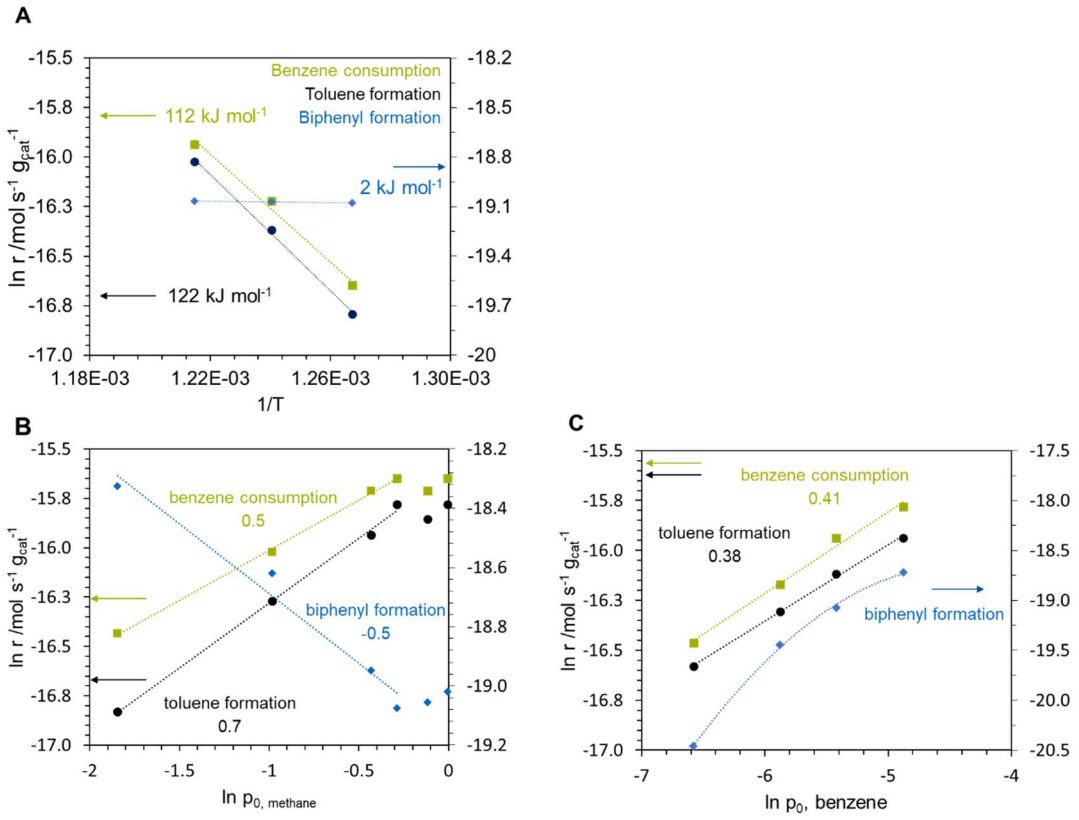

Figure S 4.8: Apparent energy of activation of Co-ZSM-5(314) determined between 783 and 833 K in A). Reaction orders in B) benzene and C) methane were determined for Co-ZSM-5(314). Benzene consumption in square (green), toluene formation in circle (black), and biphenyl formation in diamond (blue).

The data obtained for biphenyl formation shows a positive reaction order with respect to benzene. Because there is a visible deviation from linearity at higher rates, we use the kinetic data at lower partial pressures to obtain a reaction order of 1.0.

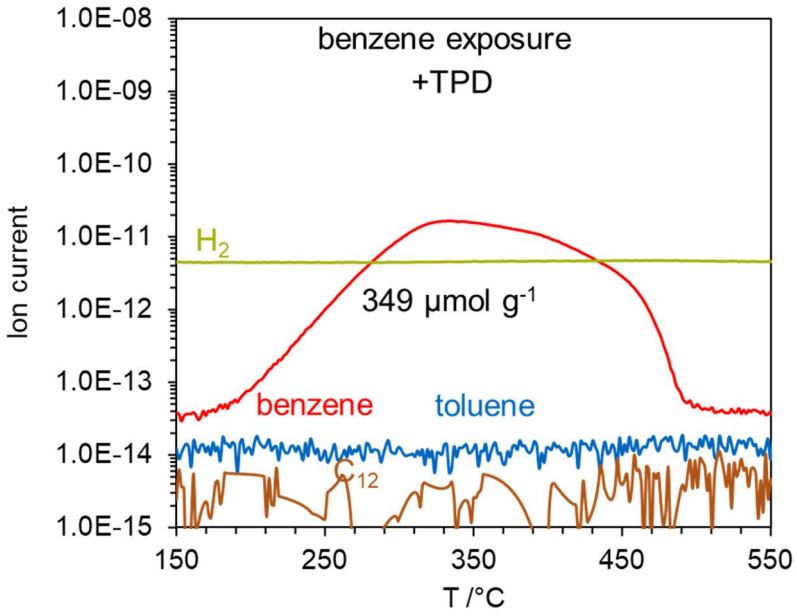

Figure S 4.9: Temperature programmed desorption after benzene exposure (200°C, 5 mbar, 0.5 h), with 5 °C min^{-1}. The y-axis represents the ion current measured by mass spectroscopy: benzene (red), toluene (blue) and biphenyl (brown) left, and hydrogen (green) on the right axis.

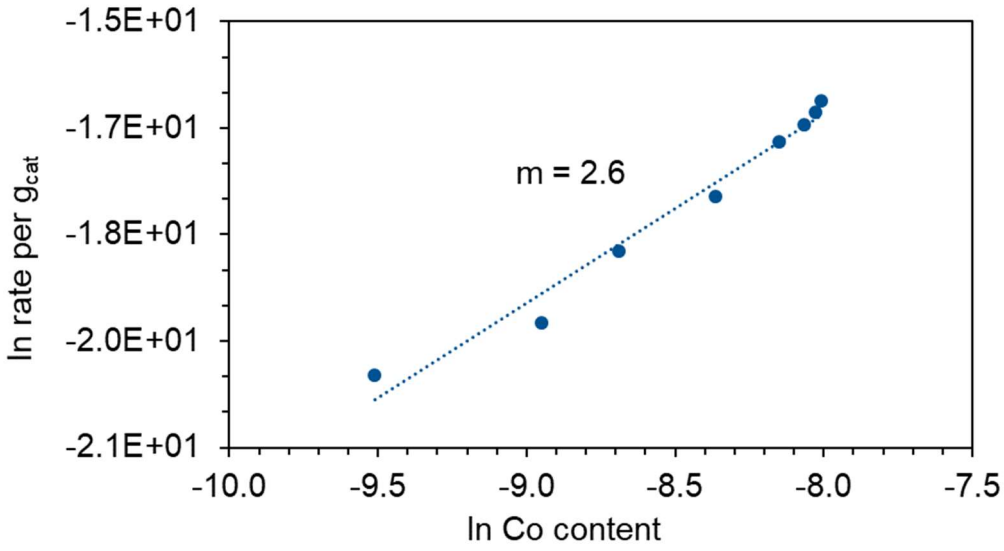

Figure S 4.10: Natural logarithm of formation rate of toluene normalized per $g_{catalyst}$ as a function of natural logarithm of Co loading. T = 550 °C, 1 atm, CH_4/ benzene = 80, WHSV = 0.6 h^{-1}.

4.5.1 Diffusion rates of benzene in H-ZSM-5 and Co-ZSM-5.

The strong adsorption of benzene over Co sites ($\Delta H_{ads} \sim 260$ kJ mol^{-1}) may affect the diffusion of this molecule through the zeolite micropores. In order to rule out any diffusion limitation, we have determined the diffusion rates of benzene in H-ZSM-5 and Co-ZSM-5, by measuring the concentration changes of benzene in an IR cell by square wave pressure perturbations according to the procedure of Fast Time-Resolved Rapid Scan IR Spectroscopy reported in a former work of Reitmeier *et al.*.[24] **Figure S 4.11** in Supporting Information shows that benzene diffusion rate is 11.0 ± 0.5 µmol s^{-1} g^{-1} in the H-ZSM-5. In contrast, the Co sample shows a slightly lower diffusion rate (4.6 ± 0.2 µmol s $^{-1}$ g^{-1}). Therefore, although the strong adsorption of benzene on the Co sites seems to impact the diffusivity of benzene, the differences are not expected to affect catalytic measurements because the reaction rates are still two orders of magnitude higher.

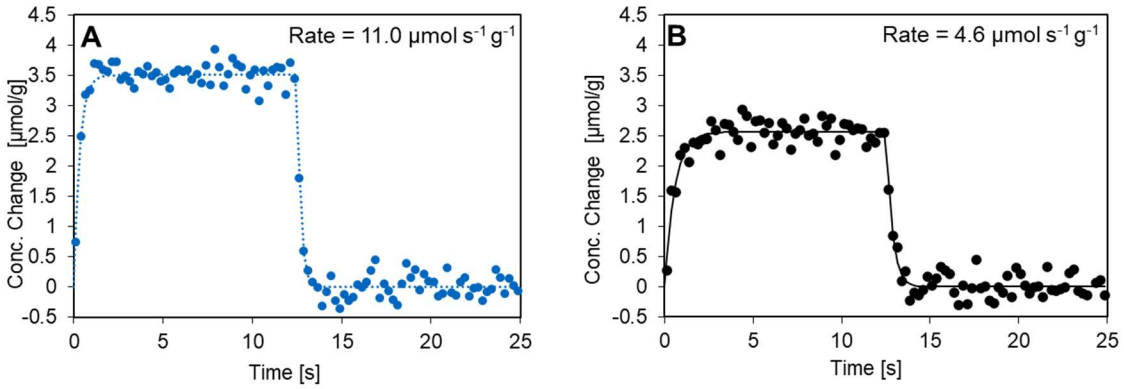

Figure S 4.11: Concentration change profile for benzene adsorbed on A) H-ZSM-5 and B) Co-ZSM-5(314) induced by square wave pressure perturbations with a modulation frequency of 1/25 s^{-1}. Activation 1h, 400°C, 10^{-7} mbar; $p_{0,equ}$ = 0.15 mbar. Concentration change was calculated from the C–C stretching vibrational band of benzene.

4.5.2 Desorption of CH_4 activation products under steam flow

The catalyst Co-ZSM-5 with 314 γmol_{Co} g_{cat}^{-1} was activated in a plug flow reactor at 500 °C in a mixture of 10% oxygen in helium (atm). After purging with inert for 1 h, the catalyst was exposed to CH_4 at 200 °C for 2.5 h. After purging with inert, the

catalyst was exposed to 20% H_2O in helium at 135°C for 1 h. Desorbed gases were analyzed by a mass spectrometer by Pfeiffer Vacuum.

No CO_2, MeOH, or DME could be detected during the steam treatment. With this absence of products, the presence of methoxy species or an oxidative activation can be ruled out.[25]

4.6 References

1. Taifan, W.; Baltrusaitis, J., CH 4 conversion to value added products: Potential, limitations and extensions of a single step heterogeneous catalysis. *Applied Catalysis B: Environmental* **2016,** *198*, 525-547.

2. Pinaeva, L. G.; Noskov, A. S.; Parmon, V. N., Prospects for the direct catalytic conversion of methane into useful chemical products. *Catalysis in Industry* **2017,** *9* (4), 283-298.

3. Wang, L.; Tao, L.; Xie, M.; Xu, G.; Huang, J.; Xu, Y., Dehydrogenation and aromatization of methane under non-oxidizing conditions. *Catalysis Letters* **1993,** *21* (1), 35-41.

4. Abdelsayed, V.; Shekhawat, D.; Smith, M. W., Effect of Fe and Zn promoters on Mo/HZSM-5 catalyst for methane dehydroaromatization. *Fuel* **2015,** *139*, 401-410.

5. Sun, K.; Ginosar, D. M.; He, T.; Zhang, Y.; Fan, M.; Chen, R., Progress in Nonoxidative Dehydroaromatization of Methane in the Last 6 Years. *Industrial & Engineering Chemistry Research* **2018,** *57* (6), 1768-1789.

6. Xu, Y.; Chen, M.; Wang, T.; Liu, B.; Jiang, F.; Liu, X., Probing cobalt localization on HZSM-5 for efficient methane dehydroaromatization catalysts. *Journal of Catalysis* **2020,** *387*, 102-118.

7. Nakamura, K.; Okumura, K.; Tsuji, E.; Suganuma, S.; Katada, N., Reactivity of Methane and Benzene over Metal/MFI Zeolite Analyzed with Temperature-Programmed Reaction Technique. *ChemCatChem* **2020,** *12* (8), 2333-2340.

8. Nakamura, K.; Okuda, A.; Ohta, K.; Matsubara, H.; Okumura, K.; Yamamoto, K.; Itagaki, R.; Suganuma, S.; Tsuji, E.; Katada, N., Direct Methylation of Benzene with Methane Catalyzed by Co/MFI Zeolite. *ChemCatChem* **2018,** *10* (17), 3806-3812.

9. Matsubara, H.; Tsuji, E.; Moriwaki, Y.; Okumura, K.; Yamamoto, K.; Nakamura, K.; Suganuma, S.; Katada, N., Selective Formation of Active Cobalt Species for Direct Methylation of Benzene with Methane on MFI Zeolite by Co-presence of Secondary Elements. *Catalysis Letters* **2019,** *149* (9), 2627-2635.

10. Hu, P.; Nakamura, K.; Matsubara, H.; Iyoki, K.; Yanaba, Y.; Okumura, K.; Okubo, T.; Katada, N.; Wakihara, T., Comparative study of direct methylation of benzene with methane on cobalt-exchanged ZSM-5 and ZSM-11 zeolites. *Applied Catalysis A: General* **2020,** *601*.

11. Adebajo, M. O., Green chemistry perspectives of methane conversion via oxidative methylation of aromatics over zeolite catalysts. *Green Chemistry* **2007,** *9* (6).

12. Lukyanov, D. B.; Vazhnova, T., Selective and stable benzene alkylation with methane into toluene over PtH-MFI bifunctional catalyst. *Journal of Molecular Catalysis A: Chemical* **2009,** *305* (1-2), 95-99.

13. Matsubara, H.; Yamamoto, K.; Tsuji, E.; Okumura, K.; Nakamura, K.; Suganuma, S.; Katada, N., Position and Lewis acidic property of active cobalt species on MFI zeolite for catalytic methylation of benzene with methane. *Microporous and Mesoporous Materials* **2021,** *310*.

14. Dědeček, J.; Kaucký, D.; Wichterlová, B.; Gonsiorová, O., Co2+ions as probes of Al distribution in the framework of zeolites. ZSM-5 study. *Phys. Chem. Chem. Phys.* **2002,** *4* (21), 5406-5413.

15. Hirschler, A. E., The measurement of catalyst acidity using indicators forming stable surface carbonium ions. *Journal of Catalysis* **1963,** *2* (5), 428-439.

16. Grundner, S.; Luo, W.; Sanchez-Sanchez, M.; Lercher, J. A., Synthesis of single-site copper catalysts for methane partial oxidation. *Chemical Communications* **2016,** *52* (12), 2553-2556.

17. Pope, C., Sorption of benzene, toluene and p-xylene on silicalite and H-ZSM-5. *The Journal of Physical Chemistry* **1986,** *90* (5), 835-837.

18. Corma, A.; Marti nez-Soria, V.; Schnoeveld, E., Alkylation of Benzene with Short-Chain Olefins over MCM-22 Zeolite: Catalytic Behaviour and Kinetic Mechanism. *Journal of Catalysis* **2000,** *192* (1), 163-173.

19. Smirniotis, P. G.; Ruckstein, E., *Ind. Eng. Chem. Res.* **1995,** *34*, 1517-1528.

20. Sealy, S.; Traa, Y., Direct alkylation of toluene with ethane on bifunctional zeolite catalysts. *Applied Catalysis A: General* **2005,** *294* (2), 273-278.

21. Mirth, G.; Lercher, J. A., Coadsorption of toluene and methanol on HZSM-5 zeolites. *The Journal of Physical Chemistry* **1991,** *95* (9), 3736-3740.

22. Oda, A.; Torigoe, H.; Itadani, A.; Ohkubo, T.; Yumura, T.; Kobayashi, H.; Kuroda, Y., An Important Factor in CH4 Activation by Zn Ion in Comparison with Mg Ion in MFI: The Superior Electron-Accepting Nature of Zn2+. *The Journal of Physical Chemistry C* **2014,** *118* (28), 15234-15241.

23. Gabrienko, A. A.; Arzumanov, S. S.; Toktarev, A. V.; Danilova, I. G.; Prosvirin, I. P.; Kriventsov, V. V.; Zaikovskii, V. I.; Freude, D.; Stepanov, A. G., Different Efficiency of Zn2+ and ZnO Species for Methane Activation on Zn-Modified Zeolite. *ACS Catalysis* **2017,** *7* (3), 1818-1830.

24. Reitmeier, S. J.; Mukti, R. R.; Jentys, A.; Lercher, J. A., Surface Transport Processes and Sticking Probability of Aromatic Molecules in HZSM-5. *The Journal of Physical Chemistry C* **2009,** *113* (4), 1640-1640.

25. Li, G.; Vassilev, P.; Sanchez-Sanchez, M.; Lercher, J. A.; Hensen, E. J. M.; Pidko, E. A., Stability and reactivity of copper oxo-clusters in ZSM-5 zeolite for selective methane oxidation to methanol. *Journal of Catalysis* **2016,** *338*, 305-312.

5 Nature of active site

The following chapter is based on unpublished results. The manuscript will be submitted by Martina Aigner[1], Rachit Khare[1], Andreas Jentys[1], Stijn Van Daele,[2] Maricruz Sanchez-Sanchez[1], and Johannes A. Lercher[1].

Martina Aigner performed the main manuscript preparation and all experiments unless otherwise noted. Rachit Khare supported and analyzed the XAS experiments. Andreas Jentys, Stijn Van Daele, Maricruz Sanchez-Sanchez, and Johannes A. Lercher supported the research. The manuscript was written with the involvement of all named authors.

Abstract

The metal precursor for the ion exchange in ZSM-5 and the resulting location of active sites within a Co-ZSM-5 played an essential role in the alkylation of benzene with methane. By benzene adsorption followed by infra-red spectroscopy, three Al sites in proximity, so-called triple sites were established. UV-Vis spectroscopic characterization showed that Co-ZSM-5 synthesized with Co acetate mainly was exchanged in the intersection and the main channel of the zeolite. In contrast, more Co was exchanged in the sinusoidal channel when Co nitrate was used to synthesize Co-ZSM-5. Combining these results made the quantification and localization of these triple sites and paired or single sites possible. Compared to active sites in different positions, the product distribution showed that Co^{2+} exchanged in sinusoidal channel enhanced secondary reactions from toluene towards xylenes and phenyltoluene.

5.1 Introduction

Besides its combustion, the most common ways to turn methane into value consists of CH_4 reforming, pyrolysis, coupling, or selective oxidation. In all processes, the most challenging part is activating the highly stable C-H bond. Efforts to overcome this high energy barrier (~ 434 kJ mol^{-1}) imply harsh conditions or the use of heterogeneous catalysts.[1-2] Noble metal catalysts such as Ru, Rh, and Pt are already known to activate CH_4, but due to their rareness and high costs, Co, Ni, Cu, and Mo have been intensively studied.[2-5]

In particular, Mo and Co exchanged zeolites like ZSM-5 have been reported to convert CH_4 via methane dehydroaromatization (MDA) or selective catalytic reduction (SCR) of nitrogen oxides[6 7] Another interesting reaction is the direct alkylation of aromatics with CH_4 using metal-supported ZSM-5. The simplest case is the alkylation of benzene with methane to produce toluene and hydrogen - both highly demanded chemicals.

Since Co-ZSM-5 got in the focus of CH_4 activation, the group of N. Katada has also tested it in the alkylation of benzene in a comparative study (500°C, p_{CH4} = 98.6 kPa, p_{C6H6} = 2.7 kPa and $W_{cat}/F_{benzene}$ = 147 g_{cat} h $mol_{benzene}$) with different metals and support.[8] They found Co-ZSM-5 to be the most suitable catalyst so far. Matsubara et al. proposed that only Co^{2+} in the α exchange position of ZSM-5 – that is, Co exchanged in the straight channels of MFI structure - is active in the reaction of CH_4 methylation of benzene.[9-10] Our recent mechanistic study has led us to conclude that CH_4 methylation of benzene on Co-ZSM-5 takes place through a concerted mechanism that requires two Co in proximity. Thus, the exchange of Co in specific sites where statistically more than one Co ion can be accessible by reactants can significantly boost the activity of the materials.

This chapter aims to gain insight into the nature and location of Co active sites in Co-ZSM-5 for the direct methylation of benzene with CH_4. The combination of several characterization methods, the use of probe molecules, and activity tests of Co-ZSM-5 materials with different Co siting allowed a quantitative analysis of Co ions exchanged in different framework positions and their role in activity and selectivity in benzene alkylation with methane.

5.2 Results and discussion

5.2.1 Catalytic performance

We tested a series of Co-ZSM-5 catalysts with different concentrations of Co exchanged by using $Co(CH_3COO)_2$ and $Co(NO_3)_2$ aqueous solutions. The rationale to use other Co salt precursors is their different behavior in an aqueous solution. Co^{2+} from nitrate mainly forms hexaaqua-complexes, while Co^{2+} in acetate solution can also form complexes in non-octahedral symmetry.[10] This, together with different pH, can influence the nature of the resulting Co sites in terms of their exchange position and dispersion.[11] Organic precursors such as acetates are reported to exchange equally within the zeolite pores compared to inorganic salts like Cobalt nitrate. [12-13]

It should be noted that when Co acetate is used for ion exchange via wet impregnation, the highest concentration that can be reached is ca. 330 μmol g^{-1} of Co, corresponding to a Co/Al ratio of 0.3. Higher Co contents were only achieved by incipient wetness impregnation, and they imply precipitation of CoO_x particles as determined by TEM (**Figure S 5.1**).

We found that the turnover frequency of Co sites for benzene alkylation with CH_4 increases with Co loading (see **Figure 5.1**). Increasing the Co content from 74 to 333 μmol g^{-1} enhances the toluene formation rates by one order of magnitude. This increase in activity per Co follows a function that points to a reaction order of 2 in Co. This is first consistent with a mechanism that requires two independent, active sites for one catalytic cycle, i.e., for the activation of CH_4 and benzene, respectively, as we previously deduced in mechanistic studies (see chapter 4). In good agreement, the activity per Co for those catalysts with a Co content above 350 μmol g^{-1} is significantly lower than for ion-exchanged samples, indicating a significant concentration of inactive Co particles. Based on this, we conclude that the main dominant active species are Co ions exchanged on Al T-sites.

The apparent activation energy for toluene formation in the temperature range 500 – 550 °C was found to be ~126 kJ mol^{-1} (**Table S 5.1** and **Figure S 5.2**). The reaction orders in methane and benzene were ~0.7 and ~0.4, respectively. Similar activation energies and reaction orders for all Co-ZSM-5 catalysts indicate that the reaction mechanism does not change with Co loading and all samples have similar active sites.

Therefore, we propose that the differences in TOF are due to different concentrations of Co active sites depending on the degree of exchange of ZSM-5.

5.2.2 Oxidation state of the active site

IR spectra of adsorbed probe molecules such as NO and CO can give insight into the oxidation state of Co sites.[14-16] **Figure 5.2A** shows the FTIR spectra of NO adsorbed on ZSM-5 samples with two different Co loadings and the parent H-ZSM-5 material. Three prominent bands can be detected at 1816, 1897, and 1943 cm^{-1}. The bands at 1897 cm^{-1} and 1816 cm^{-1} have been attributed to vibration of two NO adsorbed on one Co as ($Co^{2+}(NO)_2$). The band at 1943 cm^{-1} consists of two contributions at 1940 cm^{-1} and 1957 cm^{-1} that we attribute to Co^{3+}-NO and Co^{2+}-NO, respectively.[14] The shoulder at 1880 cm^{-1} is attributed to NO adsorbed on SiOHAl sites, which can be seen in all samples.[14] In **Figure S 5.3** in SI, the evolution of these bands with increasing partial pressure of NO can be followed. The presence of Co^{3+} might be related to Co oxide nanoclusters that migrate and aggregate to form Co_3O_4 during calcination or by stabilization of Co^{3+} ions by three negative charges/Al T-sites.[17-19] Nevertheless, due to the low intensity of these bands related to Co^{3+}, Co^{2+} species are regarded as the majority of sites in Co-ZSM-5.

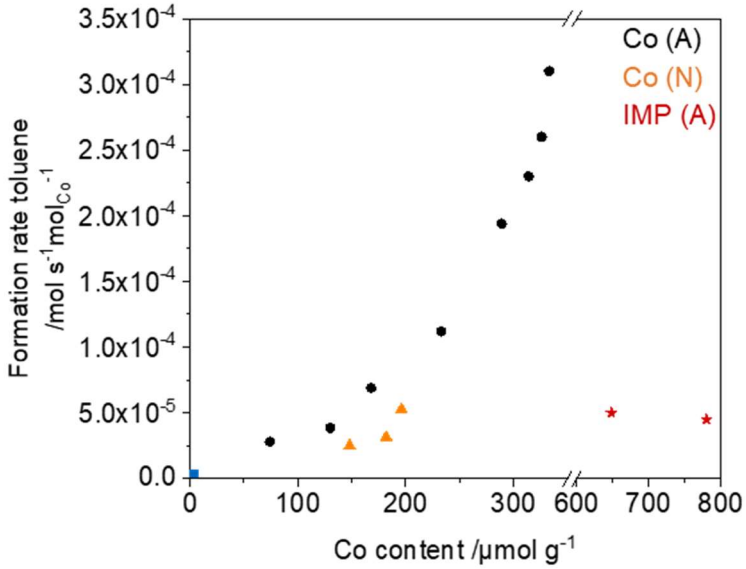

Figure 5.1: Formation rate of toluene per Co for H-ZSM-5 Co-ZSM-5 IE with acetate (circle), IE with nitrate (triangle), and impregnated (star) at WHSV 0.6 h^{-1}, 550°C, 5 mbar benzene, and 400 mbar CH_4.

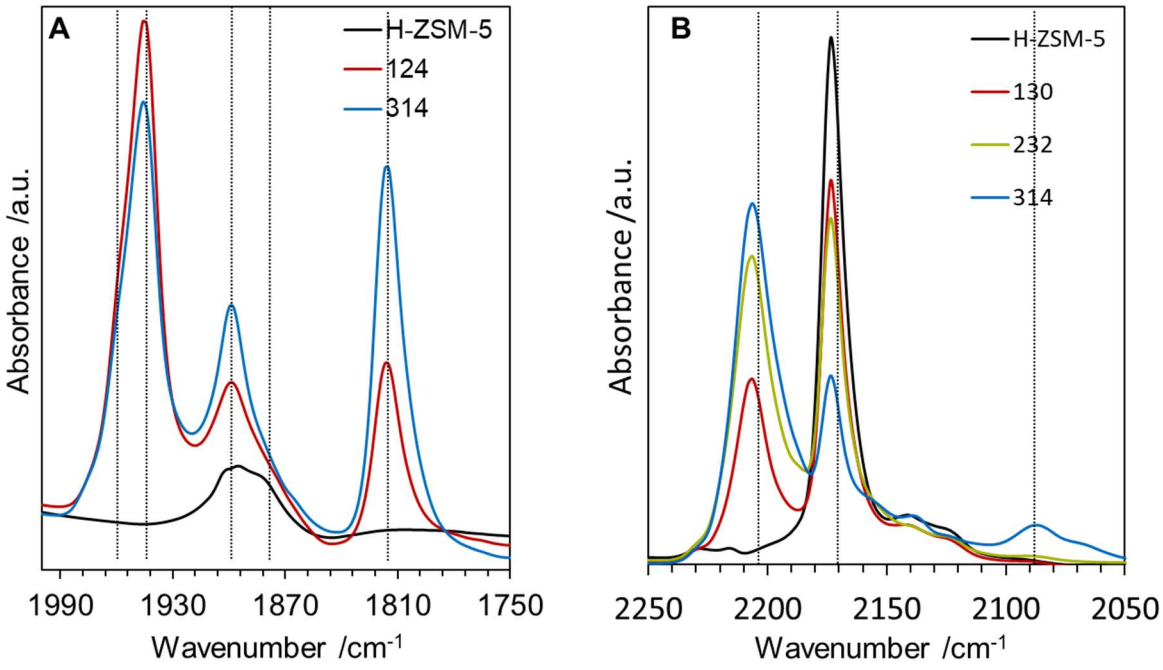

Figure 5.2: FTIR spectra of **A)** NO and **B)** CO adsorbed on ZSM-5 with different Co loading at 77 K and $p_{0,NO}$ = 1.4 ·10^{-1} mbar, $p_{0,CO}$ = 1.9 ·10^{-1} mbar. Activation for 1h at 450°C in a vacuum.

FTIR region of carbonyl stretching vibration of CO adsorbed on H-ZSM-5 and Co-ZSM-5 with different Co content is shown in **Figure 5.2**. The most intense band for all samples is at 2175 cm^{-1}, attributed to CO adsorbed on BAS (SiOHAl) of ZSM-5. The band at 2207 cm^{-1} is visible only in Co-containing samples and can therefore be assigned to CO interacting with Co^{2+} sites.[16, 20] In good agreement, the intensity of this band increases with Co loading, while the band for CO adsorbed on BAS decreases. The sample with the highest Co content in our series (314 $\mu mol_{Co}\ g_{cat}^{-1}$) shows an additional band at 2087 cm^{-1}. According to Hadjiivanov et al., this can be attributed to $Co^{+}(CO)_3$, with Co^{+} being formed via reduction with CO of $[Co\text{-}O\text{-}Co]^{2+}$ species.[16]

From NO and CO adsorption experiments, we conclude that the Co is mainly hosted as isolated Co^{2+} ions, with a small contribution of Co^{3+} and $[Co\text{-}O\text{-}Co]^{2+}$ in the samples with high Co loading.

Finally, Co K edge *in situ* X-ray absorption near-edge structure (XANES) and extended X-ray absorption fine structure (EXAFS) measurements were obtained for activated ZSM-5 catalysts with 233 and 326 $\mu mol_{Co}\ g_{cat}^{-1}$ (see **Table S 5.2**, **Table S 5.3**, **Figure S 5.4**, **Figure S 5.5**). XANES confirmed an oxidation state of Co to be primarily Co(II) with a small contribution of Co(III). The EXAFS, for both samples, suggests isolated Co sites without any significant Co-Co interactions. EXAFS fitting parameters are shown in table S1 and S2 in SI.

IR spectra of adsorbed pyridine were used to determine the degree of exchange of the zeolite BAS with Co ions. The concentration of BAS that has been exchanged by Co ions was quantified by comparison with the concentration of BAS present in the parent H-ZSM-5 (**Table S 5.1**). For catalysts with Co content < 170 $\mu mol\ g_{cat}^{-1}$ the ratio of covered BAS per Co is 2.0 ± 0.1. With increasing Co loading, this BAS/Co ratio decreases slightly but remains ≥ 1.7 ± 0.1. This is consistent with a majority of divalent Co ions at Al pairs, thus exchanging two BAS. We attribute the decrease in BAS/Co ratio to a small fraction of exchanged $[Co\text{-}O\text{-}Co]^{2+}$ species (nominal BAS/Co = 1) and/or formation of CoO_x nanoparticles (nominal BAS/Co = 0) at high Co loadings.

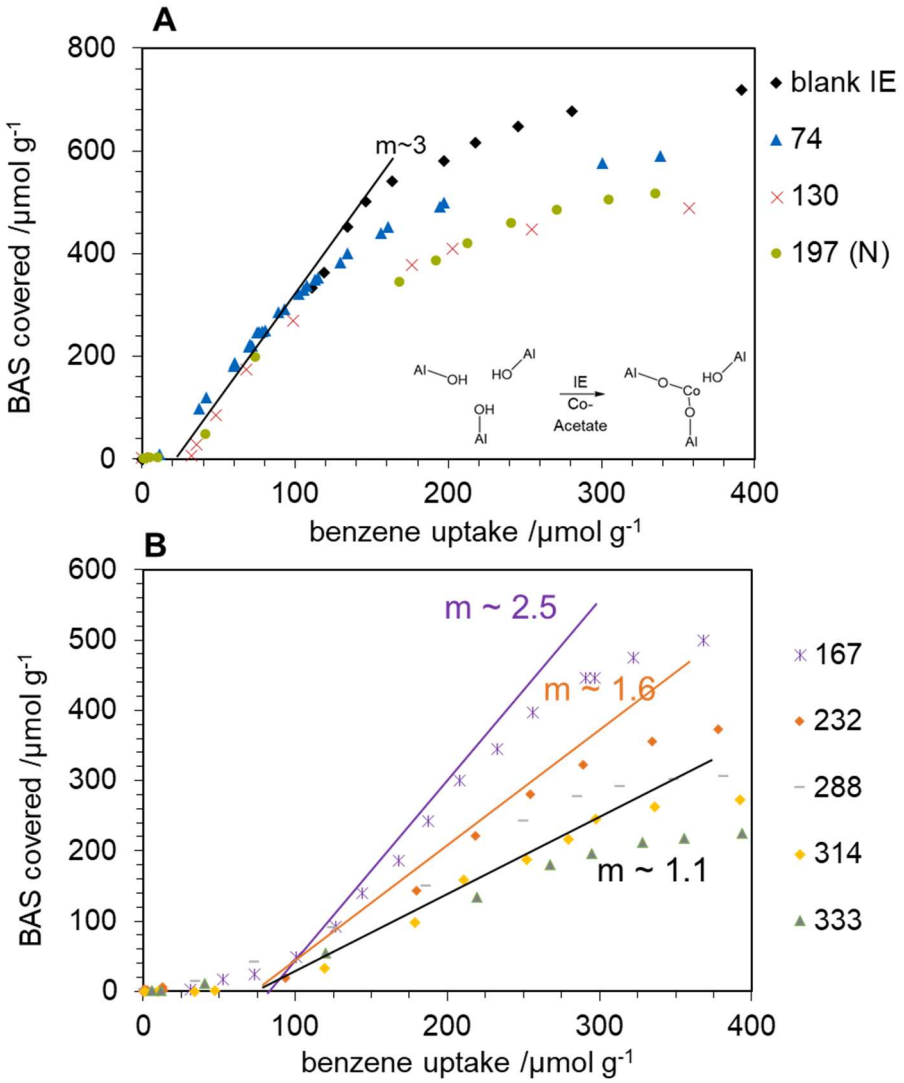

Figure 5.3: Benzene adsorption on H-ZSM-5 and Co-ZSM-5 with different Co loadings followed via FTIR. Activation for 1 h, 400 °C at vacuum. $p_{0,benzene}$ = $7.0 \cdot 10^{-3}$ – $1.1 \cdot 10^{1}$ mbar, T = 100 °C.

Overall, the spectroscopic analysis of Co-ZSM-5 with Co loadings in the range from 74 µmol g_{cat}^{-1} to 314 µmol g_{cat}^{-1} shows that Co is mainly hosted as isolated Co^{2+} ions exchanged in Al pairs, with small concentrations of $[Co\text{-}O\text{-}Co]^{2+}$ in the samples with high Co loading. With the present experimental evidence, we cannot rule out the formation of small concentrations of Co_2O_3 nanoparticles. Still, we regard them negligible in terms of the catalytic and material properties of these Co-ZSM-5 samples.

5.2.3 Location of active sites

The specific location of Co^{2+} ions exchanged in Al pairs in ZSM-5 can be determined by examining the IR spectra of Co-ZSM-5 samples after stepwise adsorption of benzene pulses. Figure S 5.6 shows the evolution in benzene uptake with increasing pressure for Co-ZSM-5 with different Co and BAS concentrations. The amount of adsorbed benzene was determined by benzene's C-C stretching vibration band at ~ 1475 cm^{-1}. The BAS coverage was inferred from the decrease of the band at ~3610 cm^{-1} for SiOHAl, based on a molar extinction coefficient for this vibration obtained for the parent H-ZSM-5, based on the BAS concentration determined by pyridine adsorption.

When small pressures of benzene are dosed to Co containing samples, a band of C-C vibration at 1472 cm^{-1} evolves with increasing p_0 of benzene without affecting BAS OH vibration (**Figure S 5.6**). This indicates preferential benzene adsorption on Co sites, in good agreement with the strong Lewis acid-base interaction between Co and benzene that we have previously reported (see chapter 4). Using TGA/DSC, we have measured a ΔH_{ads} of 260 kJ mol^{-1} for benzene over Co-ZSM-5 (314 μmol_{Co} g^{-1}) in contrast to a ΔH_{ads} of 65 kJ mol^{-1} for benzene over BAS on H-ZSM-5. Therefore, we attribute the band at 1472 cm^{-1} to benzene adsorbed on Co^{2+} sites in ZSM-5, similar to the band at 1468 cm^{-1} reported for benzene interacting with Cu on ZSM-5.[21] The slight blue shift with respect to Cu ions is also consistent with a strong Lewis acid character of Co^{2+} species, leading to a weaker C-C bond of benzene upon adsorption. At $p_0 > 8.5 \cdot 10^{-3}$ mbar, a shoulder at ~ 1478 cm^{-1} arises for Co-ZSM-5 samples, attributed to the C-C vibration of benzene adsorbed on Si-OH-Al groups in ZSM-5. [21]

Based on the benzene adsorption followed by IR spectroscopy, the amount of BAS covered per introduced benzene molecule can be calculated via the decrease of intensity of the SiOHAl band at ~3610 cm^{-1} and the increase of the C-C vibration at ~1475 cm^{-1}. In **Figure 5.3**, it can be seen that, for an H-ZSM-5 reference washed with acetate solution (blank experiment), the decrease of the BAS O-H vibration with an increase of benzene uptake follows a linear correlation with a slope of three at low pressures. This indicates that three BAS are covered by one benzene molecule, up to a coverage of ~ 600 μmol g^{-1} BAS. We attribute this to benzene adsorption in the

intersections of 10-MR sinusoidal and straight channels in MFI. In this position, one benzene molecule can perturb the O-H vibration of up to three protons in proximity[17], shifting the O-H IR absorption to lower wavenumbers. Such "triple sites" thus leading to the apparent disappearance of three BAS per molecule of benzene.

For Co-ZSM-5 catalysts with loadings below 150 $\mu mol_{Co}\ g^{-1}$, benzene adsorption on triple sites was also detected at low uptakes (**Figure 5.3A**). We can quantify the concentration of triple sites by the total benzene uptake reached when the trend deviates from the linear correlation with slope = 3. Comparing with the concentration of triple sites in parent HZSM-5, we can determine the fraction of Co in Co-ZSM-5 materials exchanged with protons that are part of triple sites (**Figure 5.4**). Having observed that Co generally exchanges with two BAS protons (Table 1 in SI), it is reasonable to assume that one BAS is left free when Co is exchanged at the triple site location.

At Co loadings above 150 $\mu mol_{Co}\ g^{-1}$, **Figure 5.3B** shows a different profile of BAS coverage vs. benzene uptake. At low benzene uptakes, the BAS are not interacting with benzene, indicative again of the preferential adsorption of benzene on Co sites. There is a linear correlation with a coverage of 2.5 to 1.1 BAS covered per benzene molecule at higher pressures. A slope of ca. 1 BAS covered by 1 benzene indicates benzene adsorption on relatively isolated BAS. For the samples with a slope between 1 and 3, benzene adsorption occurs both in free triple sites and isolated BAS. Therefore, we propose that Co ions are exchanged in different positions in such samples. Their relative concentrations can be quantified assuming proportional contributions of Co exchanged in triple sites and Co exchanged in other Al pairs. It should be noted that BAS that are isolated from the point of view of benzene adsorption (that is, they adsorb benzene in a 1:1 ratio) can be, however, paired and therefore allow the exchange of Co^{2+} ions when they are available in suitable concentrations. On the other hand, this technique cannot detect when benzene is adsorbed on Co sites that are sitting far from any other BAS (so, not in triple sites). These sites can only be quantified when they preferentially adsorb benzene at very low pressures before any BAS perturbation is detected (as in samples 167-333 $\mu mol_{Co}\ g^{-1}$). In **Table S 5.4**, we provide further details of the calculation of the concentration of Co sites in different positions of ZSM-5 based on this technique

Figure 5.4A shows the concentration of Co^{2+} exchanged in triple sites - that is, in the ZSM-5 channel intersections - as deduced from benzene adsorption experiments. The limit of ~200 μmol g^{-1} Co concentration found for the triple sites is in good agreement with the total amount of BAS in triple sites as quantified by benzene adsorption on H-ZSM-5 (~ 600 μmol g^{-1}). In **Figure 5.4A** also shows that the concentration of Co exchanged in non-triple BAS increases linearly with increasing Co loading.

Based on the benzene adsorption, it can be seen that the Co ion exchange occurs both in triple and non-triple sites. However, once all triple sites are exchanged with Co ions at about 280 μmol $g^{-1}$of Co, all the exchangeable Co excess is directed to dual/single sites within the 10-MR channels. On the other hand, one can see that catalysts without free "triple sites" correspond to those with the highest TOF_{Co} (**Figure 5.1**). Therefore, we speculate that the relatively more significant proportion of Co in the channels regarding the intersections leads to this higher activity per Co.

The finer detail of the siting of Co ions can be obtained with in situ spectroscopic UV-Vis measurements. Three different ion-exchange positions, viz. α, β, and γ, of Co^{2+}, have been proposed in the literature for ZSM-5, based on the other features in UV-Vis absorption spectra.[9-10, 22] Co^{2+} exchanged in each of these positions leads to a triplet of absorption bands that partially superimposed with the others.[6, 10, 22-23]

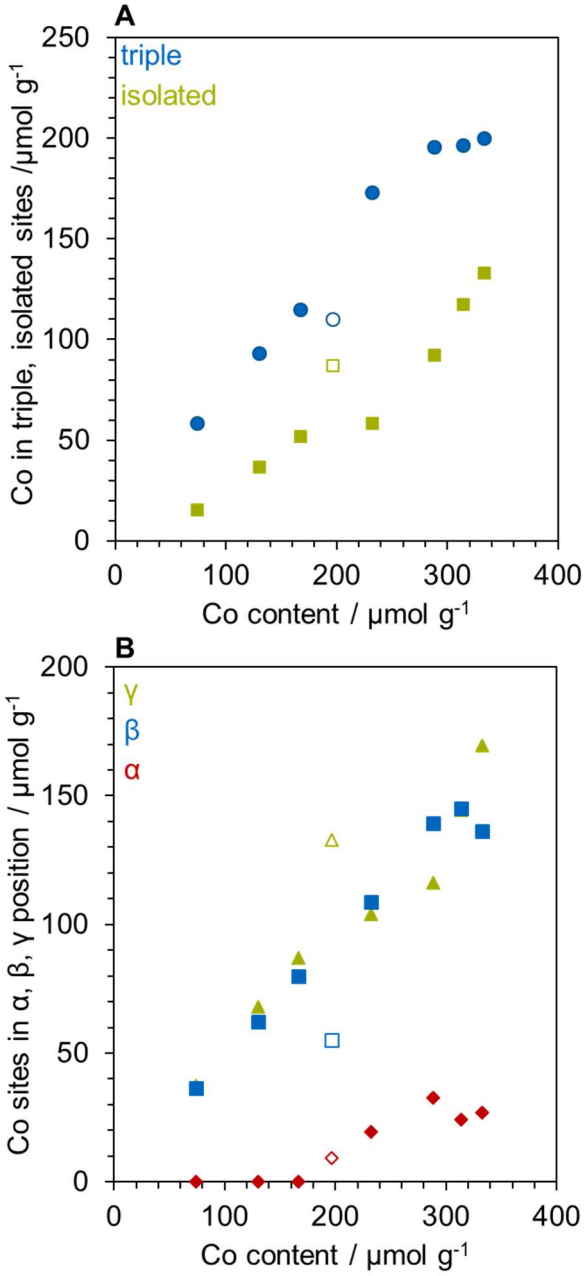

Figure 5.4: A) shows the amount of Co located in triple or isolated sites. **B)** shows Co in α, β and γ positions. Triple and isolated sites are assigned via benzene adsorption; α, β, and γ sites are assigned via UV-Vis deconvolution. Co-ZSM-5 filled, Co-ZSM-5 (N) not filled.

Figure S 5.7A in SI shows UV-Vis spectra of ZSM-5 with different Co loadings in the region from 13000 to 25000 cm^{-1}. In general, the intensity increases with Co loading over the whole spectra. Although a deconvolution of the total contribution of the three positions to experimental spectra is not possible, one can at least estimate the relative changes in the absorption of Co^{2+} in α, β, and γ positions with Co loading. For

this, we have divided the spectra into regions (A: 14000-16000 cm^{-1}; B: 16000 - 19000 cm^{-1}, and C: 19000 – 22000 cm^{-1}, corresponding to Co^{2+} in positions α, βand γ respectively.[22]

The α position, indicated by a shoulder with a maximum at 15100 cm^{-1}, can only be clearly observed for catalysts with Co loadings > 200 μmol g^{-1}. **Figure 5.4B** shows the amount of Co^{2+} in α, β, and γ positions, based on the relative proportions determined by deconvolution of the UV-Vis spectra into three main contributions (**Figure S 5.7**). Comparing the resulting trend with that of Co in triple sites deduced from benzene adsorption in **Figure 5.4A**, one can clearly see a correlation between Co in triple sites and Co in β position. In good agreement, the β position is associated to Co sites in the intersection of ZSM-5.

Regarding Co exchanged on non-triple sites, we cannot differentiate whether it is in α or γ position. However, it should be noted that catalysts at low Co loadings (74 – 188 μmol_{Co} g^{-1}) show no contribution of α sites, even though they are active in forming toluene.

On the one hand, it can be seen that below 200 μmol_{Co} g^{-1}, the position of all Co sites is equally distributed in β and γ locations. Above this value, Co also exchanges in a smaller fraction in the α position. For the samples above ~ 280 μmol_{Co} g^{-1} - those with the highest TOF per Co – the amount of Co in α and β sites is constant, and only the amount of Co in γ position increases. From this, we preliminary concluded that all Co^{2+} exchanged is active to some extent in the reaction of CH_4 alkylation of benzene. However, the sharp rise in TOF observed for high Co loadings may be linked to the more constrained γ positions of the sinusoidal channels, which are more active than Co in α and β sites.

5.2.4 On the effect of active site environment in the activity and selectivity of Co-ZSM-5

In order to direct the Co ions to distinctly different ion-exchange positions, several strategies are available. One of them is to use a different pH and Co salt precursor in the ion exchange, such as Co nitrate. Several Co-ZSM-5 materials were prepared by

ion exchange with Co nitrate. In this way, it was possible to exchange loadings of up to ~ 200 $\mu mol_{Co}\ g^{-1}$ with ratios of covered BAS per Co of 1.9. The toluene formation rates per Co are slightly lower on these samples compared with the samples synthesized with acetate solution (see **Figure 5.1A**).

Benzene adsorption on nitrate exchanged samples shows a different profile of BAS coverage compared to the acetate samples (**Figure 5.3A**). The quantification of Co in different positions show that using $Co(NO_3)_2$ for ion exchange results in a more significant proportion of Co in dual/single sites (**Figure 5.4A**).

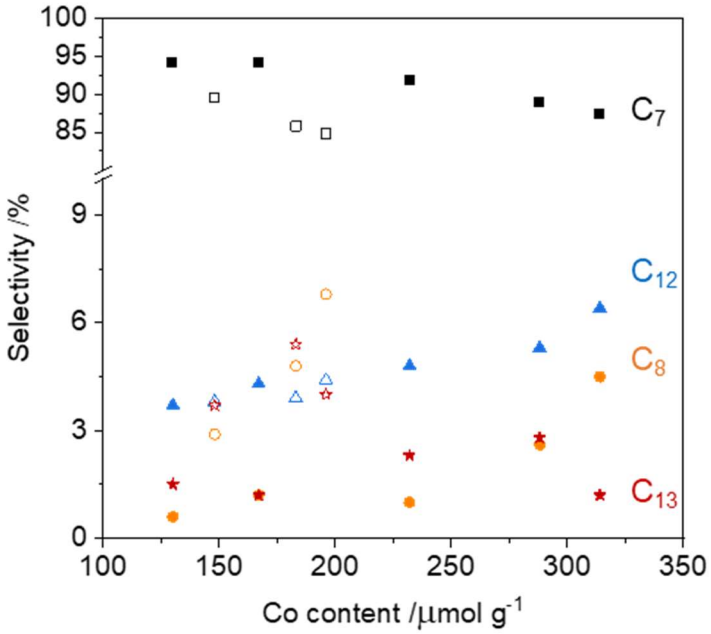

Figure 5.5: Selectivity as a function of Co content for C_7 (square), C_8 (circle), C_{12} (triangle), C_{13} (star) Co acetate samples are filled, and nitrate samples are not filled. The benzene conversion was 1.5 - 2.1 %.

In good agreement, the classification of Co exchanged in positions α, β, and γ via UV-Vis deconvolution (see **Figure 5.4B**) shows a more significant proportion of Co exchanged in non-triple sites in γ position. However, in **Figure 5.1**, one can see that the catalysts exchanged with nitrate precursor are slightly less active than the ones exchanged with acetate solution. In contrast, an apparent increase of the Co in γ sites can be seen at the expense of the β sites. This is proof that the γ position is not intrinsically more active than the others. Therefore, we conclude that the main reason for a higher TOF_{Co} in samples with high Co loading is again a higher probability of two

Co sites to be in proximity, and that is stochastic rather than related to the position of the Co ions.

Finally, we compare the selectivity of products in relation to the different positions of Co exchange sites.

Co-ZSM-5 selectivity for acetate and nitrate synthesized catalysts to products in the direct alkylation of benzene with methane was measured at similar benzene conversions. In our previous work, we reported that, in addition to the alkylation of benzene to toluene and xylene, there is a significant contribution of a parallel reaction pathway of benzene to form biphenyl (compare chapter 4). Overall, the selectivities are comparable for all samples at low conversions (X ~ 1.8%, **Figure 5.5**). However, we observed that the selectivity towards toluene decreased with increasing Co loading, while selectivity towards xylenes and biphenyl increased for acetate samples. The formation of xylenes – a secondary product- is favored at high Co loadings over the primary product because of the higher probability of an aromatic molecule encountering a second active site in its path through the zeolite microspores. However, a clear difference in selectivities is observed for those samples prepared with nitrate. In this case, a clear decrease in toluene selectivity is observed at the expenses of an increase in secondary products xylene and C_{13}. Both products are the result of the secondary reaction of toluene. The biphenyl production, however, seems independent from the Co salt. This different behavior in selectivity for the secondary products is likely an indirect result of varying position or accessibility of Co sites in nitrate exchanged samples.

The selectivity towards secondary products is higher when the ion exchange with nitrate solution is performed. We propose that xylenes and phenyltoluene are formed via an Eley-Rideal mechanism after toluene reacts with an available activated CH_3- or benzene strongly adsorbed on a Co site, respectively. We assign this increase in selectivity to secondary products to a higher concentration of Co active sites in the sinusoidal channel. The sterically constrained reorientation of alkylated aromatics through the zig-zag channel causes a ~ eight times lower diffusivity than through the main channel.[24-25] Therefore, the virtual contact time of aromatics along the sinusoidal channel is more significant than the main channel. The probability for a secondary reaction on Co sites in zig-zag channels correspondingly increases.[26]

5.3 Chapter conclusion

The location of Co sites in ZSM-5 (Si/Al = 15) was shown to influence the TOF and the selectivities in the alkylation of benzene with CH_4.

Activity tests showed that the formation rate of toluene increased with Co loading and that with acetate precursor synthesized catalysts are more active for toluene formation than nitrate precursor synthesized samples. All tested materials contain mostly Co^{2+} ions exchanged in Al pairs. Thus, the oxidation state does not explain the different behavior for these samples. However, adsorbing benzene demonstrated the presents of triple and isolated sites within the MFI structure, which influenced the location of ion exchange. Combining these findings with UV-Vis results let us relate Co exchanged in triple sites to Co in β sites in the intersection, and Co in isolated sites within α and γ positions in the main and sinusoidal channel, respectively. The position of the Co sites also influences the selectivity of products. Active sites in the sinusoidal channel enhance secondary reactions.

Regarding all together, we hypothesize to have mostly Co^{2+} sites exchange in Al pairs as active sites. The location of these active sites influences the selectivity and the TOF due to confinement and accessibility.

5.4 Experimental section

5.4.1 Chemicals

High-purity nitrogen (99.999%), synthetic air (99.995%), 10% oxygen in helium (99.995%), and CH_4 (99.995%) gases were purchased from Westfalen and used without further purification. Cobalt(II)-acetate (99.99%), cobalt(II)nitrate (99.99%) and benzene (anhydrous, 99.8%) were purchased from Merck.

5.4.2 Material synthesis

NH_4-ZSM-5 zeolite (Si/Al = 15, Zeolyst) was calcined in synthetic air (100 mL min^{-1}) for 10h at 550 °C (10 °C min^{-1}) to obtain the H-form. To prepare the metal exchanged catalysts, 1 g of H-form zeolite was stirred in 50 mL g^{-1} Co acetate or Co nitrate solution (2.5 mM – 10 mM) at 80 °C for 15 h. The pH value was adjusted to 6.5 with acetic acid or nitric acid. The resulting suspensions were filtered and washed with water, and dried in air.

5.4.3 Infra-Red spectroscopy measurement

The catalysts were characterized by FTIR measurements with a Nicolet iS50 spectrometer from Thermo Scientific to obtain their acid site concentrations. The spectra were recorded in the range of 4000 - 650 cm^{-1} on thin catalyst pellets. After heating to 450 °C for 1h under vacuum (10 °C min^{-1}, 10^{-7} mbar), pyridine (0.5 mbar) was adsorbed at 150 °C for 1h. To obtain only chemisorbed pyridine, the sample was under vacuum (10^{-7} mbar) for one hour. CO and NO adsorption was carried out in a vertex IR from Bruker at liquid nitrogen temperature. Benzene adsorption measurements were carried out in a Bruker ifs 66v/S FTIR spectrometer. The spectra were recorded in the range of 8000 - 650 cm^{-1} on thin catalyst pellets. After heating to 450 °C for 1h under vacuum (10 °C min^{-1}, 10^{-7} mbar), benzene was adsorbed stepwise from $7.0 \cdot 10^{-3}$ – 11 mbar. For analysis, the SiOHAl band at 3610 cm^{-1} and C-C band at 1478 cm^{-1} were used for BAS coverage and benzene uptake, respectively.

5.4.4 UV-Vis spectroscopy measurement

The spectra were recorded between 200 nm and 1000 nm on an AvaLight-DH-S-BAL with AvaSpec-2048 in diffuse reflection mode. $BaSO_4$ was used as a reference. Catalyst samples (150-250 µm) were activated for 1 h, at 450 °C with a rate of 10 °C min^{-1} in synthetic air. The spectra were measured at 200°C. Absorption intensities were calculated using the Kubelka-Munk equation.

5.4.5 Atomic absorption spectroscopy

For investigation of the element contents in the prepared catalysts, graphite-tube atomic absorption spectroscopy (GT-AAS) was performed on a Solaar M5 AA-Spectrometer from ThermoFischer.

5.4.6 X-ray absorption spectroscopy (XAS).

Co K-edge X-ray absorption spectra were obtained at the P65 beamline of the German electron synchrotron (DESY) in Hamburg, Germany. The storage ring was operated at 6 GeV energy and 100 mA beam-current. A water-cooled Si111 double crystal monochromator (DCM) was used for obtaining monochromatic X-rays. Two Si mirrors were installed in front of the DCM to reject higher harmonics. The DCM was calibrated for Co K-edge by measuring a Co-foil and defining the first major inflection point as 7709 eV. A Co-foil was also placed between the second and third ionization chamber for the energy calibration of each measured spectrum. The energy resolution of the beamline is estimated to be ~1.2 eV at the Co K-edge. The XAS spectra were measured in both transmission mode and in fluorescence mode using a passivated implanted planar silicon (PIPS) detector. The spot-size of X-ray beam at the sample was 1.6 mm (horizontal) × 200 μm (vertical).

Spectra for X-ray absorption near edge structure (XANES) analyses were measured between −100 eV and +200 eV around the Co K-edge while the spectra for extended X-ray absorption fine structure (EXAFS) analyses were obtained between −150 eV and +600 eV around the Co K-edge. The data were monitored for any signs of X-ray beam damage. Several successive scans were averaged to reduce signal-to-noise ratio and improve the data quality. XANES and EXAFS data analyses were performed using Athena and Artemis software packages. For XANES analyses, E_0 was fixed at 7709 eV and the spectra were normalized and flattened. For EXAFS analyses, spectra were background subtracted, normalized, k^2-weighted, and Fourier-transformed in the k range between 3 and 11 Å-1. The EXAFS fitting was performed in k-space between 3 and 11 $Å^{-1}$ simultaneously on the k^1-, k^2-, and k^3-weighted data. E_0 was set such that energy-shift (ΔE_0) obtained during the fit was less than 1 eV. A Co-foil was first fitted to obtain the amplitude reduction factor, $S0_2$ = 0.7, which was then used in the subsequent fits.

In situ XAS measurements were performed using a quartz capillary micro-reactor setup. In a typical experiment, the catalyst was placed in a quartz capillary (1 mm o.d., 20 µm thickness) supported between two quartz wool plugs. The capillary was heated from below with a hot-air gas-blower (Oxford FMB). Gas flow rates were maintained using Bronkhorst electronic mass flow controllers and the pressure was continuously monitored using a pressure gauge (Omega). The catalyst was first activated under syntetic air at 500°C for 1h.. After activation, the sample was cooled down to 100°C for XAS measurements.

5.4.7 Catalytic testing

The activity of the catalysts was tested in a 1/4" quartz glass plug flow reactor between 500 and 560 °C, under atmospheric pressure. The catalysts were activated in a mixture of 10% oxygen in helium at 550 °C (10 °C min^{-1}) for 2 h. Before starting the reaction, the reactor was purged with nitrogen. The reaction was conducted in nitrogen atmosphere with varied ratios of CH_4/benzene = 33- 170, and WHSV= 0.2 - 2.2 h^{-1}. Reactants and products were analyzed by a GC System Agilent 7890B or a mass spectrometer Omnistar® by Pfeiffer Vacuum.

5.5 Supporting Information

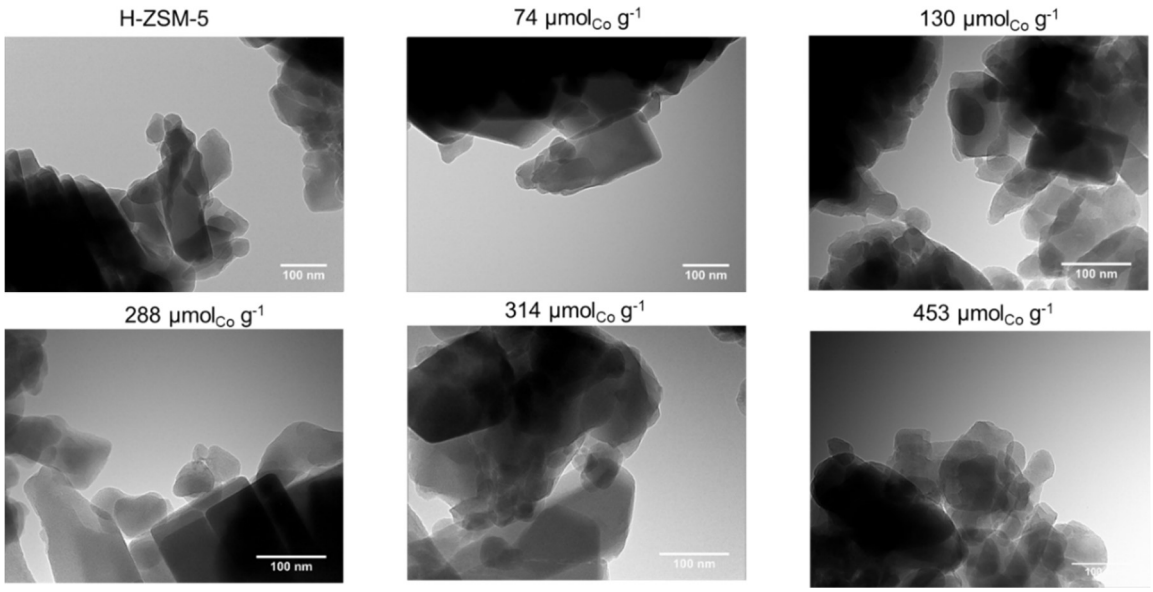

Figure S 5.1: TEM images of a selection of ZSM-5 with different Co loading. Particles are only visible at Co loading of 453 µmol g^{-1}.

Table S 5.1: Co content, LAS, and BAS concentration, BAS/Co as well as apparent activation energy, and reaction orders in benzene as well as in methane of in ZSM-5 exchanged with Co. Si/Al = 15.

Co content /µmol g_{cat}^{-1}	**LAS /µmol g_{cat}^{-1}**	**BAS /µmol g_{cat}^{-1}**	**BAS/Co**	**Apparent energy of activation /kJ mol^{-1}**	**Reaction order for toluene in methane**	**Reaction order for toluene in benzene**
333	1122	182	1.8	N/S	N/S	N/S
326	1051	214	1.7	N/S	0.7	0.4
314	1061	227	1.8	122	0.7	0.4
288	1040	277	1.8	N/S	N/S	N/S
232	910	354	1.8	N/S	0.7	0.4
167	725	450	2.0	130	N/S	N/S
130	541	519	2.0	126	0.7	0.4
74	438	630	2.0	N/S	N/S	N/S
196 (N)	632	400	1.9	N/S	0.7	N/S
181(N)	889	445	1.9	N/S	0.7	N/S
148 (N)	546	428	2.3	N/S	0.7	N/S
Blank IE	190	780	-	-	-	-

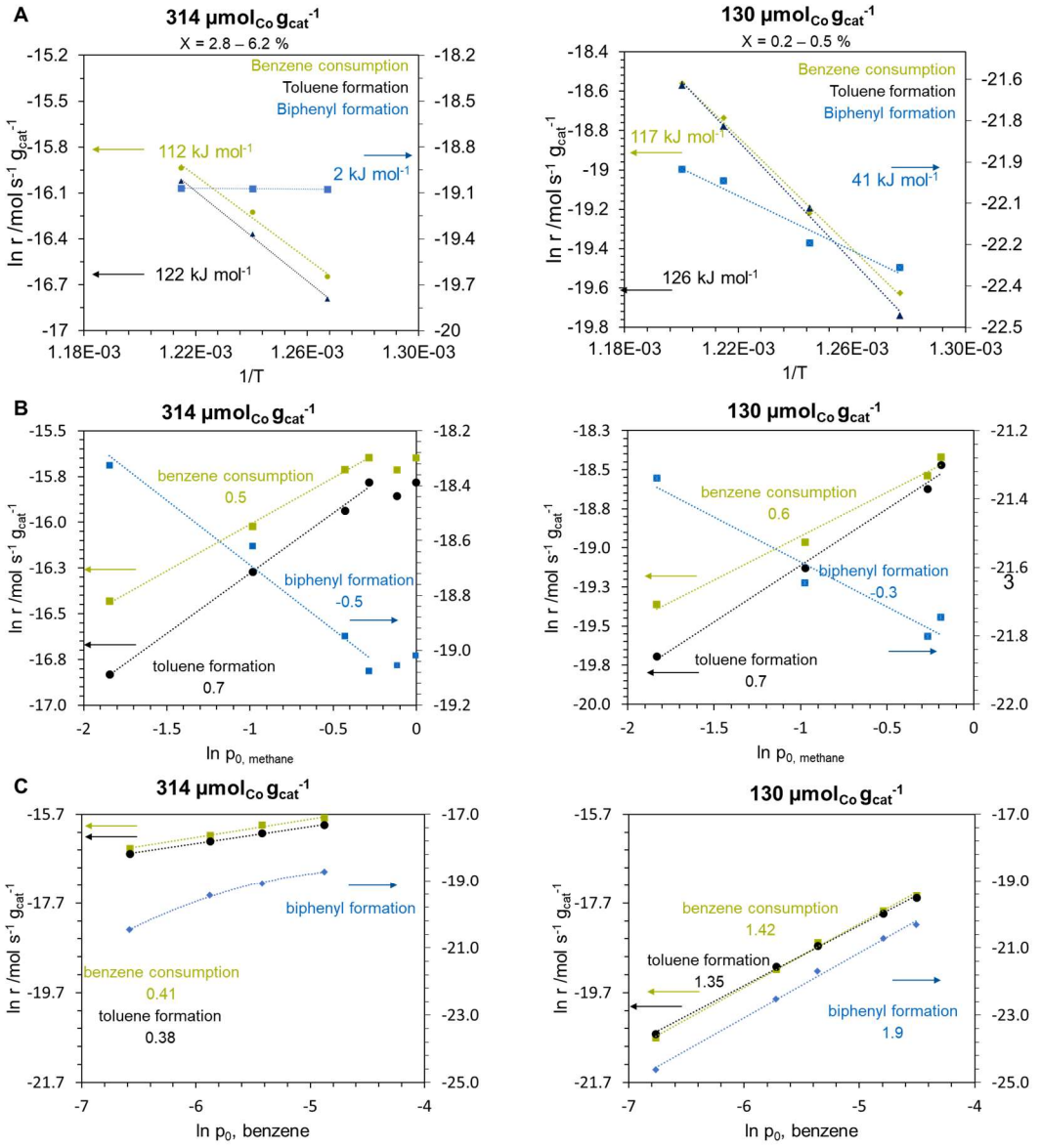

Figure S 5.2: Apparent energy of activation of Co-ZSM-5(130) and Co-ZSM-5(314) determined between 783 and 833 K in A). Reaction orders in methane (B) and benzene (C) determined for Co-ZSM-5(130) and Co-ZSM-5(314). Benzene consumption in circles (green), toluene formation in triangle (black), and biphenyl formation in square (blue).

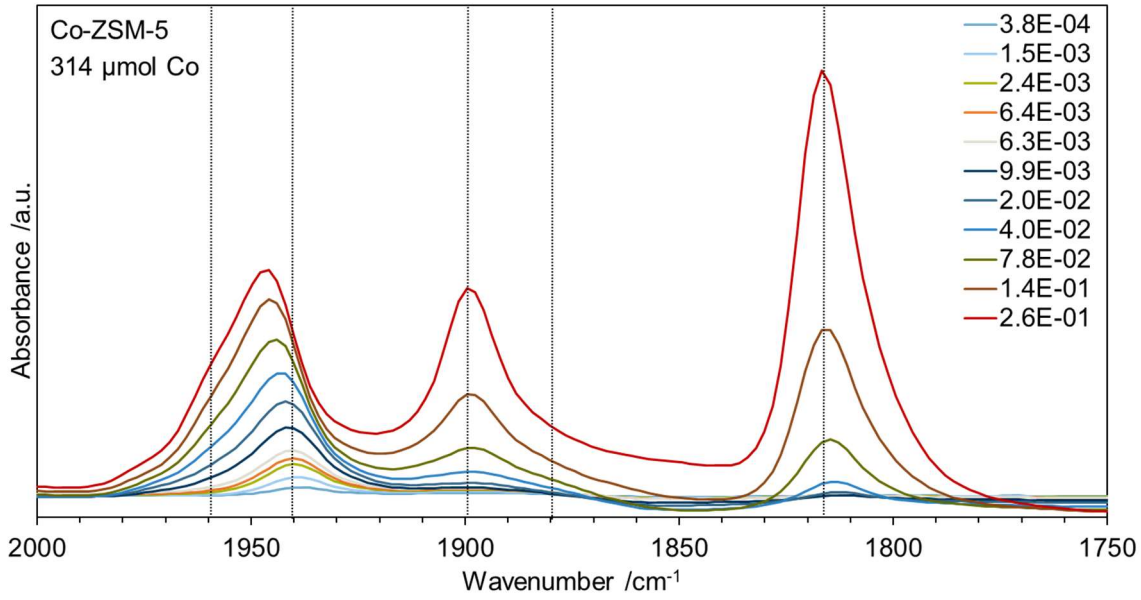

Figure S 5.3: FTIR spectra of NO adsorbed on ZSM-5 (314 $\mu mol_{Co}\ g^{-1}$) with different p_0 of NO at liquid N_2 temperature. Activation for 1h at 450°C in vacuum.

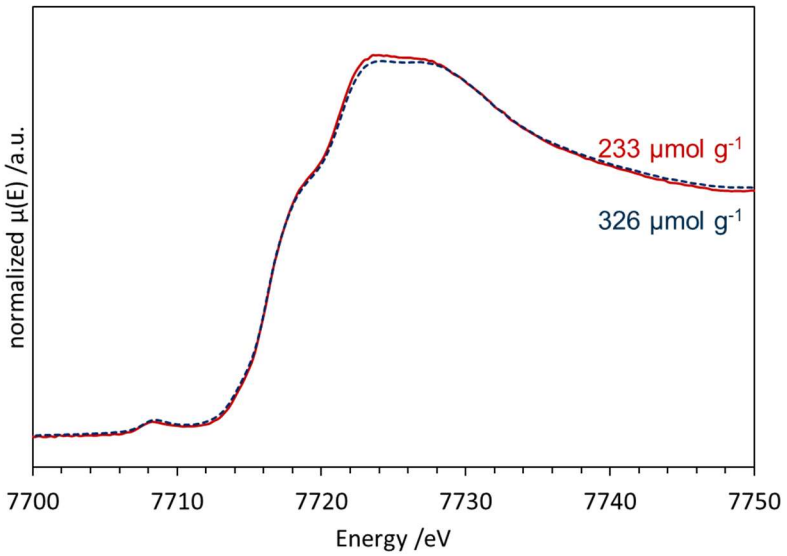

Figure S 5.4: Cobalt XANES data Co-ZSM-5 with 233 $\mu mol_{Co}\ g_{cat}^{-1}$ (line) and 326 $\mu mol_{Co}\ g_{cat}^{-1}$ (dashed line) activated in synthetic air at 450°C.

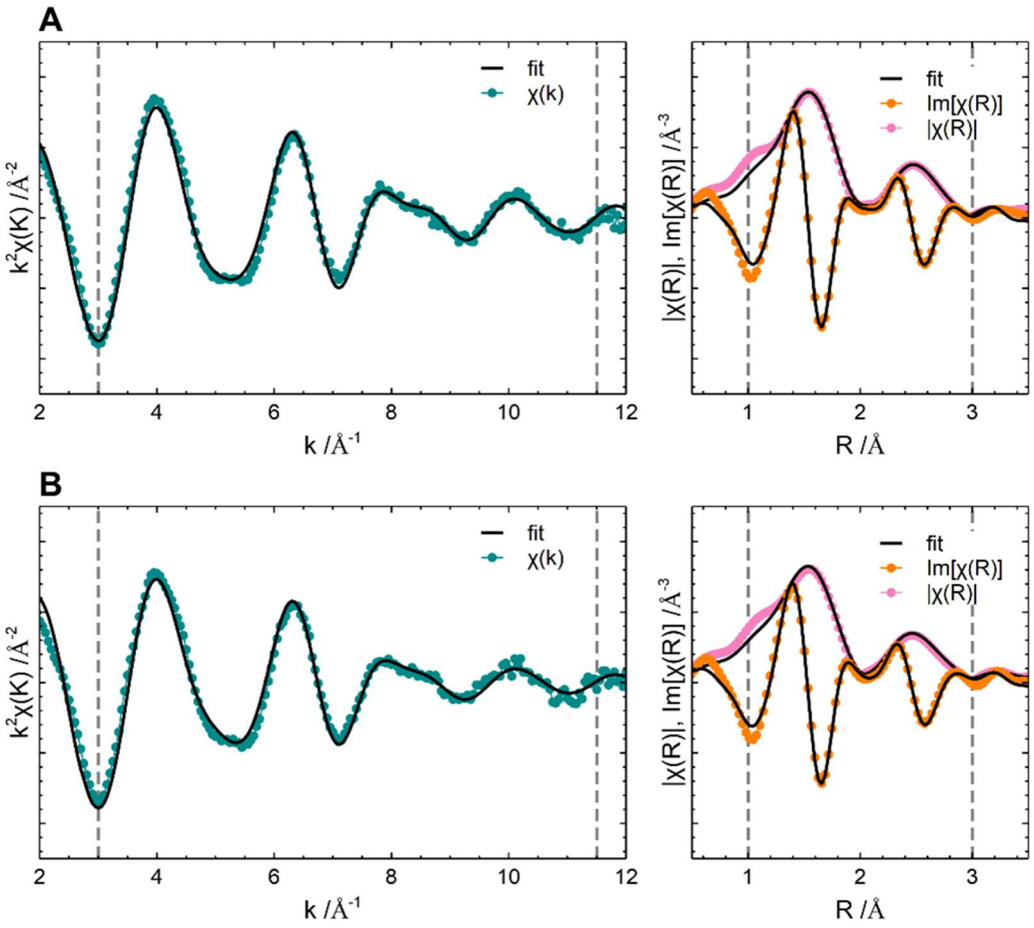

Figure S 5.5: Cobalt EXAFS data and fitting in k-space and R-space for Co-ZSM-5 with A) 233 $\mu mol_{Co}\ g_{cat}^{-1}$ and B) 326 $\mu mol_{Co}\ g_{cat}^{-1}$. The materials were activated in synthetic air at 450°C prior measurement at 100°C.

Table S 5.2: EXAFS fitting parameter for Co-ZSM-5 with 233 $\mu mol_{Co}\ g_{cat}^{-1}$. E_0 = 7717 eV; ΔE_0 = -1.5 ± 7.0 eV; R-factor = 0.02606; S_0^2 = 0.80

Path	**CN**	***d* /Å**	**$\sigma^2 \times 1000$ /Å^2**
Co-O	4.0 ± 2.3	2.001 ± 0.042	7.3 ± 5.6
Co-Al	1.0 ± 2.9	2.758 ± 0.087	3.6 ± 24
Co-Si	1.1 ± 4.3	3.183 ± 0.107	5.0 ± 33

Table S 5.3: EXAFS fitting parameter for Co-ZSM-5 with 326 $\mu mol_{Co}\ g_{cat}^{-1}$. E_0 = 7717 eV; ΔE_0 = -0.8 ± 8.5 eV; R-factor = 0.03168; S_0^2 = 0.80

Path	**CN**	***d* /Å**	**$\sigma^2 \times 1000$ /Å^2**
Co-O	4.1 ± 2.9	2.003 ± 0.053	8.6 ± 7.3
Co-Al	1.5 ± 5.0	2.763 ± 0.112	7.6 ± 31
Co-Si	1.1 ± 6.0	3.199 ± 0.162	7.7 ± 51

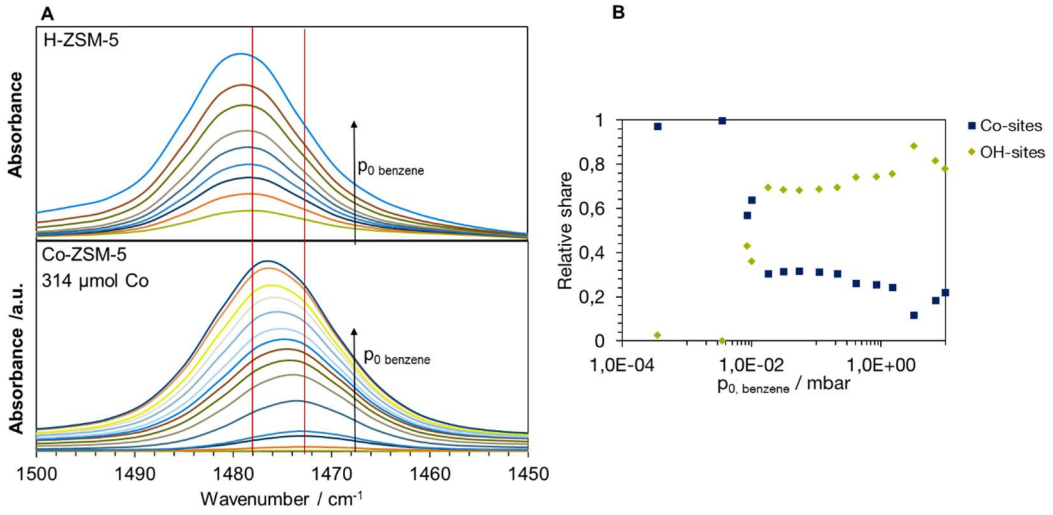

Figure S 5.6: A) FTIR spectra of benzene adsorbed on H-ZSM-5 and Co-ZSM-5 with different p_0 at 100 °C. Activation for 1h at 450°C in vacuum. **B)** Band at ~1475 cm^{-1} deconvoluted into two bands corresponding to CC vibration interacting with AlOH and Co sites.

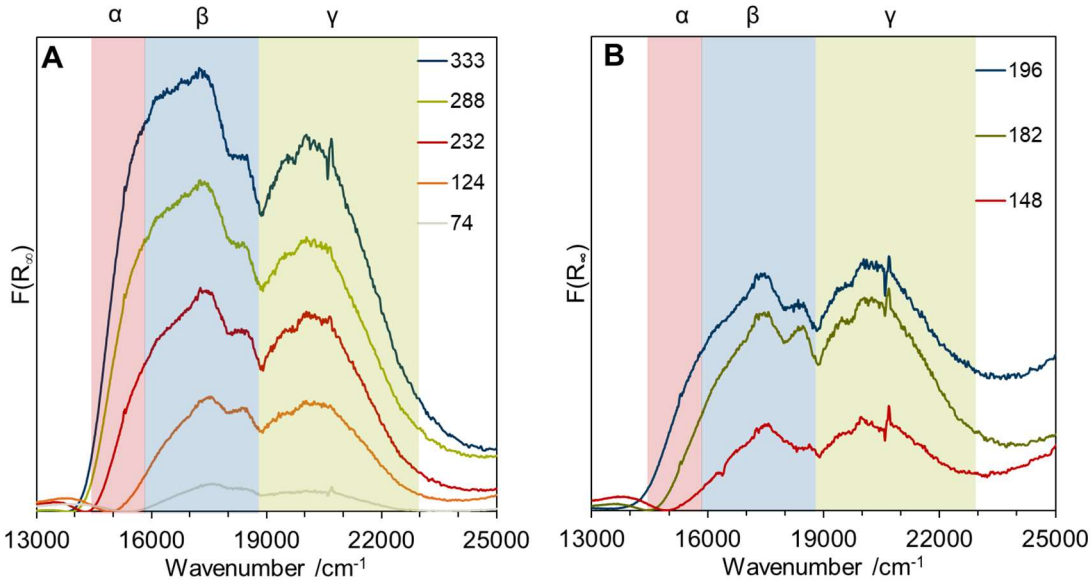

Figure S 5.7: UV-Vis spectra (FT) of dehydrated Co-ZSM-5 with different Co loading synthesized with A) Co acetate and B) Co nitrate Co-ZSM-5. Activation 1h in synthetic air, 450°C. $T_{measurement}$ = 200°C. Spectra are not normalized.

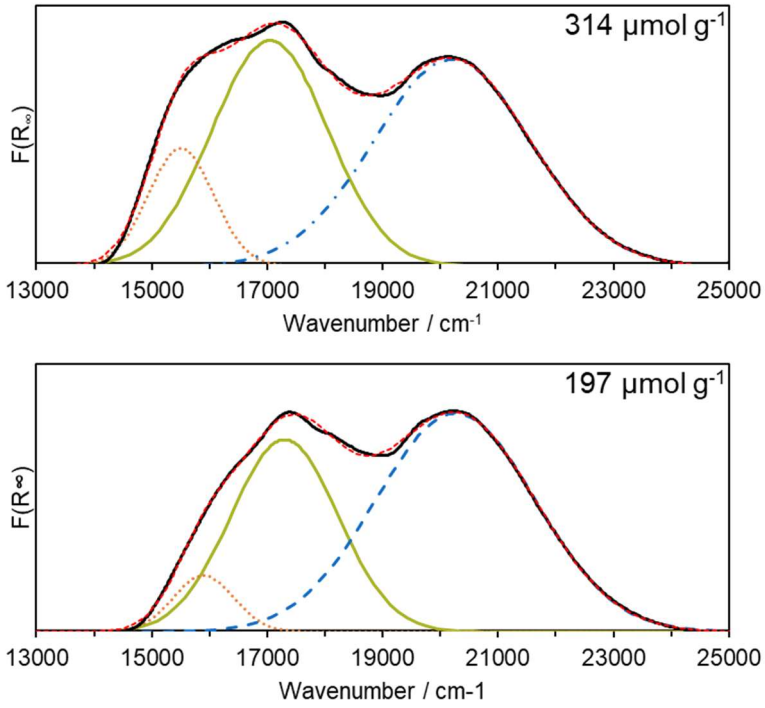

Figure S 5.8: Example of deconvolution of UV-Vis spectrum of samples with 314 and 197 $\mu mol_{Co}\ g^{-1}$. Original spectrum (line), fitted (--), α site (··), β site (–), γ site (- -).

Table S 5.4: Distribution of Co sites deconvoluted from UV-Vis spectra (FT) shown in Figure S6.

* [(total number of BAS) – (number of BAS covered in the linear part) * (fraction of BAS with slope 3)] / 3.

** (Total number of Co – number of Co in triple sites).

Co content /µmol g^{-1}	**Slope (linear part)**	**Co in triple sites***	**Co in isolated sites****
74	3.0	58	16
130	3.0	93	37
167	2.5	115	52
232	1.6	173	59
288	1.1	196	92
314	1.1	196	118
333	1.0	200	133
197(N)	3.0	110	87

Table S 5.5: Distribution of Co sites deconvoluted from UV-Vis spectra (FT) shown in **Figure S 5.7**.

Co content /µmol g^{-1}	α site /%	β site /%	γ site /%
74	0	49	51
130	0	48	52
167	0	48	52
232	8	47	45
288	11	48	40
333	8	41	51
148 (N)	2	31	67
182 (N)	4	30	66
197(N)	5	28	67

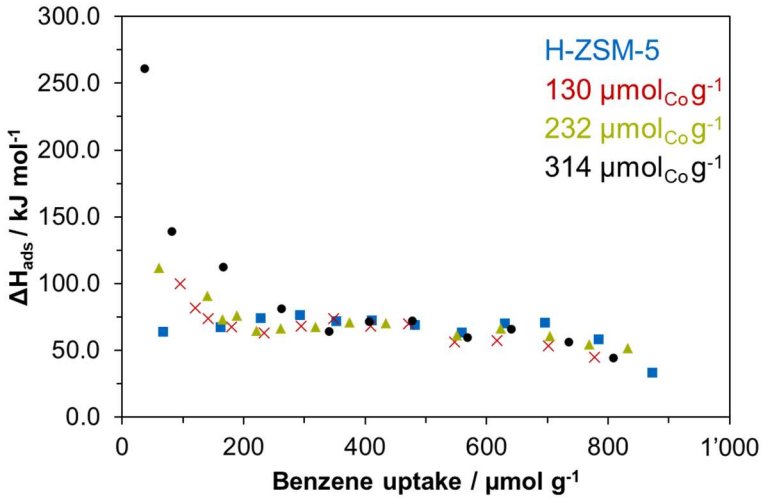

Figure S 5.9: ΔH_{ads} determined via benzene adsorption in vacuum TGA.

5.6 References

1. Horn, R.; Schlögl, R., Methane Activation by Heterogeneous Catalysis. *Catalysis Letters* **2015,** *145* (1), 23-39.

2. Spivey, J. J.; Hutchings, G., Catalytic aromatization of methane. *Chemical Society Reviews* **2014,** *43* (3), 792-803.

3. Taifan, W.; Baltrusaitis, J., CH 4 conversion to value added products: Potential, limitations and extensions of a single step heterogeneous catalysis. *Applied Catalysis B: Environmental* **2016,** *198*, 525-547.

4. Sun, L.; Wang, Y.; Guan, N.; Li, L., Methane Activation and Utilization: Current Status and Future Challenges. *Energy Technology* **2019,** *8* (8).

5. Sun, K.; Ginosar, D. M.; He, T.; Zhang, Y.; Fan, M.; Chen, R., Progress in Nonoxidative Dehydroaromatization of Methane in the Last 6 Years. *Industrial & Engineering Chemistry Research* **2018,** *57* (6), 1768-1789.

6. Bellmann, A.; Atia, H.; Bentrup, U.; Brückner, A., Mechanism of the selective reduction of NOx by methane over Co-ZSM-5. *Applied Catalysis B: Environmental* **2018,** *230*, 184-193.

7. Xu, Y.; Chen, M.; Wang, T.; Liu, B.; Jiang, F.; Liu, X., Probing cobalt localization on HZSM-5 for efficient methane dehydroaromatization catalysts. *Journal of Catalysis* **2020,** *387*, 102-118.

8. Nakamura, K.; Okuda, A.; Ohta, K.; Matsubara, H.; Okumura, K.; Yamamoto, K.; Itagaki, R.; Suganuma, S.; Tsuji, E.; Katada, N., Direct Methylation of Benzene with Methane Catalyzed by Co/MFI Zeolite. *ChemCatChem* **2018,** *10* (17), 3806-3812.

9. Matsubara, H.; Yamamoto, K.; Tsuji, E.; Okumura, K.; Nakamura, K.; Suganuma, S.; Katada, N., Position and Lewis acidic property of active cobalt species on MFI zeolite for catalytic methylation of benzene with methane. *Microporous and Mesoporous Materials* **2021,** *310*.

10. Dědeček, J.; Kaucký, D.; Wichterlová, B.; Gonsiorová, O., Co2+ions as probes of Al distribution in the framework of zeolites. ZSM-5 study. *Phys. Chem. Chem. Phys.* **2002,** *4* (21), 5406-5413.

11. Hirschler, A. E., The measurement of catalyst acidity using indicators forming stable surface carbonium ions. *Journal of Catalysis* **1963,** *2* (5), 428-439.

12. Panpranot, J.; Kaewkun, S.; Praserthdam, P.; Goodwin, J. G., Effect of Cobalt Precursors on the Dispersion of Cobalt on MCM-41. *Catalysis Letters* **2003,** *91* (1), 95-102.

13. Kraum, M.; Baerns, M., Fischer–Tropsch synthesis: the influence of various cobalt compounds applied in the preparation of supported cobalt catalysts on their performance. *Applied Catalysis A: General* **1999,** *186* (1), 189-200.

14. Ivanova, E.; Hadjiivanov, K.; Klissurski, D.; Bevilacqua, M.; Armaroli, T.; Busca, G., FTIR study of species arising after NO adsorption and NO+O2 co-adsorption on CoY: comparison with Co-ZSM-5. *Microporous and Mesoporous Materials* **2001,** *46* (2), 299-309.

15. Hadjiivanov, K.; Saussey, J.; Freysz, J. L.; Lavalley, J. C., FT-IR study of NO + O2 co-adsorption on H-ZSM-5: re-assignment of the 2133 cm-1 band to NO+ species. *Catalysis Letters* **1998,** *52* (1), 103-108.

16. Hadjiivanov, K.; Tsyntsarski, B.; Venkov, T.; Klissurski, D.; Daturi, M.; Saussey, J.; Lavalley, J. C., FTIR spectroscopic study of CO adsorption on Co–ZSM-5: Evidence of formation of Co+(CO)4 species. *Physical Chemistry Chemical Physics* **2003,** *5* (8), 1695-1702.

17. Chupin, C.; van Veen, A. C.; Konduru, M.; Després, J.; Mirodatos, C., Identity and location of active species for NO reduction by CH4 over Co-ZSM-5. *Journal of Catalysis* **2006,** *241* (1), 103-114.

18. Pietrzyk, P.; Dujardin, C.; Góra-Marek, K.; Granger, P.; Sojka, Z., Spectroscopic IR, EPR, and operando DRIFT insights into surface reaction pathways of selective reduction of NO by propene over the Co–BEA zeolite. *Physical Chemistry Chemical Physics* **2012,** *14* (7), 2203-2215.

19. Wang, X.; Chen, H.-Y.; Sachtler, W. M. H., Catalytic reduction of NOx by hydrocarbons over Co/ZSM-5 catalysts prepared with different methods. *Applied Catalysis B: Environmental* **2000,** *26* (4), L227-L239.

20. Campa, M. C.; De Rossi, S.; Ferraris, G.; Indovina, V., Catalytic activity of Co-ZSM-5 for the abatement of NOx with methane in the presence of oxygen. *Applied Catalysis B: Environmental* **1996,** *8* (3), 315-331.

21. Ene, A. B.; Archipov, T.; Roduner, E., Spectroscopic Study of the Adsorption of Benzene on Cu/HZSM5 Zeolites. *The Journal of Physical Chemistry C* **2010,** *114* (34), 14571-14578.

22. Bellmann, A.; Rautenberg, C.; Bentrup, U.; Brückner, A., Determining the Location of Co2+ in Zeolites by UV-Vis Diffuse Reflection Spectroscopy: A Critical View. *Catalysts* **2020,** *10* (1), 123.

23. Drozdová, L.; Prins, R.; Dědeček, J.; Sobalík, Z.; Wichterlová, B., Bonding of Co Ions in ZSM-5, Ferrierite, and Mordenite: An X-ray Absorption, UV−Vis, and IR Study. *The Journal of Physical Chemistry B* **2002,** *106* (9), 2240-2248.

24. Gobin, O. C.; Reitmeier, S. J.; Jentys, A.; Lercher, J. A., Diffusion pathways of benzene, toluene and p-xylene in MFI. *Microporous and Mesoporous Materials* **2009,** *125* (1), 3-10.

25. Toda, J.; Corma, A.; Abudawoud, R. H.; Elanany, M. S.; Al-Zahrani, I. M.; Sastre, G., Influence of force fields on the selective diffusion of para-xylene over ortho-xylene in 10-ring zeolites. *Molecular Simulation* **2015,** *41* (16-17), 1438-1448.

26. Lukyanov, D.; Vazhnova, T., A kinetic study of benzene alkylation with ethane into ethylbenzene over bifunctional PtH-MFI catalyst. *Journal of Catalysis* **2008,** *257* (2), 382-389.

6 Summary and final conclusion

By combining reaction kinetics, temperature-programmed surface reactions, and *in-situ* and *operando* spectroscopic methods, we clarify within this thesis the main questions concerning the mechanism and the catalytic active sites for the direct alkylation of benzene over Co-ZSM-5 catalysts. These concerned (i) the product distribution, (ii) the reaction pathways, (iii) the reaction mechanism, (iv) the nature and location of active Co sites, and (vi) the influence on selectivity and reactivity of the location of active sites.

For this purpose, Co-ZSM-5 with different Co concentrations (74 – 333 $\mu mol_{Co}\ g^{-1}$) were prepared via aqueous ion exchange. Testing these materials revealed that the modified tailored catalysts are active for the direct alkylation of benzene with CH_4 at 550 °C at atmospheric pressure. Toluene and hydrogen were identified as the main products with a carbon selectivity of up to > 90%. Xylene isomers and phenyltoluene were found to be the main secondary products. A competitive reaction pathway is the dimerization of benzene to form biphenyl. However, the rate of competitive biphenyl formation can be reduced by increasing the partial pressure of CH_4. It has a positive impact on the selectivity of the toluene route. However, high selectivity and activity to produce target products require a large amount of CH_4 in excess. As a result, most of the methane must be recycled. From an industrial point of view, this might not be profitable enough, for which reason this method might remain academic.

The heat of benzene adsorption on Co in Co-ZSM-5 catalysts showed a strong interaction of the probe molecule with the active sites with ΔH_{ads} = 260 kJ mol^{-1}. Temperature programmed surface reactions underline this strong adsorption of benzene on Co sites. The controlled activation of CH_4 is only possible if it is fed prior benzene. Otherwise the Co sites will be poisoned by benzene, and the reaction pathway of alkylation is hindered. Furthermore, the TPSR showed toluene production at two temperatures: at mild temperatures of 200-400 °C and above 500 /°C. An energy barrier of 69 kJ mol^{-1} at lower temperatures indicates an Eley-Rideal mechanism. In comparison, more inadequate benzene coverage at higher temperatures allows a Langmuir-Hinshelwood mechanism with an E_{app} of 112 kJ mol^{-1}.

Based on these findings, the proposal is that CH_4 and benzene are activated on similar Co^{2+} sites. A dependency of 2.6 Co sites required per toluene formed suggests that at least two different cobalt sites are part of the mechanism.

This increase of activity, per mass as well as per Co, with Co concentration raises the question of whether the mechanism or the active sites involved are changing with Co content.

Therefore, several probe molecules like carbon monoxide, nitric oxide, and pyridine were adsorbed on catalysts with various Co loading. The latter combined with XAS measurements point to the majority of Co being exchanged as single Co^{2+} ions on Al pairs throughout the series of different Co content. Hence, the oxidation state does not explain different activities.

However, different precursors' applications during catalyst synthesis also showed another activity. Samples synthesized with Co nitrate are slightly less active than those synthesized with Co acetate.

The adsorption of benzene on this series of samples from 74 – 333 $\mu mol_{Co}\ g^{-1}$ indicated the presence of cobalt in triple Al sites and isolated sites. The classification of Co sites in α, β, and γ locations obtained by UV-Vis spectroscopy, showed that the triple sites are located in the intersection of the straight and the sinusoidal channel of ZSM-5. In contrast, isolated sites are located inside the channels. While all locations seem to be active for the alkylation of benzene with CH_4, Co in β position - in the intersection of the straight and the sinusoidal channel - appears to be slightly more active than Co in other positions. With this, the main reason for a higher TOF in samples with high Co loading is not the location of Co. However, a higher probability of two or more co-locations being close to each other is based on stochastic reasons rather than depending on the position of the Co sites.

However, the position of the Co sites has an impact on the product selectivity. Co sites inside the sinusoidal channel appear to enhance secondary reactions. A lower diffusivity of aromatics through the zig-zag channel increases the contact time and therefore, increases the probability of a secondary reaction.

To summarize, the hypothesis is to have mostly Co^{2+} sites exchange in Al pairs as active sites. The location of these active sites influences the selectivity and the TOF due to confinement and accessibility.

7 Attachments

7.1 List of figures

7.2 Publications

- Katz, A., Okrut, A., Aigner, M., Ouyang, X., Zones, S. I., 2019. U.S. Patent Application No. 16/275,945.

- Okrut, X. Ouyang, M. Aigner, A. Palermo, N. Grosso-Giordano, S. Hwang, S. Zones, A. Katz, Dalton Trans., 2018, 47, 15082-15090.

- M. Aigner, N. A. Grosso-Giordano, C. Schöttle, A. Okrut, S. Zones, A. Katz, React. Chem. Eng., 2017, 2, 852-86.

- M. Aigner, N. A. Grosso-Giordano, A. Okrut, S. Zones, A. Katz, React. React. Chem. Eng., 2017, 2, 842-851.

7.3 Conference contributions

- FEZA 2021, Brighton (virtuel), GB
  Poster & short talk

- 54. Jahrestreffen Deutscher Katalytiker 2021, Weimar (virtuell)
  Poster

- JOURNÉES DOCTORALE DE L'ÉNERGIE 2019, Paris, FR
  Poster

- InnoEnergy PhD conference pitching competition 2019, Paris, FR
  Poster & short talk

- DGMK 2018, Berlin
  Poster

7.4 Awards

- FEZA 2021, Brighton (virtuell), GB
  Poster prize

- InnoEnergy PhD conference pitching competition 2019, Paris, FR
  „Top 3“